Measurement of radon concentrations and temperature profiles in boreholes

by

Mayasa H Rashed

Supervisor:professor Bjarne Stugu

Master Thesis in Energy Physics

August 2013

Department of Physics and Technology

University of Bergen/ Norway

ABSTRACT

This thesis is based on a research project aimed at measuring temperature gradients and radon concentrations in boreholes. This was done by observing radon activity and temperature profiles in twelve boreholes that were investigated between October 2012 and May 2013. The boreholes located in Bergen and Osterøy were drilled for extracting underground heat by means of heat pumps and heat exchangers at shallow depths.

Underground heat flow results from the decay process of radioactive elements such as U-235, U-238, Th-232, and K-40 with high concentrations in granitic rocks. Using this the total energy of decay chain of U-238 to Pb-208 was calculated to understand how much energy located in the ground was due to uranium.

Temperature profiles were measured in bore holes by means of sensitive temperature sensors. The logger reads temperature in 10 second intervals. Samples were recorded for 60 and 30 sec at each depth (5 m). The time however was not long enough for the logger to have stable temperature readings.

Therefore, the temperature logger calibration was performed for an unbiased estimate of the temperature at each depth. The logger was placed in a container full of ice water for 15 minutes. Obtained calibration data were plotted on the same figure with the measured data. Figures show in total a variation in some points near the surface.

Radon calibration by using a canary meter with a radioactive source and coalboxes sealed in a plastic box for three days at the laboratory room was used to determine the calibration constant K to be used in field measurements. Energy calibration was done in order to convert the channel number to energy by using known energy values of isotopes such as Cs-137, Na-22, and Ra-226 to determine the energy for unknown sources. Radon concentration was detected by placing coal boxes on top of boreholes in order to absorb radon gas. They were left for three days because the half-life of radon is about three days. The coal boxes were then placed in a gamma ray detector for gamma spectroscopy. Clear peaks were noted from area 2 bore holes, which indicates high radon concentration emanated from boreholes in such area.

Results shown in this thesis were taken from twelve water boreholes: four 250 m deep holes at the Haukeland university hospital (area1), three 180 m deep holes in Osterøy (area2), four 210 m deep holes in Åsane (area3), and one 500 m deep hole in Fyllingsdalen (area4)

Thermal studies show no variation between bore holes, whereas radon concentration is hole dependent. No significant correlation was observed between thermal energy and radon concentration.

The next few chapters in this thesis are presenting the results of the Rn-222 concentration and temperature data in boreholes.

Acknowledgment

I would like to thank:

Professor Bjarne Stugu, my supervisor, for his hard work and guidance, especially during fieldwork and for driving under poor weather conditions. Thank you for your patience with me and for the constructive feedback.

Dr. Kristi Midttomme from CMR for providing me with assistance during fieldwork.
Professor Haakon Fossen and Eivind Bastesen for supporting with geological information in regards to my research area.

The staff at the mechanical workshop at the Department of Physics and Technology for their assistance in making the tools for the experiments.

Dr. Enver Alagoz for his suggestions, discussions, and support throughout the writing process.

PHD candidate Mahdi pur Muhammadi for always welcoming me to his office and for his help with the computer programming.

Student consult Kristine Indahl Helle for her general guidance during my master's study.
The students in my program: Tjalve, Kina, Tordis, and Daniel for their friendship and support.

My family, especially my wonderful children, Jwan and Rojan for their patience while I worked long hours on my master's thesis.

My husband, Thank you for providing us with love and support, even from afar.

My sister, Balkes, thank you for keeping in contact by telephone since we were not able to be close in proximity this time.

Mayasa Rashed
Augest, 2011

LIST OF ABBREVIATIONS AND SYMBOLS

Abbreviations	Meaning
TRT	Thermal Response Test
BHE	Borehole heat exchanger
HDR	Hot Dry Rock
HWR	Hot Wet Rock
GHP	Geothermal Heat Pump
WHO	World Health Organization
NGU	Geological Survey of Norway
NGI	Norwegian Geothermal Institute
HVAC	Heating, Cooling, Ventilation, Air-Condition.

Symbols	Meaning	
λ	Thermal conductivity	[W $m^{-1} k^{-1}$]
ρ	Density	[$kg\, m^{-3}$]
c_p	Specific heat capacity	[$J\, kg^{-1} k^{-1}$]
α	Thermal diffusivity	[$m^2 s^{-1}$]
T	Temperature	[C°]
Q	Constant heat injection rate	
r_b	Borehole radios	[cm]
t	time	[sec]
γ	Euler's constant	[0.5772]
R_b	Thermal borehole resistance	[m KW^{-1}]
R	Decay rate	
Q	Disintegration energy of the system	[J]
E_k	Kinetic energy	[MeV]
Ex	Excitation energy	[MeV]
K	Calibration constant	[Bq m^{-3} /count]
C_1, C_2	Correction factors	
R	Radon concentration	[Bq/m^3]

Contents

Table of figures

1. Introduction

The energy release of naturally occurring radioactive substances is one of the components necessary to explain the temperature of the crust of the earth. One of the most important naturally occurring elements is Uranium-238. Radon-222 is part of the decay chain originating from U-238. Since Rn-222 is an inert gas, these elements will emanate from substances containing U-238. If the radioactive material is lying deep in the ground, it may be difficult to identify its existence. However, when drilling deep holes for purposes of exploiting geothermal energy, it is conceivable that Radon is emitted into the hole, and subsequently diffusing up to the surface of the earth. Identifying Rn-222 emanating from the borehole, may therefore serve as an indicator of the presence of layers of U-238, possibly located deep underground, at least if the bore hole is filled with air, through which it is expected that the radon diffuses relatively fast.

Finding Rn-222 concentrations in the boreholes is of interest in its own right, adding information about the geology vertically along the boreholes which are around 200 m deep. In addition, since U-238 is a source of heat generation, identifying its presence through the presence of Rn-222 could add information on how much energy that might be extracted from the hole (see chapter 2). In this thesis we therefore also measure temperature profiles in a number of boreholes. The goal is to see if it is possible to correlate features of the temperature profile to the measured radon concentration in the hole.

This thesis is presented as the following:

Chapter 1	Introduction motivation
Chapter 2	Presents the source of geothermal heat production and how much energy is related in underground due to uranium.
Chapter3	Presents the description of radon gas and how has negative impact on human health according to some research results data.
Chapter 4	Present description of the field works area in details.
Chapter 5	Presents the methodology and measurements for temperature profile with calibrated data.
Chapter 6	Presents the methodology and measurements of radon concentration with gamma-ray spectroscopy.
Chapter 7	Conclusions and future work suggestion with the appendixes and references.

2. RENEWABLE ENERGY

2.1 Introduction

Each renewable energy type is tied to one of three primary energy sources; solar radiation, gravitational forces, and heat generated by radioactive decay. Renewable energy has a long history, as for centuries man has attempted to find reliable, renewable sources of energy. Geothermal energy from hot springs has been used for bathing since Paleolithic times and for space heating since ancient Roman times. Wind power has been used for powering sailing ships for centuries, but it is now better known for electricity generation. In 2010, energy produced by wind accounted for over 2.5% of total worldwide electricity usage [1].

In 1902, electricity was first produced using geothermal steam at Larderello (Italy). Since that time other developments have taken place, including the steam field at the geysers in California and the hot water systems in Wairakei, New Zealand, Iceland and several other countries. These developments have led to an installed world electrical generating capacity of more than 10 000 Mw in twenty-one countries, and a direct use nonelectric capacity of more than 100 000 $Mw_{(th)}$(thermal megawatts of power) at the beginning of the 21st century.

Renewable energy can be integrated in to all types of electricity systems, from large, interconnected continental scale grids to small autonomous buildings. Whether for electricity, heating, cooling, gaseous fuels or liquid fuels, renewable energy integration is contextual. Wind and solar energy can be more difficult to integrate than hydropower, bioenergy and geothermal energy.

Table2.1: Renewable energy theoretical potential expressed as annual energy fluxes of EJ/yr compared to 2008 global primary energy supply [1].

Renewable source		Annual Flux(Ej/yr)	Ratio(Annual energy flux/2008 primary energy supply)	Total reserve
Bioenergy		1,548	3,1	_
Solar energy		3,900,000	7,900	_
Geothermal energy		1,400	2,8	_
Hydropower		147	0,3	_
ocea power		7,400	15	_
Wind energy		6,000	12	_
Annual primary energy source		Annual Use 2008(EJ/yr)	Lifetime of proven Reserve(years)	Total Reserve(EJ)
Total fossil		418	112	46,700
Totaluranium		10	100-350	1,000_3,500
total RE		64	_	_
primary energy supply		492(2008)	- _	_-

2.2 Geothermic

Heat is created in some parts of the interior of the earth by radioactive disintegration of atomic nuclei. In addition, the material of the earth is in the process of cooling down from an initial high temperature. This is a result of heat carried away after being released within the interior by condensation and possibly other physical and chemical processes.

The radioactive elements mainly responsible for geothermal heat production at present are U-235(decay rate $9.7\times 10^{-10}y^{-1}$), U-238(decay rate $1.5\times 10^{-10}y^{-1}$), Th-232 (decay rate $\times 10^{-11}y^{-1}$), and K-40 (decay rate $5.3\times 10^{-10}y^{-1}$) [4].

These isotopes are present in different concentrations in different geological formations. They are more abundant in the granite-containing continual shields than in the ocean floors. Most of the material containing the radioactive elements is concentrated in the upper part of the earth's crust.

In the lower, half of the crust (total depth around 40 km), radiogenic heat production is believed to be fairly constant, at a value of about$2 \times 10^{-7}Wm^{-3}$. [5]

From the radioactive decay of the above –mentioned isotopes, it can be deduced that the temperature of an average piece of rock near the surface of the crust must have decreased approximately 900 C° during the last 4.5×10^{9} years.

At present, radiogenic heat production accounts for an estimated 40% of the continental average heat flow at the surface. The rest, as well as most of the heat flow at the oceanic bottom, may then be due to cooling associated with the expenditure of stored heat.

The global geothermal flow rates to the surface are more than twice the rate of human energy consumption from all primary sources.

2.3 Geothermal energy

Geothermal energy is defined as energy stored in form of heat beneath the surface of solid earth [2].

Fundamentally, geothermal energy results from radioactive decay of isotopes of certain elements contained in the earth's interior. 80% of the geothermal energy of the crust of the earth originates from radioactive decay.

Thermal energy in the earth is, distributed between the constituent host rock and the natural fluid that is contained in its fractures and pores at temperatures above ambient levels.

Heat extracted is from geothermal reservoirs using wells or other means. Reservoirs that are naturally sufficiently hot and permeable are called hydrothermal reservoirs. Once at the surface, fluids of various temperatures can be used to generate electricity or can be used more directly from applications that require thermal energy, including district heating while other use lower temperature heat flow from shallow wells for geothermal heat pumps in heating or cooling application. A ground energy system uses the temperature differences to extract geothermal energy from the ground and transfer it to a building for heating, cooling and hot water supplies.

Effectively the earth becomes a heat source in winter and heat sink in summer. Below five meters under the Earth's surface the underground temperature is relatively stable throughout the year, generally higher than the air temperature in winter and cooler in summer. The normal ground water temperature in Norway is between "4 and 9"℃. [3]

Overall, geothermal technologies are environmentally advantageous because there is no combustion process emittingCo_2, with the only direct emissions coming from the underground fluids in the reservoir.

2.3.1 Types of geothermal energy

There are two kind of geothermal energy that we should distinguish. Shallow geothermal energy, which is also called ground source heat, is from energy stored in the upper 300m of the ground. The main source of energy is the absorption of solar or atmospheric energy by the ground surface. The sun is the primary source of heat renewal at this shallow depth to 300m according to (Banks, 2008) [6] 47% of the sun energy is absorbed by the ground (see figure 2.1).

In this thesis, we work with geothermal energy at a depth less than 300m. With the main source of energy being the radioactive disintegration of naturally occurring radionuclides in the bedrock. The decay process of these radionuclides creates heat, which is stored in the bedrock.

In Norway no deep geothermal energy plants has established because it is a cold country and no hot geothermal sources (such as geysers) have been found. The geothermal temperature gradients in Norway vary between 10-30 ℃ / km

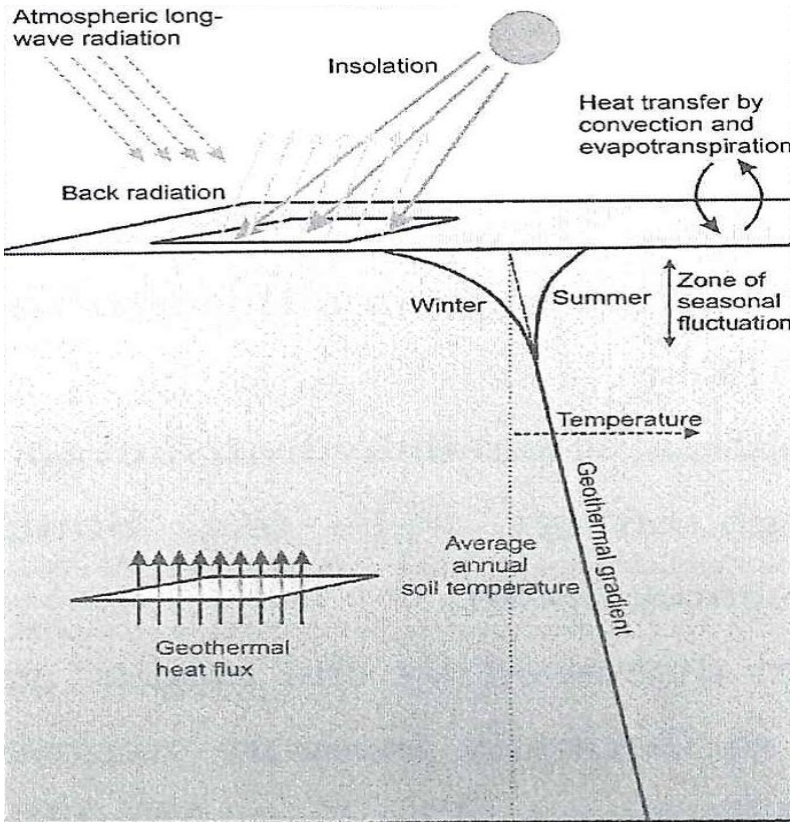

Figure2.1: Schematic presentation of heat fluxes at the ground and atmosphere [6].

2.3.2 Using geothermal energy to generate electricity

To develop electricity from geothermal resources, wells are drilled into a geothermal reservoir and the wells then bring the geothermal water to the surface. Its heat energy converted into electricity at a geothermal power plant, which offer constant output. Like wind and solar power plant, this is a clean source of energy, which does not require the burning of fuels to manufacture steam to turn the turbines. Thus generating electricity by geothermal energy helps to conserve non-renewable fossil fuels, and decreasing the use of these fuels will reduce the harmful emissions to the atmosphere. For heating applications the geothermal heat used directly, without involving a power plant or a heat pump. These applications include space heating and cooling, hot spring bathing, agriculture, green house and some other industrial uses.
Geothermal energy is currently used for base load electric generation in 24 countries, with an estimated 67.2TWh/yr. (0.24EJ/yr) of supply provided in 2008 at a global average capacity factor of 74.5 % [1]. In the USA installed capacity of direct use systems totals 470Mw, enough to heat 40,000 average-sized houses according to the (Geo heat centre) [7]. About 10 GW of geothermal electric capacity installed around the world as of 2007. This generates 0.3% of global electricity demand. An additional 28 GW of direct geothermal heating capacity was installed for district heating, space heating, spas, industrial processes, desalination and agricultural applications. Because heat is flowing through every square meter of land, it can be used as a source of energy for heating, air

conditioning (HVAC) and ventilating systems using ground source heat pumps almost anywhere. In areas where modest heat flow is present, geothermal energy can used for industrial applications that presently rely on fossil fuels.

Table2.2: Average annual growth rate in geothermal power capacity uses including GHP in the last 40 years [1].

Year	Electric capacity		Direct uses capacity	
	Mwe	%	$Mw_{(th)}$	%
1970	720	_	N/A	_
1975	1,180	10,4	1,300	_
1980	2,110	12,3	1,950	8,5
1985	4,764	17,7	7,072	29,4
1990	5,834	4,1	8,064	2,7
1995	6,833	3,2	8,664	1,4
2000	7,972	3,1	15,200	11,9
2005	8,933	2,3	27,825	12,9
2010	10,715	3,7	50,583	12,7
total annual average		7.0		11,0

Notes:

%: Average annual growth in percent over the period.

N/A: Reliable data not available.

2.3.3 Geothermal heat reservoir

There are two kinds of geothermal reservoirs, hot dry rock (HDR) and hot wet rock (HWR). A (HDR) system target deep, hot, low permeability (dry) bedrock. A (HWR) system utilizes deep, warm, permeable bedrock aquifers or regional fractures systems and the heat transfer fluid is natural ground water.

In Norway, the bedrock in general is very low permeability and so is generally suited to HDR- plants. However, certain locations contain permeable rock, which can be used for an HWR system.

The subsurface temperature exhibits variation associated with the magnitude of the heat flow and heat capacity (in general) the thermal properties of the material.

The presence of water or steam or other molten material is important for the transportation and concentration of heat. Dry rock accumulation of heat is probably the most common type of geothermal heat reservoir, but it does not lend itself so directly to utilization because of the difficulties in establishing sufficiently large heat transfer surface. Therefore, the smoothly varying average heat flow from the interior of the earth can considered as renewable energy resource. At the World Energy Conference 1974, the total amount of geothermal heat stored in water or steam to a depth of 10km is estimated to be

4×10^{21}J. They estimate also the total amount of energy stored in dry rocks to a depth of 10km as around 10^{27}J. steam of temperatures above 200 C° represents an average power of 240×10^{9}W for a period of 50 years [8].

Geothermal energy from hot dry rock could be available anywhere.

2.3.4 How does a convection geothermal reservoir work?

A geothermal system requires heat, permeability, and water. Heat comes from the earth's core continuously flows outward. The heat (as magma) sometimes reaches the surface as lava, but usually remains below the earth's crust, heating nearby rock and water. When water is heated by the earth's heat, hot water or steam can be trapped in preamble and porous rocks under a layer of impermeable rock and geothermal reservoir conform. This geothermal hot water can manifest itself on the surface as hot springs, however most of it stays deep underground trapped in rocks and cracks.

This natural collection of hot water called a geothermal reservoir.

However, most often the magma remains below earth's crust, heating the rock water (rainwater that has leaked deep in to the earth).

Figure 2.2 below shows the conversion of geothermal energy from hot dry rocks to electricity based on geothermal reservoir by using pumps and heat exchanger [R].

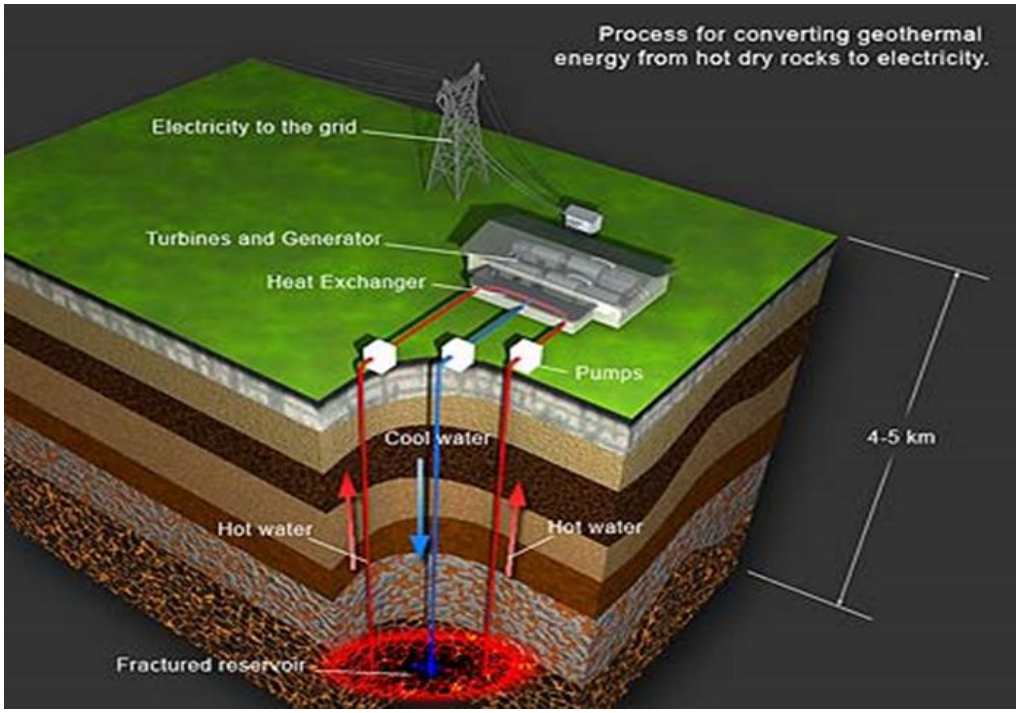

Figure2.2: Electricity generation from hot dry rocks HDR.

2.4 Heat extraction with boreholes

Shallow geothermal energy or ground- coupled heat pump systems are consider one of the key technologies to reduce greenhouse gas emissions in the buildings sector [9]. The heating and cooling of buildings accounts for 8% of the total greenhouse gas emissions, but geothermal heat pumps are one of the fastest growing types of renewable energy in the world. With annual increases of 10% in approximately 30 countries in the last 10 years, (Lund 2010) [10] current interest is very high due to the high prices of natural gas, heating oil and propane.

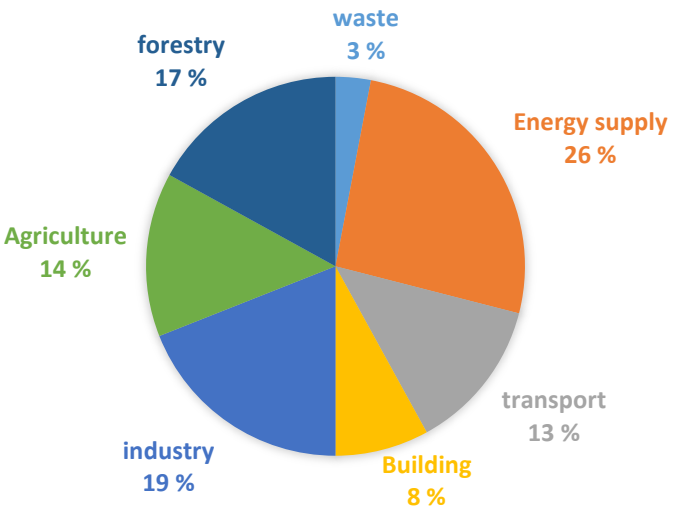

Figure2.3: Global, greenhouse gas emission sources (IPCC2007)

One method of extracting heat from the ground to support a heat pumps system (which has two sources sun and earth) for domestic heating is to use a deep borehole.

The depth of the borehole varies according to the place and demand of energy, between 40 and 180 m. For household heating is commonly heat extracted from shallow boreholes with depths between 100-200 m.

Many systems of this kind have been built in the United States, Canada, Sweden, and many in operation in Norway now. Multiple borehole systems can used to support large heat pumps. In this case, it is often necessary to re-inject heat to the ground, normally during the summer. In systems with both air conditioning and heating, heat injected to the ground in the cooling mode and extracted in the heating mode.

The fluid is heated by the rock while it flows down to the bottom of the borehole in one channel and back up in the second channel. The ground water in the borehole can also be used directly as the heat carrier fluid, using a single pipe down to the bottom.

2.4.1 Geothermal heat pumps

Geothermal heat pumps (GHP) circulate water or other liquids through pipes buried in continuous loop (either horizontally or vertically) next to a building.

These pumps use very little electricity and are therefore very clean on the environment.

The heat pumps can be used for indoor heating during the winter. In regions with hot summers, the pump can be reversed, and be used for indoor cooling, transferring excess heat in to the ground.

The coefficient of performance of a typical GHP is about four or more, meaning that four units of thermal energy are transferred for every one unit of electrical energy supply. [3].

2.4.2 Definition of borehole

A borehole is a common term for any narrow shaft bored in the ground, either vertically or horizontally. Borehole can be drilled in the earth for many different purposes, including: extraction of heat, water well and other liquid such as petroleum, releasing gases as a part of geotechnical investigations, mineral exploration and borehole temperature measurements. In this thesis, we have investigated holes that will use in geothermal installations.
Engineers and environmental consultants use the term to collectively describe all of the various types of holes drilled as part of a geotechnical investigation or environmental site assessment.

2.4.3 Borehole heat exchanger

A down hole heat exchanger (DHE), also called a borehole heat exchanger (BHE), and is a heat exchanger installed inside a borehole. It used to capture or dissipate heat to and from the ground, which is an absorbed into the fluid from the ground, which then circulates into the indoor heat pumps. The heat exchanger concentrates the heat, which is then distributed throughout the structure. Part of this heat also distributed to the hot water heater to preheat the water going in to it. The fluid constantly cycles back through the loops, and then the process repeats itself. To cool the building, the process of heating is reversed. The ground stays at a constant temperature under the surface, so the heat pump can used throughout the year, even in the middle of winter. Because 80% of the heat comes from the surrounding air (while the rest comes from electricity supply), this saves electricity and money. For this reason, geothermal energy extracted from DHE has less of an impact on the environment than electrically driven GHPs.

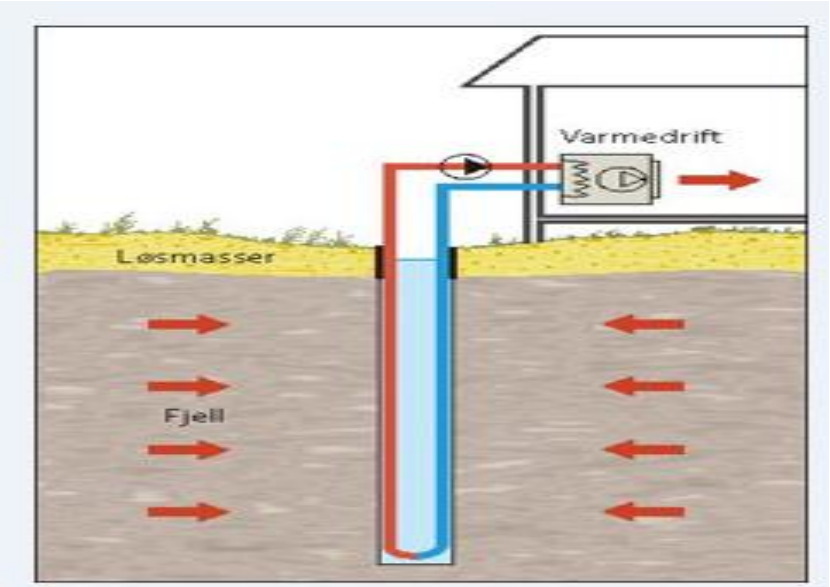

Figure 2.4: Ground-source heat pump systems use borehole heat exchanger to transfer heat to and from the ground [11].

Figure2.5: Top end of down hole heat exchanger in Åsane

2.4.4 U-tube

The BHE design usually consists of one or two U-tubes through which the carrier fluid (usually water) circulates. The space around the u-tubes is filled with ground water. This was the case for the boreholes we investigated.

A vertical borehole with a" closed loop" collector installation is the most popular way of utilizing ground-source energy in Norway.

2.5 The physical transmission of heat

Heat transport between a system and the surroundings is possible because of a temperature difference between two locations. These temperature differences are called the temperature potential. Most heating systems involve the transport of heat via fluids such as water, or via gases such as air, through the pipes or channels.

Assuming that a hot fluid or gas is produced at the central conversion plant, transmission may be accomplished by pumping the fluid or gas through a pipe line which is placed under ground to the load points.

Heat pumps and solar heating system are individual systems providing heat for single building, a community, a whole village, or city with certain size. Many of these combined heat and power (CHP) systems use heat transmission through distance of 10-50km, which has average heat cusses of 10%-15%. These systems depend strongly on radiated heat transfer, because a difference in temperature causes heat transfer by three mechanisms: conduction, convection, and thermal tradition. However, for thermal tradition the heat transmission rate are nonlinear in the temperature difference ΔT.

To understand in practical heat transfer problem we need to know some properties of the material such as**,** temperature, density, heat flow, capability of mater to transmit, and divest heat. Examples for that thermal conductivity, thermal diffusivity, specific heat coefficient,

Emittance and absorptivity. Which all this proprieties are continuous function of time and position.

2.5.1 Thermal conductivity and temperature of the bedrock

Thermal conductivity and temperature are two important natural factors for the design of borehole heat exchanger systems. When the ground source (heating, cooling) scheme increases, it will be important to know more precision about these factors. As a general rules the temperature in the ground is 1-2℃ higher than the average annual air temperature, partly reasons due to the natural geothermal gradient, and also because snow isolates the ground from the worst extremes of winter temperature.

In Norway the ground temperature ranges from 2 ℃ (in mountainous) to 8 ℃ (near the coast and near the south) (NGU) and the thermal conductivity of the bedrock typically varies between 2 and 4.5W/mk, and it is measurement of how heat transport through the rocks towards the borehole. The thermal conductivity of the bedrock is generally dependent on the rocks quarts content. Greater quantities of heat can obtained per drilled borehole meter from bedrock with high thermal conductivity. Heat transport via ground water is another important factor in addition to temperature and thermal conductivity for performance of borehole heat exchanger systems. The thermal conductivity of a sample (λ, [W/mk]) is estimated as a product of the measured thermal diffusivity (a, [m^2/s]), density (ρ, [kg/m^3]) and specific heat capacity (c_p[ws/kgk])

$$\lambda = c_p \text{ a } \rho \qquad \textbf{(2.1)}$$

2.5.2 Thermal response test TRT

Thermal response test (TRT) is an indirect measurement method that is considered the simplest and most exact way to determine the effective thermal properties [12], or effective thermal conductivity in a borehole that integrates over the thermal conductivity of the bedrock, of the water in the borehole.

The idea of measuring the thermal response of boreholes was first introduced by (Mogensen 1983) [13], which suggests a simple arrangement in which heat at constant power is injected into a borehole and the mean temperature is measured. From TRT we can estimate the certain amount of power, and energy from borehole by measuring thermal borehole resistance and thermal conductivity in situ [14].

TRT equipment consists of a borehole, pipe system, circulation pump, heater with constant power rate. The inlet and outlet temperature of the flow is continuous logged.

The undisturbed ground temperature should be determined before the test starts. The thermal conductivity λ_{eff} of the ground and the borehole resistance R_b can determine when the temperature increases in the heat carrier fluid during a test run.

The TRT analysis is generally based on Kelvin's line source theory, and therefore the closed loop BHE approximated by alien source in a homogeneous medium with a constant thermal property.

The temperature variation around the line source in space and time can described as:

$$T_{(r,t)} = T_o + \frac{Q/Z}{4\pi\lambda} \int_{r^2/4kt}^{\infty} \frac{e^{-\mu}}{u} du \qquad \textbf{(2.2)}$$

$$T_{(r_2.t_)} = T_o + \frac{Q/Z}{4\pi\lambda} \left[\ln\left(\frac{4kt}{r^2}\right) - \gamma \right] \qquad \textbf{(2.3)}$$

Where

T is temperature field as a function of time (t) and radius r

$$Z = \frac{at}{r^2}$$

$T_\circ$ Undisturbed ground temperature

K= $\frac{\lambda}{\rho c}$ the isobaric rock thermal diffusivity

Q =constant heat injection rate.

Z = length of the BHE

γ = Euler's constant (0.5772)

The average borehole temperature T(r=r_b) caused by the specific radial heat flow q=Q/Z through the BHE is

T=T(r=r_b, t) + qR_b

$$= \underbrace{\frac{q}{4\pi\lambda}}_{a} \ln(t) + \left[qRb + \frac{q}{4\pi\lambda}\left[\ln\left(\frac{4k}{r^2 b}\right) - \gamma \right] \right] + T_o \qquad \textbf{(2. 4)}$$

Rb is thermal borehole resistance between the BHE fluid and the borehole wall

T= (Tin + Tout)/2 (Signorelli 2007) [15]

T=a ln (t) +b

As a linear function of logarithm of time t thus, the rock thermal conductivity can be derived from the slope of this linear relation:

$$\lambda = \frac{q}{4\pi} \frac{\ln(t2) - \ln(t1)}{T(t2) - T(t1)} \qquad \textbf{(2.5)}$$

Here the temperatures at time t_1 and t_2 that are used to calculate the regression line to estimate λ normally between 20 (t_1) and 70 hours (t_2) [15]

This commonly accepted as sufficient for an appropriate heat yield prediction.

TRT have been performed in the sites that we have investigated. GECCO [16] has kindly shared the TRT results with us from ostrøy. Table 2.3 summarizes these. The most important parameter is the thermal conductivity, found to be 4.49W/mK as shown in table below.

Table2.3: data collected and calculated from boreholes at area2 from the TRT results.

Measured values		Calculated Values	
Power Input,P(W)	8500	Thermal Conductivity,λ, (W/mK)	4,49
Borehole Length, H(m)	170	Thermal transitivity, λH (W/K)	763,44
Borehole Radius, r(m)	0,06	Thermal Diffusivity, a(m^2/s)	2,09
Gradient	0,886	Borehole Thermal resistance(mK/W)	0,155
Specific Heat capacity, S,(MJm/k)	2,15	Critical Time for Theory to be valid,(minutes following power on)	144

2.6 Geothermal gradient

Geothermal gradient is the rate of increasing temperature with respect to increasing depth in the earth's interior. Away from tectonic plate boundaries, it is about 25°C per km of depth in most of the world [4].

The geothermal gradient varies with location in deep boreholes. The temperature of the rock below the inflection point generally increases with depth at rates of the order of 20 k/km or more. Fourier's law of heat flow applied to the earth gives q = Mg where q is the heat flux at a point on the earth's surface. λ the thermal conductivity of the rocks there, and g the measured geothermal gradient. A representative value for the thermal conductivity of granitic rocks is M = 3.0 w/mk. Using the global average geothermal conducting gradient of 0.2k/m we get that q = 0.06 Wm^{-2}.

This estimate, corroborated by thousands of observations of heat flow in boreholes all over the world, gives a global average of $6\times10^{-2}Wm^2$. Thus, if the geothermal heat rising through an acre of granite terrain could efficiently captured, it would light four 60W light bulbs.

The temperature gradient decreases with depth for two reasons:

First, radioactive heat production is concentrated with in the crust of the earth, and particularly with in the upper part of the crust, as concentrations of uranium, thorium and potassium are highest there. These three elements are the main producers of radioactive heat with in the earth.

Second, the mechanism of thermal transport changes from conduction, as within the rigid tectonic plates, to convection, in the portion of earths metal that convicts.

Despite its solidity, most of the earth's mantle behaves over long time scales as a fluid, and heat transported by advection, or material transport. this heating up can be both beneficial or detrimental in terms of engineering geothermal energy can be used as a means for generating electricity, by using the heat of the surrounding layers of rock underground to heat water and then routing the steam from this process through a turbine connected to a generator.

2.6.1 Heat flow

Geothermic is the branch of geophysics that studies earthly heat flow [17]. And heat flow is defined as the transfer of heat from Earth's interior to the surface and is the main driver of geological processes. The major source of the heat interior is decay of radioelements in the earth crust and upper mantle. Up to 70% of continental heat flow may be generated within the upper (10-20)km of the crust, while 96% of the oceans heat flow is from beneath the oceanic crust which devoid of radioactive elements. The Earth's internal heat comes from a combination of residual heat from planetary accretion (about 20%) and heat produced through radioactive decay (80%). The major heat-producing isotopes in the Earth are potassium-40, uranium-238, uranium-235, and thorium- 232.

Heat flow can measured from boreholes by combining of temperature and thermal conductivity by the Fourier's equation which define the heat conductive transport

$$Q = \lambda \, (dT/dz) \qquad \textbf{(2.6)}$$

Where Q is rate of heat flow
λ thermal conductivity
T is the temperature
z is the depth

Where T is temperature and x is the coordinate in the direction of temperature variation [18], a basic physical property of rocks and fluids are thermal conductivity, which is proportional to thermal gradient (see E.q2.6).

2.6.2 The source of heat

Temperature increases with depth, its sign to the continental crust of earth, decay of natural radioactive isotopes which has significant involvement in the area of geothermal heat in some layer to earth's surface, naturally occurring isotopes are enriched in the granite and basaltic rocks, however the continental crust is abundant in lower density minerals but also contains concentration of heavier minerals such as uranium which has high density. The mantle is mostly made up of high density minerals with high contents of atoms. There an estimated 45-90% of the heat escaping from the earth originates from radioactive decay of elements within the mantle which is considered one of the heat sources.

Table 2.4: Present-day major heat-producing isotopes [19].

Isotope	Heat release [W/kg isotope]	Half-life[years]	Mean mantle concentration [kg isotope/kg mantle]	Heat release [W/kg mantle]
^{238}U	9.46×10^{-5}	4.47×10^{9}	30.8×10^{-9}	2.91×10^{-12}
^{235}U	5.69×10^{-4}	7.04×10^{8}	$0{,}22 \times 10^{-9}$	1.25×10^{-13}
^{232}Th	2.64×10^{-5}	1.40×10^{10}	124×10^{-9}	3.27×10^{-12}
^{40}K	2.92×10^{-5}	1.25×10^{9}	36.9×10^{-9}	1.08×10^{-12}

2.6 Radioactive and radiogenic isotopes

The emission of radiation by unstable atomic nuclei undergoing radioactive decay. Radioactive nuclei are generally classified into two groups: unstable nuclei found in nature (which cause natural radioactivity) and unstable nuclei produced in the laboratory through nuclear reactions, which exhibit artificial radioactivity.

The term radioactivity refers to the particles emitted by unstable nucleus. U-238, is an example of a naturally occurring radioactive element, goes through 19 stages of decay before becoming a stable isotope of pb-206. The amount of Pb-206 will increase while that of U-238 decreases all steps in the decay chain have this same rate of 3×10^{6}decayed particles per second per mole U-238.

Some of the intermediate stages include the heavier elements thorium, radium, radon, and polonium (table 2.4)

Each element remains radioactive for a characteristic length of time, ranging from mere microseconds to billions of years. An elements rate of decay is proportional to half-life. This refers to the time interval during which half of a given number of radioactive nuclei decay, and is a useful parameter in characterizing nuclear decay.

While radiogenic nuclide is a nuclide that is produced by a process of radioactive decay, and may itself be radioactive or stable in the most important tools in geology radiogenic nuclide refer to radiogenic isotopes. Some naturally occurring isotopes are entirely radiogenic, and they are radioactive with half-lives too short therefor they present as radiogenic daughters of their ongoing decay processes or cosmic ray induced process.

The three isotopes Pb-206, Pb-207, and Pb-208 may occur as radiogenic decay products of uranium and thorium. In rocks that contain uranium and thorium the excess amount of the three heavier lead isotopes allows estimating the time from when the rock solidified [18].

Table 2.5: the total energy released from uranium-238 to lead-206 [20].

nuclide	historic name (short)	historic name (long)	decay mode	half-life (*a*=year)	energy released, MeV	product of decay
238U	U_I	Uranium I	α	4.468·109 a	4.270	234Th
^{234}Th	UX_1	Uranium X_1	β−	24.10 d	0.273	234mPa
^{234m}Pa	UX_2	Uranium X_2	β^- 99.84%	1.16 min	2.271	234U
		Brevium	IT 0.16%		0.074	^{234}Pa
^{234}Pa	UZ	Uranium Z	β^-	6.70 h	2.197	^{234}U
^{234}U	U_{II}	Uranium II	A	245500 a	4.859	230Th
^{230}Th	Io	Ionium	A	75380 a	4.770	226Ra
^{226}Ra	Ra	Radium	A	1602 a	4.871	222Rn
^{222}Rn	Rn	Radon, Radium Emanation	A	3.8235 d	5.590	218Po
^{218}Po	RaA	Radium A	α 99.98%	3.10 min	6.115	214Pb
			β^- 0.02%		0.265	218At
^{218}At			α 99.90%	1.5 s	6.874	214Bi
			β^- 0.10%		2.883	218Rn
^{218}Rn			A	35 ms	7.263	214Po
^{214}Pb	RaB	Radium B	β^-	26.8 min	1.024	^{214}Bi
^{214}Bi	RaC	Radium C	β^- 99.98%	19.9 min	3.272	^{214}Po
			α 0.02%		5.617	210Tl
^{214}Po	RaC'	Radium C'	A	0.1643 ms	7.883	210Pb
^{210}Tl	RaC"	Radium C"	β^-	1.30 min	5.484	^{210}Pb
^{210}Pb	RaD	Radium D	β^-	22.3 a	0.064	210Bi
^{210}Bi	RaE	Radium E	β^- 99.99987%	5.013 d	1.426	210Po
			α 0.00013%		5.982	206Tl
^{210}Po	RaF	Radium F	A	138.376 d	5.407	206Pb
^{206}Tl	RaE"	Radium E"	β^-	4.199 min	1.533	^{206}Pb
^{206}Pb	RaG	Radium G	-	stable	-	

2.6.1 Decay process

The decay process is probabilistic in nature and can be described with statistical calculations for a radioactive substance of macroscopic size containing a large number of radioactive nuclei.

For such large numbers, the rate at which a particular decay process occurs in a sample is proportional to the number of radioactive nuclei present (that is, the number of nuclei that have not yet decayed). If N is the number of non-decayed radioactive nuclei present at some instant, the rate of change of N with time is

$$\frac{dN}{dt} = -\lambda N \qquad \textbf{(2.7)}$$

Where λ called the decay constant, which is the probability of decay per nucleus per second. The negative sign indicates that dN/dt is negative, that is, N decreases in time.

Eq. 2.7 can written in the form

$$\frac{dN}{N} = -\lambda dt$$

Which, upon integration gives

$$N = N_o e^{-\lambda t} \qquad \textbf{(2.8)}$$

Where the constant No represents the number of undecided radioactive nuclei at t= 0. Eq. 2 shows that the number of undecided radioactive nuclei in a sample decreases exponentially with the time.

The decay rate or activity A which is the number of decays per second, can be obtained by combining Eq. (2.7) and (2.8)

$$A = \left|\frac{dN}{dt}\right| = \lambda N = \lambda N_o e^{-\lambda t} = A_o e^{-\lambda t} \qquad \textbf{(2.9)}$$

Where

$A_o = \lambda N_o$ Is the decay rate at t=0.

The decay rate A of a sample referred to as its activity.

To find an expression for the half-life, we first set

N=No/2

And t= T1/2. In Eq.2.8 to give

$$\frac{No}{2} = No \; e^{-\lambda T_{1/2}}$$

Taking the natural logarithm of both sides gives

$$T_{1/2} = \frac{\ln 2}{\lambda} = \frac{0.693}{\lambda} \qquad \textbf{(2.10)}$$

As we stated up in (radioactivity), a radioactive nucleus spontaneously decays by one of the three processes, alpha decay, beta decay, or gamma decay.

2.6.2 Alpha decay

A nucleus emitting an alpha particle ($^{4}_{2}He$) loses two protons and two neutrons. Therefore, the atomic number Z decreases by 2, the mass number A decreases by 4, and the neutron number decreases by 2. The decay can written

$$^{A}_{Z}X \rightarrow {}^{A-4}_{Z-2}Y + {}^{4}_{2}He \qquad (2.11)$$

Where X is the parent nucleus and Y the daughter nucleus. As a general rule in any decay expression such as this one, (1) the sum of the mass numbers A must be the same on both sides of the decay and (2) the sum of the atomic numbers Z must be the same on the both sides of the decay [22].

In figure below, a U-238, it will spontaneously decay in to a Th-234 nucleus, releasing an alpha particle. The companied mass of the decay daughter (Th+α) is less than the parent nucleus. The different accounts for the energy released according to Enstian Eq. E=m.c^2 Mass can converted to energy.

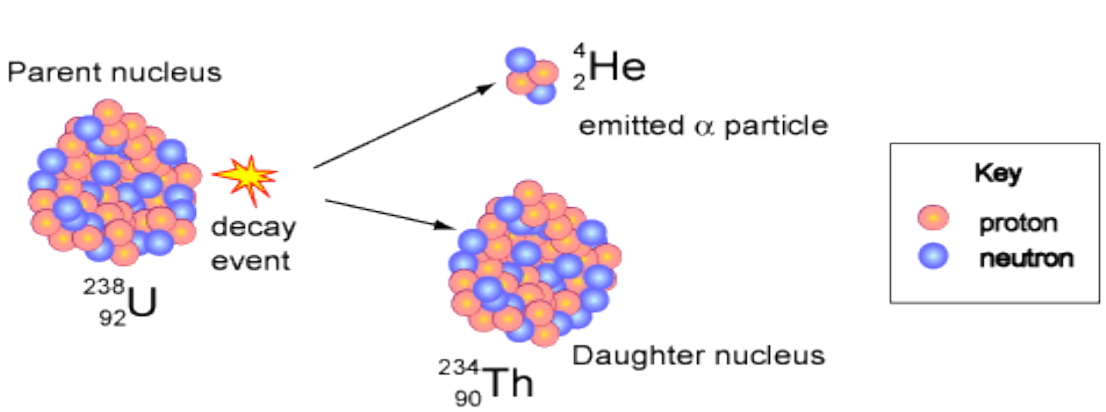

Figure2.6: Alpha decay of U-238[21].

As examples, ^{238}U and ^{226}Ra are both Alpha emitters and decay according to the schemes

$$^{238}U \rightarrow {}^{234}Th + {}^{4}He \qquad \textbf{(2.12)}$$

$$^{226}Ra \rightarrow {}^{222}Rn + {}^{4}He \qquad \textbf{(2.13)}$$

When the nucleus of one-element changes into the nucleus of another as happens in alpha decay, the process called spontaneous decay. In any spontaneous decay, relativistic energy and momentum of the isolated parent nucleus must conserved. If we call

M_x The mass of the parent nucleus
M_y The mass of the daughter nucleus
M_α The mass of the alpha particle

We can define the disintegration energy Q of the system as [23]

$$Q = (M_x - M_y - M_\alpha)C^2 \qquad \textbf{(2.14)}$$

The energy Q is in joules when the masses are in kg and C is the speed of light (3.00×10^8m/s). When the masses expressed in atomic mass units u, however, Q can calculated in MeV using the expression

$Q = (M_x - M_y - M_\alpha) \times 931.494$ MeV/u

The disintegration energy Q appears in the form of kinetic energy in the daughter nucleus and the alpha particle, and sometimes referred to as the Q value of the nuclear decay.

As an example, we calculate the Q value, and the kinetic energy of the emitted alpha particle in decay 2.13.

The nucleus is initially at rest. After the decay, the radon nucleus has kinetic energy K_{Rn} and momentum $\overrightarrow{P_{Rn}}$. In addition, the alpha particle has kinetic energy Kα and momentum Pα.

If the parent nucleus is at rest before the decay, the total kinetic energy of the product is 4.87 MeV. Using Eq.2.14

= (226.025410u-222.017578u-4.002603u)*931.494 MeV/u
= (0.005229u)* 931.494 MeV/u
= 4.87 MeV

The value of 4.87 MeV is the disintegration energy for the decay. It includes the kinetic energy of both the alpha particle and the daughter nucleus after decay. Therefore**,** the kinetic energy of the alpha particle would be less than 4.87Mev.

We try to find E_k (kinetic energy) for the alpha particle by using momentum equation for the daughter nucleus and alpha particle.

Initial momentum of the system equal to zero

$0=M_y\ \upsilon_y - M\alpha\ \upsilon_\alpha$

Where M_y mass of daughter nucleus
υ_y Velocity of daughter nucleus
$M\alpha$ Mass of alpha particle
υ_α Velocity of alpha particle

We set the disintegration energy Q equal to the sum of the kinetic energies of alpha particle and the daughter nucleus.

$$Q=\frac{1}{2}M\alpha\upsilon^2\alpha+\frac{1}{2}My\upsilon^2 y \qquad \textbf{(2.15)}$$

We find υ_y and substitute in to Q Eq. (2.14)

$$Q=\frac{1}{2}M\alpha\upsilon^2\alpha+\frac{1}{2}My\upsilon^2\left(\frac{M\alpha\upsilon\alpha}{My}\right)$$

Solve for the kinetic energy of the alpha particle we obtain

$$K\alpha=Q\left(\frac{My}{My+M\alpha}\right) \qquad \textbf{(2.16)}$$

In the present example, we evaluate the kinetic energy for the decay of Ra-226

$$K\alpha=(4.87\ MeV)\left(\frac{222}{222+4}\right)$$

$K\alpha=4.78MeV$ less than Q Value.

Most of this kinetic energy is associated with alpha particle because this particle is much less massive than the daughter nucleus, Rn-222. Because momentum must conserved, the lighter alpha particle recoils with a much higher speed than does the daughter nucleus.

Experimental observations of alpha-particle energies show a number of discrete energies rather than a single energy because the daughter nucleus may be left in one of several possible excited quantum state after the decay. The emission of an alpha particle followed by one or more gamma rays as the excited nucleus decays to the ground state. The observed discrete alpha-particle energies represent evidence of the

quantized nature of the nucleus and allow a determination of the energies of the quantum states.

If one assumes U-238(or any other alpha emitter) decays by emitting either a proton or a neutron, the mass of the decay products would exceed that of the parent nucleus, corresponding to a negative Q value. A negative Q value indicates that such a proposed decay does not occur spontaneously.

The Q values for the U-234 decay using Eq.2.14 gives 4.1984 MeV. In table 2.5, we summarize the Q-values of all parts of the decay chain of U-238 and we find that the total energy value is 23.6 MeV per decaying U238-nucleus.

So total energy release due to decay in 2.12 is 0.11188 MeV. The activity A and decay rate Lambda for the interaction 2.12 can calculated as,

$A = 0.11188.\lambda_U 238.N_{u238} \text{Mev} s^{-1}$

$\lambda_{U238} = \frac{\ln 2}{T_{1/2}} = 0.49 \asymp 10^{-17} s^{-1}.$

Average uranium content on earth is 4mg/kg, which includes (N_{U-238}) 1.01×10^{22} of U-238 atoms.

The total decay energy from the decay chain of Uranium-238 is equal to

$E = \lambda_U 238.N_{u238}.\ Ex$ **(2.17)**

Ex=23.5684 MeV $=3.77\times 10^{-12}$ J (for all decay chain U-238 to Pb-208 stable).

Including Ex value in Eq. 2.17 one gets

$E = 4.9\times \mathbf{10^{-18}} s^{-1} \times 1.01\times \mathbf{10^{22}}$ atom $\times 3.776\times 10^{-12}$J

$E = 1.85\times 10^{-7}\ J\times s^{-1} = 1.85 \times 10^{-7} W$

2.6.3 Beta energy spectra

In the process of beta decay, either or a positron is emitted. Because either a neutrino or an antineutrino emitted as well, there is a spectrum of energies for the electron or positron, depending upon what fraction of the reaction energy Q carried by the massive particle.

In figure below, beta decay of thorium-234 results in a high energy electron released from the nucleus. The daughter nucleus has same mass number of the parent but higher in atomic number. Pa-234 emit a high-energy gamma photon (gamma ray).

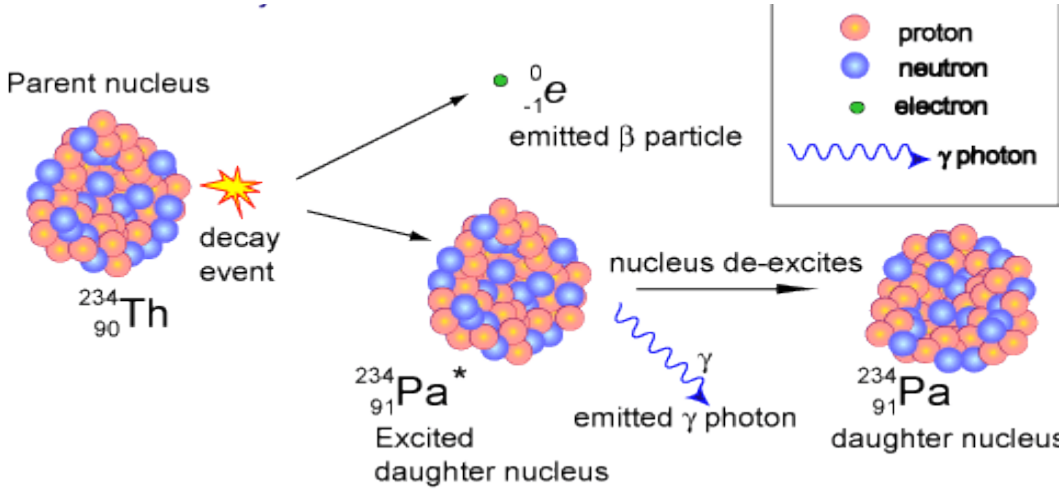

Figure2.7: Beta decay of a Thorium-234 nucleus.[21]

$^{A}_{Z}X \rightarrow {}_{Z+1}^{A}Y + {}^{-}e$ Designates an electron

$^{A}_{Z}X \rightarrow {}_{Z+1}^{A}Y + {}^{+}e$ Designates an a positron

$$^{234}Th \rightarrow {}^{-}e\ {}^{234}Pa + \upsilon^{-} \qquad \textbf{(2.18)}$$

$Q_{\beta^-} = (M_X - M_y)c^2$

= (234.043601_234.043308)931.49Mev

$Q_{\beta^-} = 0.27292657$

2.6.4 Gamma Emission

Radioactive decay by alpha, beta, positron emission or electron capture often leaves some of the energy resulting from these changes in the nucleus. As a result, the nucleus raised to an excited level. None of these excited nuclei can remain in this high-energy state. Nuclei release this energy returning to ground state or to the lowest possible stable energy level. The energy released is in the form of gamma radiation (high-energy photons) and has an energy equal to the change in the energy state of the nucleus. Gamma and X-rays behave similarly but differ in their origin, gamma emissions originate in the nucleus while X-rays originate in the orbital electron structure.
U, Th, and K decay series have radioisotopes producing gamma rays of sufficient energy and intensity for gamma-ray spectrometer measurements. The most direct method to measure the abundance of these radioisotopes in rocks is to use a gamma-ray spectrometer [24].

Figure2. 8: Shows how high energy photon released through gamma decay each gamma ray photon released has a discreet energy, which is characteristic of the source isotope. By measuring the energies of these gamma ray-photons, it is possible to determine the source of the radiation.

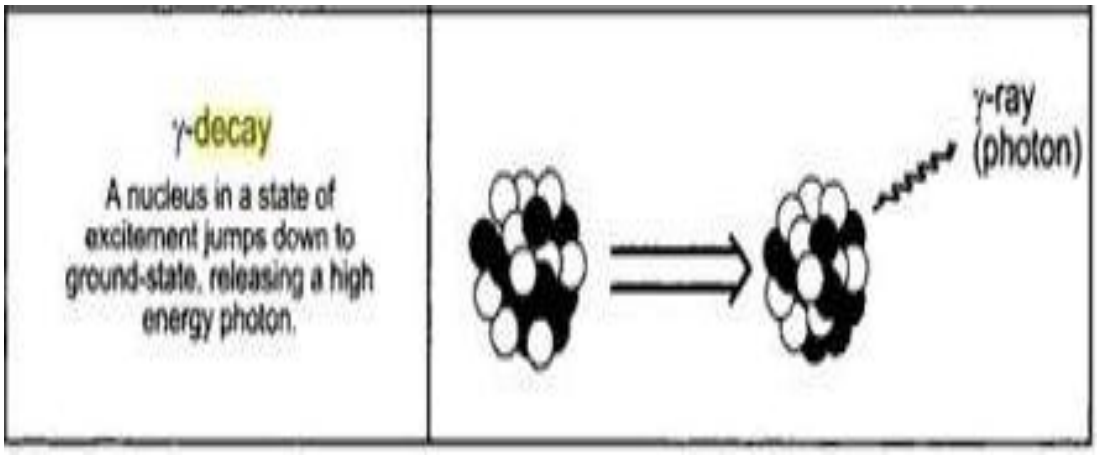

Figure2.8: Gamma-decay where a high energy gamma-ray photon is release.

3. Radon

3.1 Introduction

Radon is a radioactive noble gas, produced by decay of the naturally occurring radionuclide Ra-226, which is a part of decay chain of U-238. Radon-220 (Thoron) is a member of decay chain of Thorium-232.

Since radon is a gas under normal condition, it can move through the air easily from the material in which it is formed, and since uranium and radium occur in soil, rocks and spring waters or hot springs, Radon gas can be found both indoors and out, and even the air that we inhale contains radon [25].

All Radon isotopes are radioactive and constitute a health hazard. It is responsible for the majority of the public exposure to ionizing radiation. Radon-222 is the most long-lived isotope with half-life of 3.8 days (9.68 hours) and decay to a number of short life decay products that are themselves radioactive. Radon progeny rather than radon gas itself presents the greater risk.

In 1970 radon was regarded as a radiation health hazards encountered only in the mining and processing of uranium ore. As natural radiation (or "background") increased attention has been paid to exposure to radon which counts as average for about half of all human exposure to radiation from natural sources in both industrialized and developing countries.

Indoor dose by thoron to the human exposures usually small compared with that due to radon, because it has short half-life (55 second) compare to radon (3.8 days).

Radon is a monatomic gas with a density of 9.73 kg/m^3at standard temperature and pressure about 8 times the density of the earth's atmosphere at sea level. Radon emanation from the soil varies with soil type and with surface uranium content, Uranium which is present in small amounts in most rocks and soil, breaks down to Radium, which then decay to radon. Some of this moves to the soil surface and enters air, while some remains below the soil surface and enters the ground water.

Radon also undergoes radioactive decay, this means that one-half of a given amount of radon will changed or decayed to other products every 3.8 days, two parts will be the result of the decay, one called radiation, and second will called a daughter. The daughter also will divide in to radiation and daughter because it is not stable. The dividing process will continue until it is stable. During the decay process alpha, beta, and gamma radiations released. Alpha particles can move short distances and cannot go through human's skin. Beta particle can however penetrate the skin, and gamma radiation however can go all the way thought the body (see chapter 5).

In addition, uranium, thorium, radium, and radon will continue to occur for millions of years at about the same concentrations as they are now.

Table 3.1: Half-lives of the three natural isotopes of Radon.

Isotope	Common name	Half-life	Decay Chain Coming With
Rn-222	Radon	3.8 days	U-238
Rn-220	Thoron	54.5 sec	Th-232
Rn-219	Actinon	3.92 sec	U-235

3.1.1 Sources of indoor radon

For indoor radon, the main source its immediate parent, Radium-226 in the ground of the site and in the building material. As a gas radon can move through the soil and when enters a building it can sometimes build up to very high concentrations, and can accumulate especially in confined area such as basements.
Sometimes indoor radon levels may rise due to the kind of building materials, some of which contain high level of radium-226. Well water considers being another kind of radon source indoors. Water that comes from an underground source such as rivers or lakes will collect more radon than surface water (water with radon concentration of 4000 Bq/m^3 can increase the indoor air by 40 Bq/m^3 (under normal conditions) [26].
Although well water is often a more significant source of radon than building materials, it is not the only one and some dwellings with high radon concentration do not have wells. The ground is the major source of radon inside most homes, as we mentioned for the decay process at the introduction. Since radon as a part of the decay chain, it decays quickly. This makes it more dangerous as radon gas enters homes through pores, cracks, and accumulation on the lower floors, because it is coming from the ground and is heavier than air.

3.2 Radon concentration

As we mention in previous section that radon is produced by the radioactive decay of radium 226 that is found in uranium ores, phosphate rock, shales, igneous and metamorphic rocks such as granite, gneiss, schist and to a lower degree in common rocks types such as limestone.

There is a possibility for any granite sample to contain varying concentrations of uranium and other naturally occurring radiation and produce radon gas, which is a source of β, α particles and gamma rays.

This granite contributes to indoor radon levels, and some types of granite may emit gamma radiation above typical background levels. Granite is a naturally occurring igneous rock, meaning that the cooling of molten rock formed it. Crystalline aquifers of igneous and metamorphic rocks generally have higher radon levels than other aquifer types with granites consistently showing the highest level of radon concentration.

It is estimated that every square mile of surface soil contains approximately 1 gram of radium, which releases radon in small amounts to the atmosphere on global scale; it is estimated that also 2400 million curies (90 tbq) of radon are released from soil annually [27, 28].

Radon concentration varies significantly from place to place. In the open air it ranges from one to 100 Bq/m^3, and even less (0.1 Bq/m^3) above the ocean. In caves or houses with poor ventilation, its concentration varies between to 20-2000 Bq/m^3.

Hence, ground water has higher concentration of Rn- 222 than surface water, because radon continuously produced by radioactive decay of Ra 226 present in rock [29].

Likewise, the saturated zone of as soil frequently has higher radon content than the unsaturated zone because of diffusion losses to the atmosphere.

3.2.1 Unit of Radon concentration

When we discuss radon concentration in the environment we refer to Rn-222, while the average rate of production of Rn-220 from the thorium decay series is about the same amount of Rn-222 but because Rn-220 has very short half-life (1 minute) it is present in lower amounts in the environment.

Radon concentration usually measured in the atmosphere, in Becquerel per cubic meter (Bq/m^3) indoor. In the USA normally Pico per litter pci/l is used for measuring radon concentration, which is equal to 37 Bq/m^3.

When Rn-222 released in to the air, it decays into Pb-210. The average concentration of radon in the atmosphere is about 6×10^{-20} of radon for each molecule in the air, or about 150 atoms in each mole of air.

3.3 Dose limit

Dose is defined as the limit value of the effective dose or the equivalent dose to individuals from controlled practices that shall not be exceeded [30]. The limits on effective dose for occupational exposure apply to the sum of effective doses due to external sources and the committed effective doses due to intakes over the same period. Specifies limits on occupational exposures are as follows:

An effective does of 20 mSv per year over five consecutive years.

An effective does of 50 mSv in any single year.

An occupational exposure to Radon progeny of 1Bq/m^3, equilibrium equivalent concentration (EEC) Radon, for 1 h corresponds to a committed effective dose of 8 nSv, and an occupational exposure to Thoron progeny of 1Bq/m^3 (EEC) for 1 h corresponds to a committed effective dose of 36 nSv. For 2000 hour working years, this leads to the following derived air concentrations corresponding to the does limits:

- 20 mSv corresponds to radon gas concentration of 3000 Bq/m^3.
- 50 mSv corresponds to radon gas concentration of 8000 Bq/m^3.

In Norway, radiation dose from Radon is about 3 mSv, from natural background is 4.2 mSv, and from medical applications is about 1.6 mSv.

3.4 Risk of Radon

According to epidemiological studies there is a clear link between breathing high radon concentration and incidence of lung cancer. There is some theoretical possible increased risk of leukaemia of radon but there is no empirical support proved yet.

Radon has risk effect on health indoor and outdoor (work places), as indoor radon is considered a significant contaminant that effects indoor air quality worldwide. It is also present as a hazard in wide range of work places, including below ground work places such as subway, tunnels, stores, show caves, closed-out mines open to visitors, and radon spas. However, the majority of such work places are above ground such as factories, shops, schools and offices, but they are still affected by high radon concentrations. As shown in section (3.1.1), the main mechanism by which radon can entry the building is the pressure driven flow of gas from soil through cracks in the floor. Flow arises when the building is under pressure with respect to their surroundings. Being under pressure is the result of the air inside buildings being wormer than outside, especially in cold regions, in addition to other mechanisms, which effect the limited level of radon in dwellings. The World Health Organization (WHO) recommends an action level not above 300bq/m3.

Work places such as laundries and restaurant kitchens that have a high level of radon are the result of the use of such water, because radon can be high in ground water especially in areas of granite rock (more in chapter5). Generally however the annual exposure time of workers in these work places is low and some countries have recommendations level of radon in drinking water.

Table3.2: Radon concentration in work places in above ground in Nordic Europe [31]

Work place type	Location	Number surveyor	Radon concentration
Public building	Finland	155 400	Mean 505, 37%>300 Mean284.17%>300
Kindergarten	Norway	3600	Range5-2800,mean88
Various workplaces	Finland	3050 993	Mean 255,37%>300 Mean 171,12%>300
	Sweden	150	10%>400

Table3.3: Radon concentration underground work places [31]

Work place type	Country	Radon concentration rang bq/m3
Tunnels	Finland	500-7000
	Norway	250(mean)
Power station	Norway	20-4000
Underground railway	Finland	45-200(station) 20-790(work places)

3.5 Uranium measurement in Norway

Norwegian geology research center NGU, has drawn care map showing the most radon prone areas in southeastern Norway. This is used so that both municipalities and private homeowners can implement recommended safeguards.

The figure below shows that parts of Bergen from Fyllingsdalen to the east side of Sotra have high uranium in the subsurface. Because of Løvstakken granite, a rock which also from previous studies are known to contain uranium, according to NGU"s elevated uranium value there is a high value of uranium between OS and Bergen.

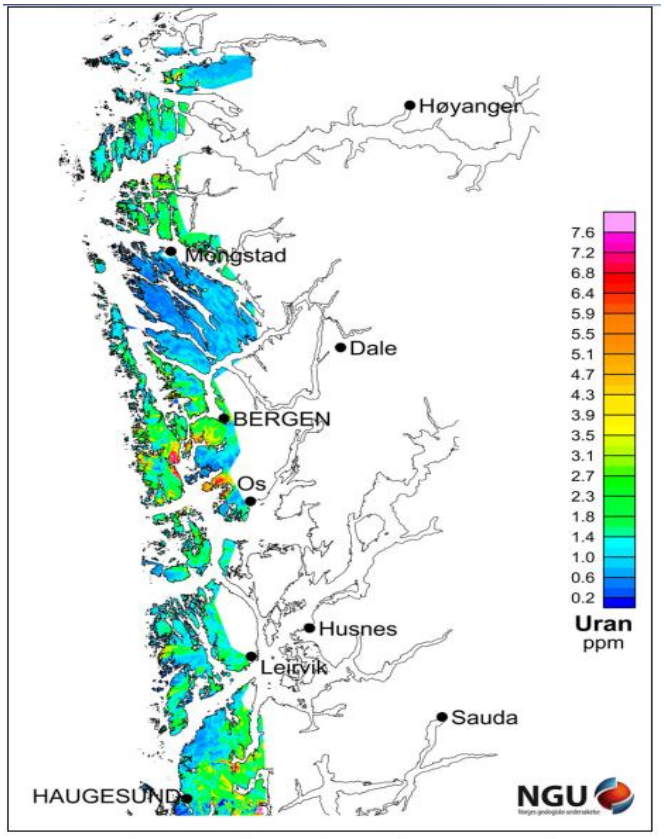

Figure 3.1: Uranium map for the Bergen area. [32]

3.5.1 Data from Norway

Norway is among the countries in the world where indoor radon reaches its highest concentration (NRPA) [33]. About 9 %(17500) of Norway's housing stock has a radon concentration higher than recommended action limit of 200Bq/m3.

Doses from radon are larger than doses from all other natural radioactive materials. It is estimated that long term exposure to radon indoor air is responsible for between 250 to 300 new cases of lung cancer each year in Norway (NGU 2010).

According to the U.S geological survey (USGS 2008)[34] Norway has one of the major thorium resources in the world, approximately 170 000 tones, which has a potential energy content which is about 100 times larger than all the oil extracted to date by Norway, plus that of the remaining reserves.

Table 3.4: Radon concentration in dwellings in Nordic countries (NRPA 2009) [33].

Country	Number of dwelling exceeding 200Bq/m^3
Sweden	450 000
Finland	200 000
Danmark	65 000
Norway	170 000
ICE land	No dwellings have radon level above 200Bq/m^3*

*due to the Icelandic bedrock.

3.6 Principles of testing radon gas

There are several simple tests for radon gas. Radon test kits for short-term uses for screening purposes are generally inexpensive, and even free in some cases such as charcoal. The tests can be completed in (48-96 hours), while for long-term take more than 90 days, in some case taking collections for up to one year. Its detectors that have abroad result range average, the average is important because radon levels vary from day to day and month to month. The open coal box after absorbing gas from the air for (2-7 days) should be sent to a laboratory for analysis. There is another type of radon detector, called canary meter (see appendix C) which is capable of long term and short-term results. This is easy to use because it requires no lab to analyze the data. It is however recommended to not make use of short-term test for times with high humidity, storms or high winds.

Figure 3.2: Radon test equipment (coal box).

3.7 Method to reduce radon levels

There are deferent methods to reduce radon concentration depending on the specific circumstances of the situation. Generally for elevated radon levels in above ground homes or work places, as we stated before radon can entry through cracks or other openings in the floor, or by diffusion from soil in contacts with the building foundations by diffusion from construction materials. The radon level can be lowered by:

- Increasing under floor ventilation.
- Sealing the cracks and other openings through which radon enter structure, even this method less effective than the sub-floor ventilation.
- Increasing ventilation of indoor space without door air, it might be reason to diluted radon level indoor in cooler climates this method can be costly in terms of energy loss, which can reduced by using heat exchanger.
- Putting plastic sheeting below the basement.
- Water treatment by aeration or other methods.

3.8. Some industrial uses of radon

Radon has some industrial uses, due to its part of the uranium decay chain. When it is present in soil or air near the ground, it is indication for the presence of uranium there, so industries that explore for uranium can find it by detecting radon. In addition, oil companies can locate petroleum by measuring for radon [25] because radon dissolves well in oil it used also to check for flows in products. It is possible to add to gas or liquid flowing through the tub, if any radiation detected outside the tub this indicates a leak.

4. Field work

4.1 Descriptions of the areas

The Bergen area consists of bedrocks of mostly metamorphic origin of Pre-Cambrian and early Palaeozoic ages (Fossen, 1988). Rocks can generally be differentiated between gneisses of granitic, amphibolite, quartz tic composition and different types of a north sites and mafic units.
The most important geological event in forming the bedrock of Bergen area was the Caledonian progeny (c. 400 ma.) forming a mountain chain similar to the Himalaya. After this progeny, the mountain was severely eroded, and today we can only observe the deep roots of this mountain chain. The bedrock is very complex, consisting of Caledonian folded deep metamorphosed thrust sheets. The geological units of Bergen area forms a characteristic arc shape with stacked units of the aforementioned different bedrock units.

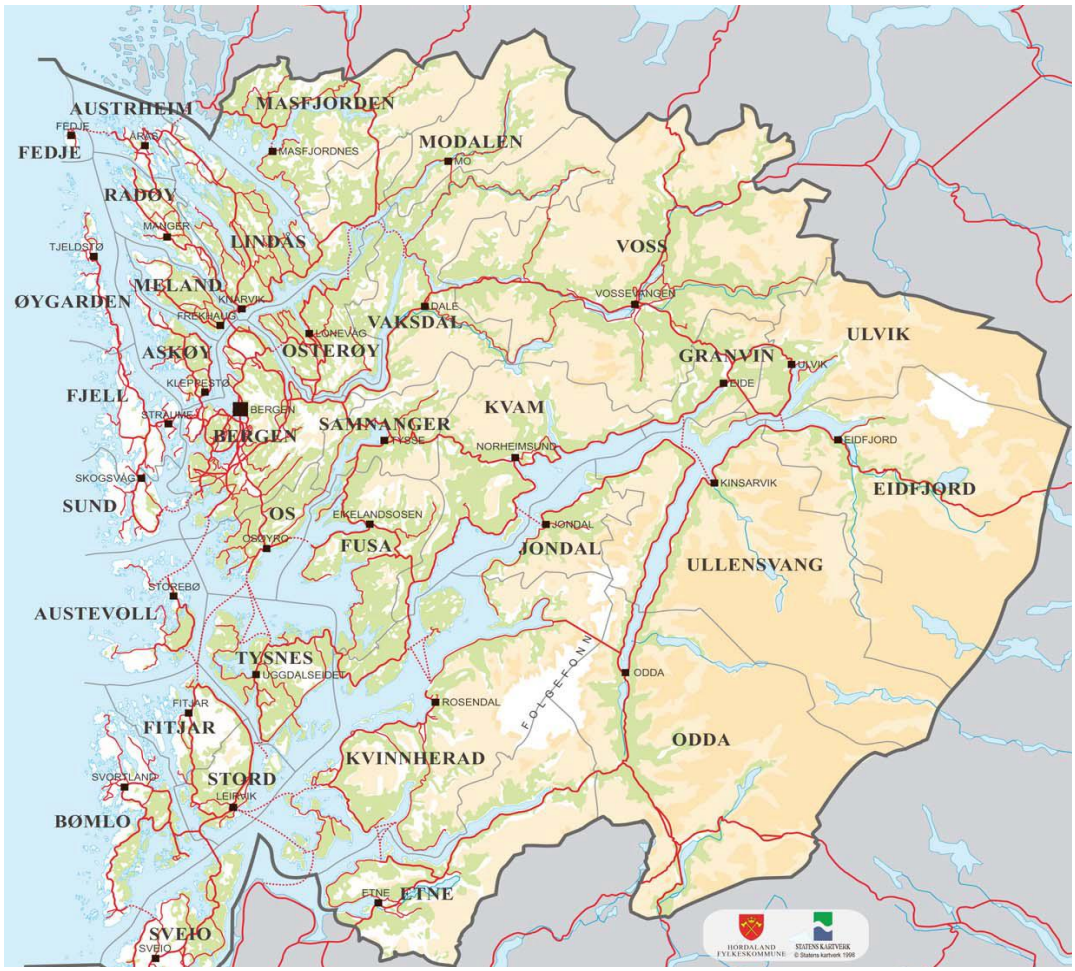

Figure4.1: The main point of Bergen ark system [35].

4.1.1 Area1-Haukeland (university hospital)

It is close to Bergen center, on the southeast side of the city. Is resting on rocks of the Minor Bergen arc, which is characterized as complex mixture of granitic gneisses, amphibolite's, quartzite's, mica schist's and marble. At the Haukeland the bedrock is probably of granitic gneiss, but may as well also be quartzite.

4.1.2 Area2-Hosanger in osterøy

Our research studies was at Hosanger It is located northeast of Bergen. Consists of rocks derived from the Lindås Nap, which dominantly comprises amphibolite, and gneisses. The radioactivity considered low in these rock units. In ch.6, we show that we have measured anomalously high Radon values here. This may be a result of hydrothermal enrichment of radioactive elements. Both Cu and Ni mines have been discovered in this area. This is still enigmatic and needs further investigation to confirm source of radioactivity.

4.1.3Area 3-Åsane

Åsane is precinct of the city of Bergen; it lays at the north western part of the city. Our test area was closed to åsane center. It consists of the Blåmannsdekket, which dominantly comprises granitic gneisses and quartzite. These rocks shows moderately low radioactivity (based on some scattered).

4.1.4 Area4-Fyllingsdalen

It lays south-west of the city center in the valley to the west of Løvstakken. Consists of granitic gneisses of the Øygarden gneiss complex, which underlies the Bergen arc units. Some of these granitic gneisses show anomalous high radioactivity (Rudlaug 2010), high indoor Radon concentrations also reported from the area. [36]

4.2 Description of the borehole

All boreholes were filled with natural ground water. The overall depth and diameter were different in our sampling areas. The borehole depth (diameter) in area1 was 250 m (139 mm), in area2 was 180 m (115 mm), in area3 was 220 m (139 mm), and area4 was 500 m (56 mm).

5. Field work – part one

5.1 Measurements of temperature profile

5.1.1 Overview

Temperatures at the surface of the Earth are controlled by the sun and the atmosphere, except for areas such as hot springs and lava flows. This leads to different temperatures at the surface in different times year round.
At shallow depths of about 6 m below the surface, the temperature is constant, between 10 and 16 °C depending on latitude. In the zone between the near surface and about 120m depth temperatures are affected by atmospheric changes and circulating groundwater. Below that zone, the temperature normally increases with depth. However, the geothermal gradient (the rate of change in temperature with depth) varies with respect to tectonic setting and the thermal properties of the rocks.
The geothermal gradient is an important factor for the geothermal energy industries. A high temperature gradient leads to high heat flow, which is an important factor to estimate the potential extracted energy.

5.2 Experimental set up

Temperature profiles in boreholes have been measured in order to understand if one can correlate to the amount of radon emanating from holes. In fieldwork, data loggers used a Vemco temperature logger [37] for temperature measurement below the surface of the ground in boreholes (see appendix C). The temperature logger is fastened to a several hundred meters long rope, and attached to a cylindrical bar to be able to lower the logger smoothly down which allows for a good and correct temperature profile (see figure 5.1). The logger was lowered directly in the borehole, not in the heat exchanger tube. The reason for this was to avoid risking that losing our equipment in the hole would result in blocking circulation of heat exchanger liquid.

Figure 5.1: Temperature logger was fasted with rope and weight in area 3.

Temperature samples were recorded in ten second time intervals with control over the depth and the rate of descent. The logger reads temperature at every 10 seconds. In the first hole, we took samples in one-minute time intervals in steps of 5 m, and for the rest of holes data was taken in 30 seconds time intervals and in steps of 5 m in areas 1, 2, and 3.

5.3 Correcting temperature measurements

After the temperature measurements, it was realized that neither 60 second nor 30 second time intervals (3 consecutive readings) were not long enough for the logger to have stable temperature readings at each depth. Therefore, the temperature logger calibration was performed for an unbiased estimate of the temperature at each depth, which is particularly important for the thermal gradient in each area (see table5.1).

5.2.1 Calibration of temperature logger corrections.

Temperature logger calibration was carried out in ice water at the laboratory in the physics department. Calibration data was taken by putting the logger in a container filled with ice water for 15 minutes and studying the temperature readings as function of time (see figure 5.2).

We assume that the rate of change of the temperature is proportional to the temperature difference ΔT between measured T and the real temperature, T_0, of the ice water. Using Eq. 5.3 that extracted from the slope of ice water curve shown in Figure 5.2.

$dT / dt = -K\Delta T$ **(5.1)**

$dT / \Delta T = -kdt$

$\Delta T = T_o \, e^{-kt}$ **(5.2)**

The ice water temperature profile is fitted with an exponential function plus a constant term. Eq. 5.3 is extracted from the fit function.

$T(t) = 0.867 + 20.68 e^{-0.005t}$ **(5.3)**

The time constant of stabilisation, k, is thus determined from Eq. 5.3 as 0.005 per second and the temperature of the ice water is estimated to be .

$T_o = 0.8$ °C

The derivative, using the first and last measurement at a given depth, is found for each depth in each hole and is used to the correct the average found for each depth, defined as

$$\text{Correction} = \frac{\Delta T}{\Delta t} / K \qquad \textbf{(5.4)}$$

The corrected value we obtained by

$$T_{Av} - \left[\frac{\Delta T}{\Delta t} / K \right] = T_{\text{corrected}} \qquad \textbf{(5.5)}$$

Where T_{AV} is the average temperature at a given depth.

We plot the corrected temperature data that we obtained from the calibration of the logger and the measured temperature data from the borehole together in one plot (see 5.2.2).

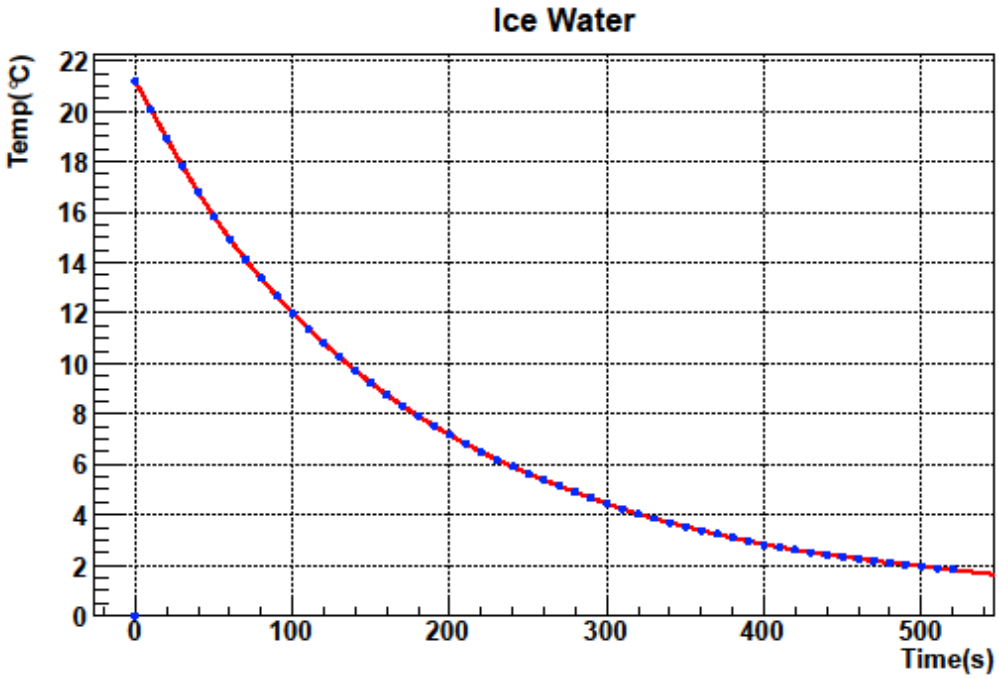

Figure 5.2: Temperature profile in ice water

5.2.2 Thermal gradient from boreholes

The thermal gradient is an important parameter to know when evaluating the potential for extraction of ground heat.

In order to obtain thermal gradient from boreholes we plot the corrected temperature data as a function of depth and different fitting range for each area to get an exponential function. From fit slope, we record the thermal gradient for each borehole. See figure below.

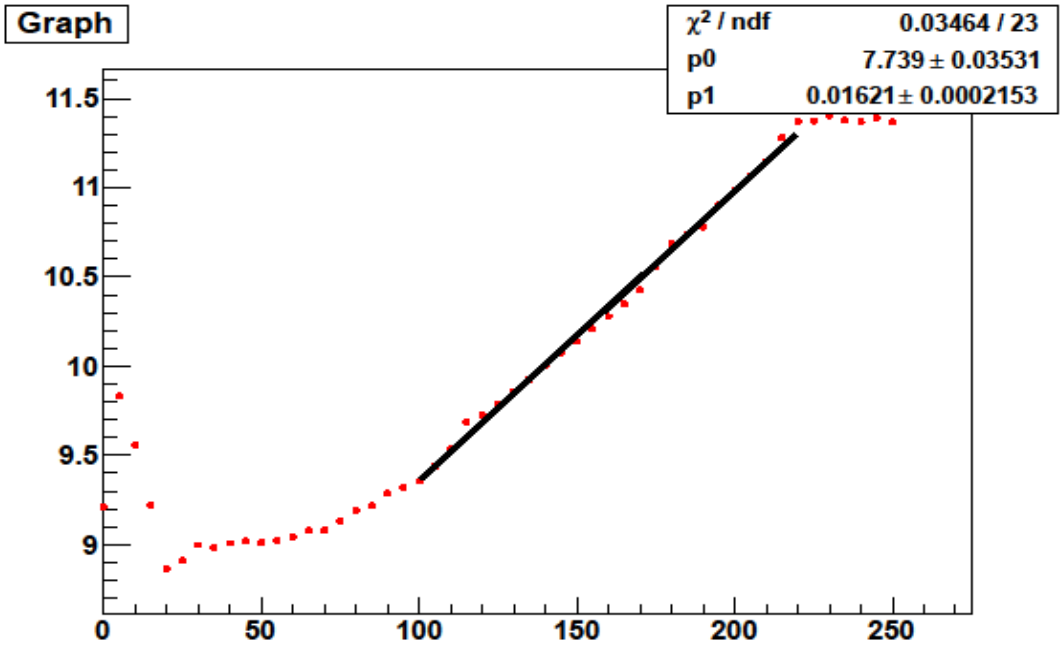

Figure 5.3: An example of thermal gradient obtained from fitting slope of the corrected temperature profile for area1 hole 1.

It is clear that only the central parts of the temperature profiles show a linear dependence. Therefore, the fit range used to determine the gradient is determined by studying the figure first. Table 5.1 show the fit ranges and the resulting gradients.

The first few measurements just below the surface are expected to be affected by the ground weather conditions and our handling of the temperature meter. Although most of the hole is filled with ground water, we did not determine the depth of the ground water surface, which was probably somewhere between 5 and 15 meters. Our correction procedure is therefore probably not valid for the most shallow depths.

For the measurements at the largest depths, we recall that our impression was that the equipment was moving more slowly when lowering it. It was difficult to determine if we had reached the bottom. Therefore, the depth for these measurements may have been smaller than we plot in the figures.

Table 5.1: Thermal gradient from all the boreholes.

	Hole number	Fit range (m)	Thermal gradient (°C/m)
Area1	1	100-220	0.01621
	2	100-220	0.01669
	3	100-220	0.01558
Area2	1	80-160	0.01395
	2	80-200	0.01474
	3	60-160	0.01266
Area3	1	60-160	0.0134
	2	100-200	0.01585
	3	60-160	0.01395

Assuming that the thermal gradient is the same in the three boreholes of a given area, we use the three measurements to get estimates of the thermal gradients in the area by taking the mean value, and using the spread of results to estimate the uncertainty by the "max-min" method [38]

$$S_x = \frac{\max - \min}{3}$$

Result shown in table below:

Table 5.2: Uncertainty in thermal gradient

Area number	thermal gradient with uncertainty
Area-1	0.0162± 0.0004
Area-2	0.0138±0.0004
Area-3	0.0144±0.0008

5.3 Results

We measure temperature as a function of time. For the first borehole in each of the areas samples were taken each 30 sec for each five meter depth. The logger records temperatures every ten seconds. That gives readings with two digits after the decimal point. In tables for temperature measurement series given in Appendix A, we can see six readings each minute. For the other boreholes, samples were taken for one minute every five meters. We assumed that the relative precision between the points corresponds to the precision of the readings, i.e. ± 0.01 degree.We plot temperature as a function of depth in order to see how temperature gradient develops while going deeper.

As we can see from the plots, the initial temperature starts to decrease from 0-90 m and increasing again going deeper. Results are in good agreement with many other previous measurements and searches. We learn from the plots that the temperature underground is relatively stable throughout the year, generally higher than the air temperature in winter, and cooler in summer. There is no major variation in temperature gradient underground, for example at 150m depth, the temperature ranged from 8.60℃ and 9.90℃ across all of the boreholes.

For dissection of the temperature gradient, results, and the correction procedure those data are described in a series of table in appendix A

The ffigure below shows the temperature profile from all the boreholes. From the plots below we observed that there is some variation between measured data closer to the surface which indicates that surface temperature is affected by air temperature.

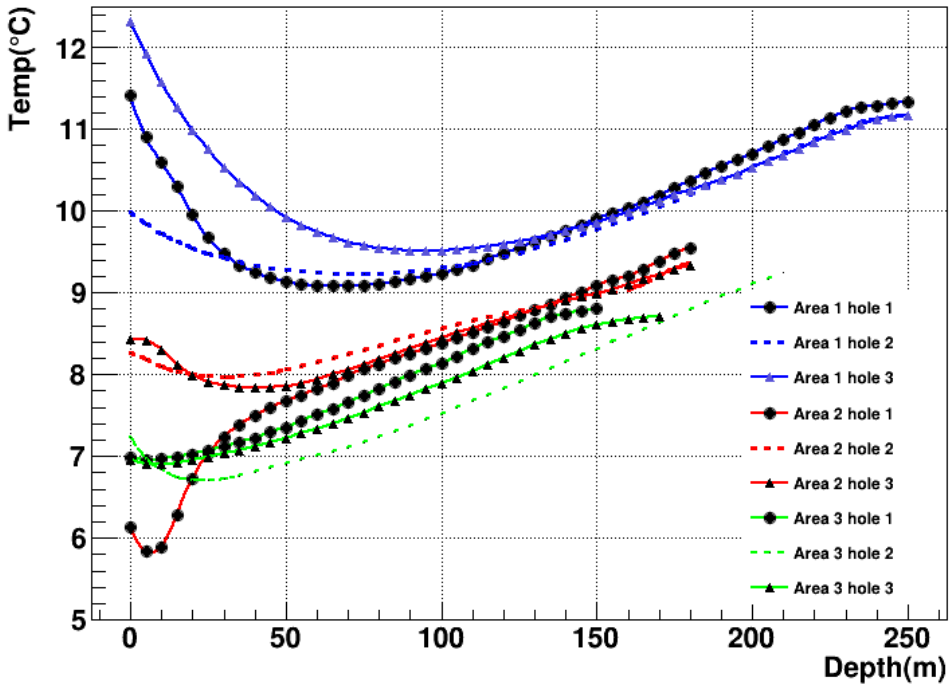

Figure 5.4: The distribution of measured temperature data for nine boreholes with different depth.

We plot the corrected temperature data that we obtained from the calibration of the logger and the measured temperature data from the borehole together in one plot. The same procedure was applied to the other boreholes, data analyzed, and as shown down in the plots, we can observe a significant variation between the measured and calibrated data, this indicates some uncertainty in the process of controlling the time and temperature while moving from one hole to another.

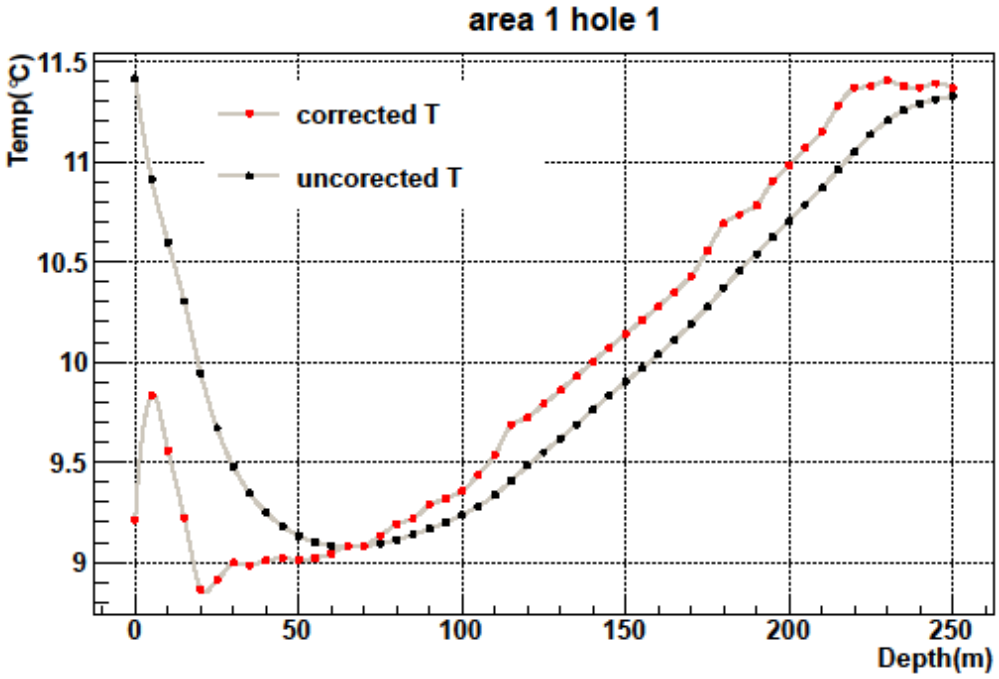

Figure 5.5: The distribution of measured and corrected temperature data, for area 1 hole 1, which shows that the initial measured Temperature at the surface and a few meters below the surface are much higher than the corrected data.

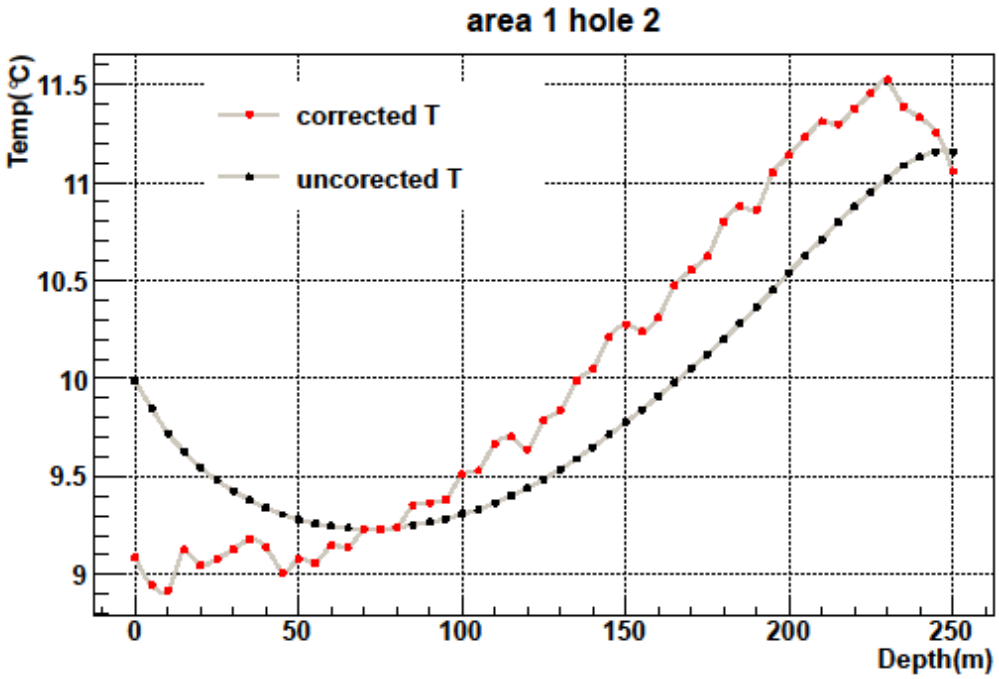

Figure 5.6: the distribution of the measured and corrected temperature data, for area 1 hole 2, which shows some different measurements between the corrected and measured data at all depths.

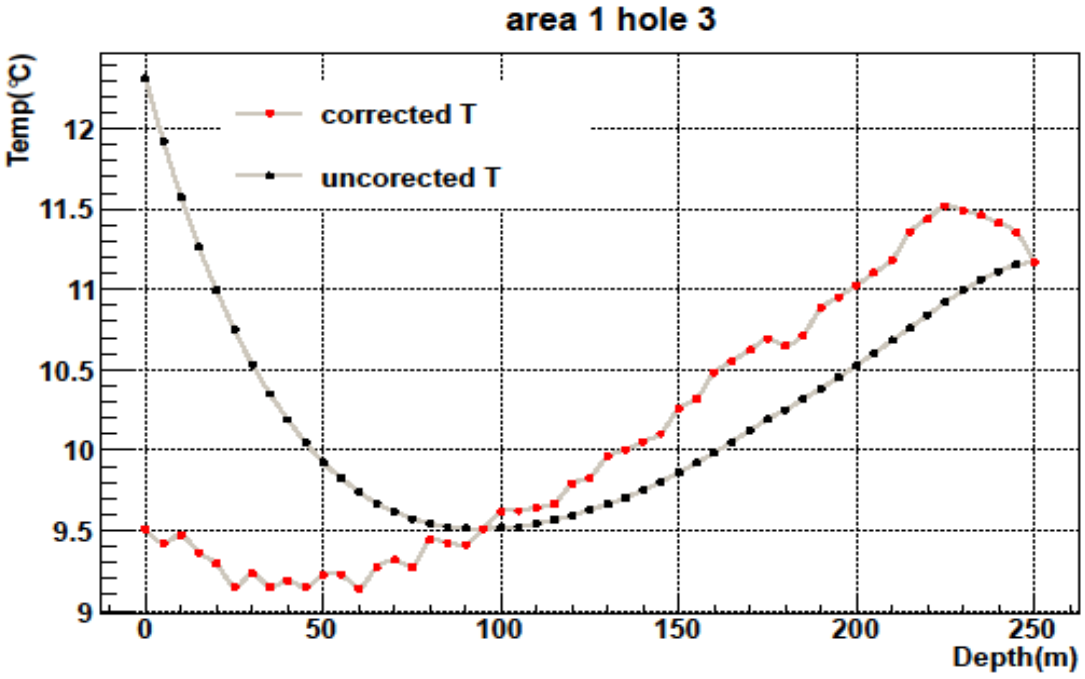

Figure 5.7: The distribution of measured and corrected temperature data in area1 hole 3. Results show some variation between the two data's, at different depths.

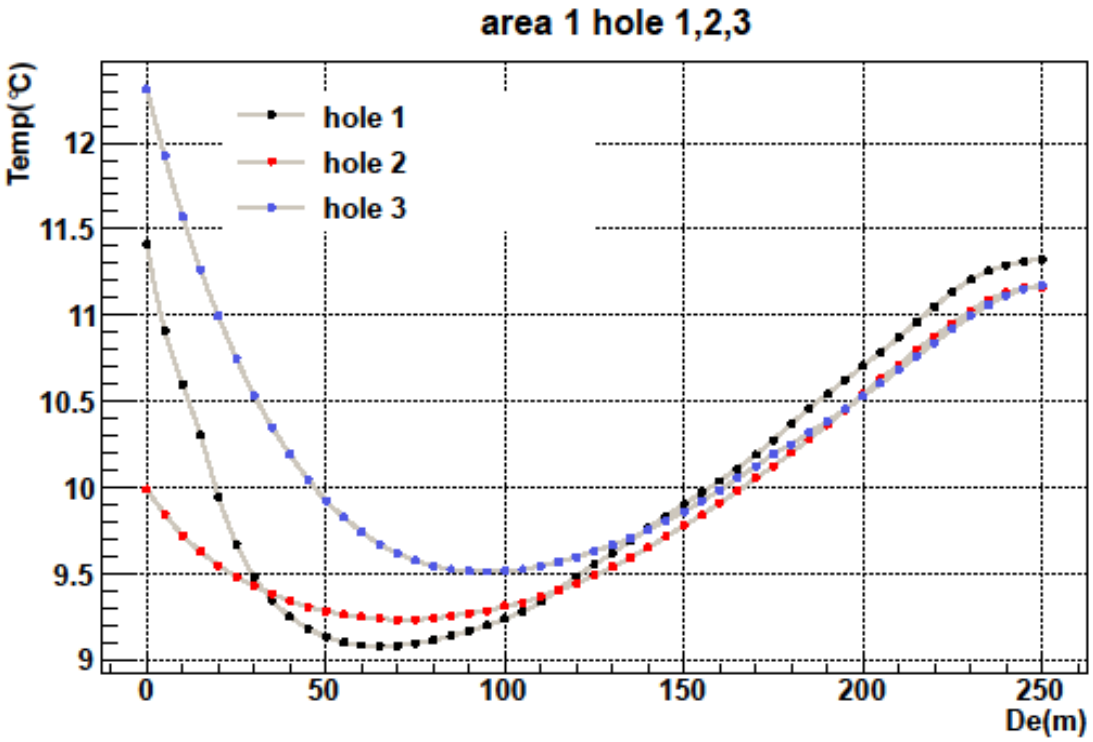

Figure5.8: The distribution of the measured temperature data of all boreholes in area 1 in one plot. The results show variation in initial temperature measurement at the surface.

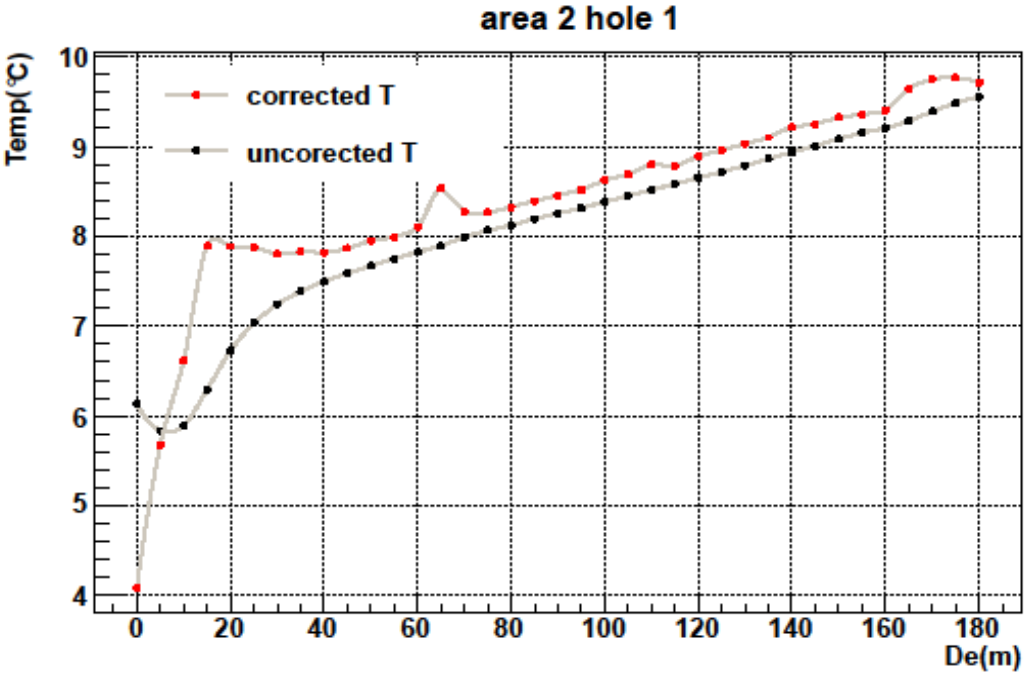

Figure5.9: The distribution of the measured and corrected data of area 2 hole 1. The results show significant variation between 0m-80m, and little difference further down.

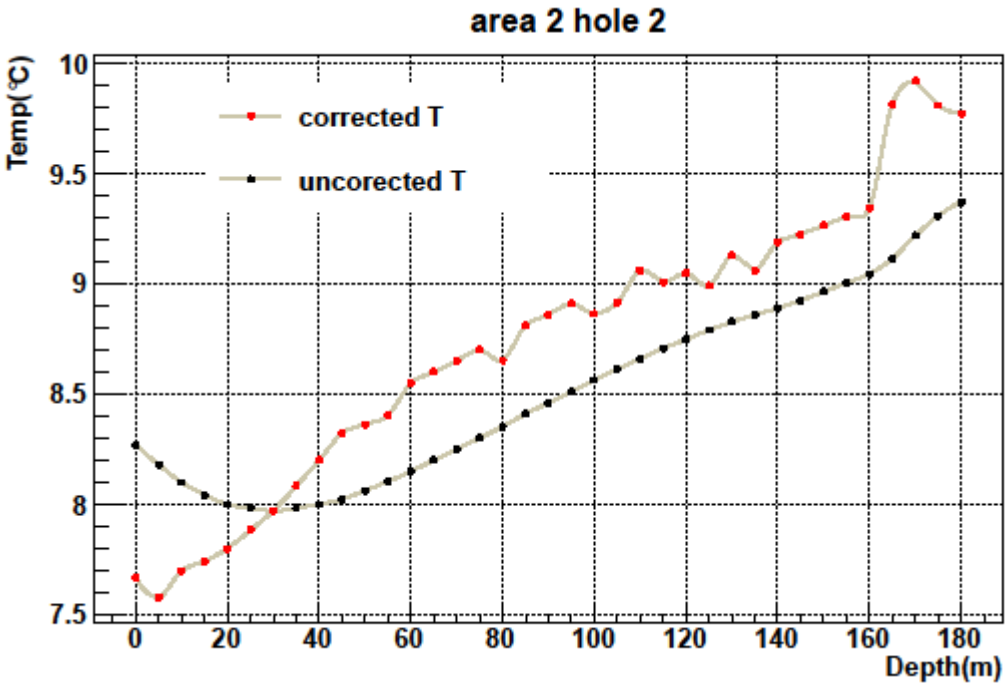

Figure 5.10: The distribution of the measured and corrected data for hole 2 in area2. This shows significant difference between the two data at all depths.

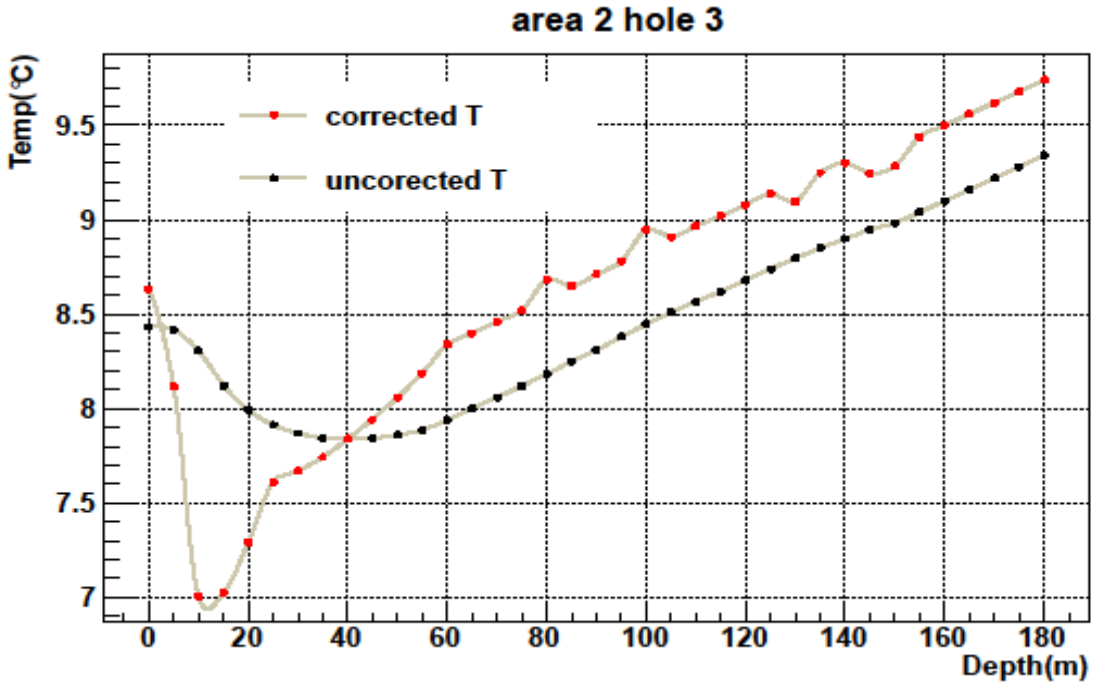

Figure5.11: The distribution of the measured and corrected data for hole 3 in area2. This shows significant difference between the two data at all depths.

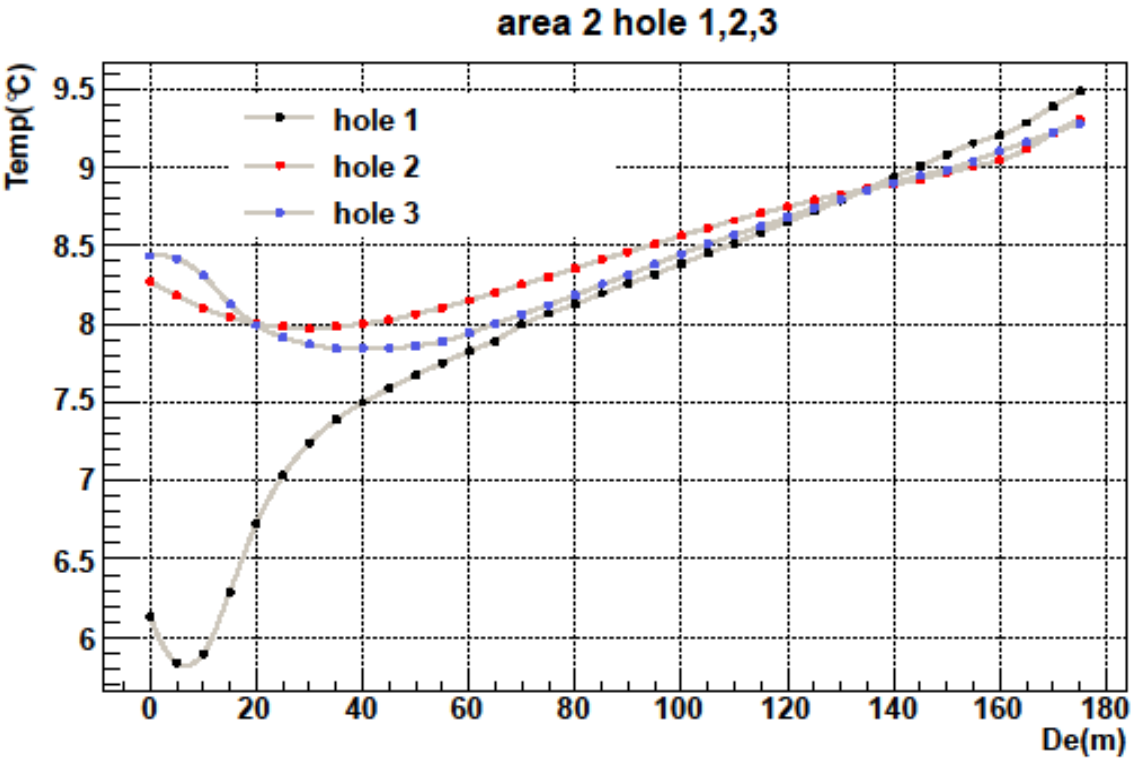

Figure 5.12: The distribution of the measured temperature data of all boreholes in area 2 in one plot. The results show variation in initial temperature measurement at the surface.

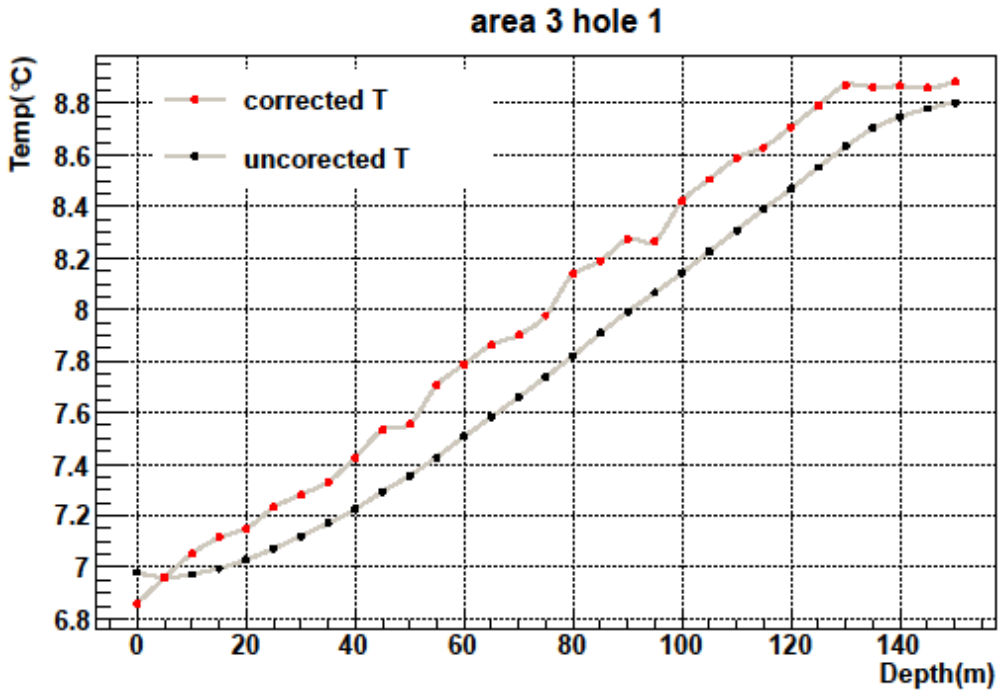

Figure 5.13: The distribution of measured and corrected data for area3 hole 1, results show very big similarity between the two data at all the points.

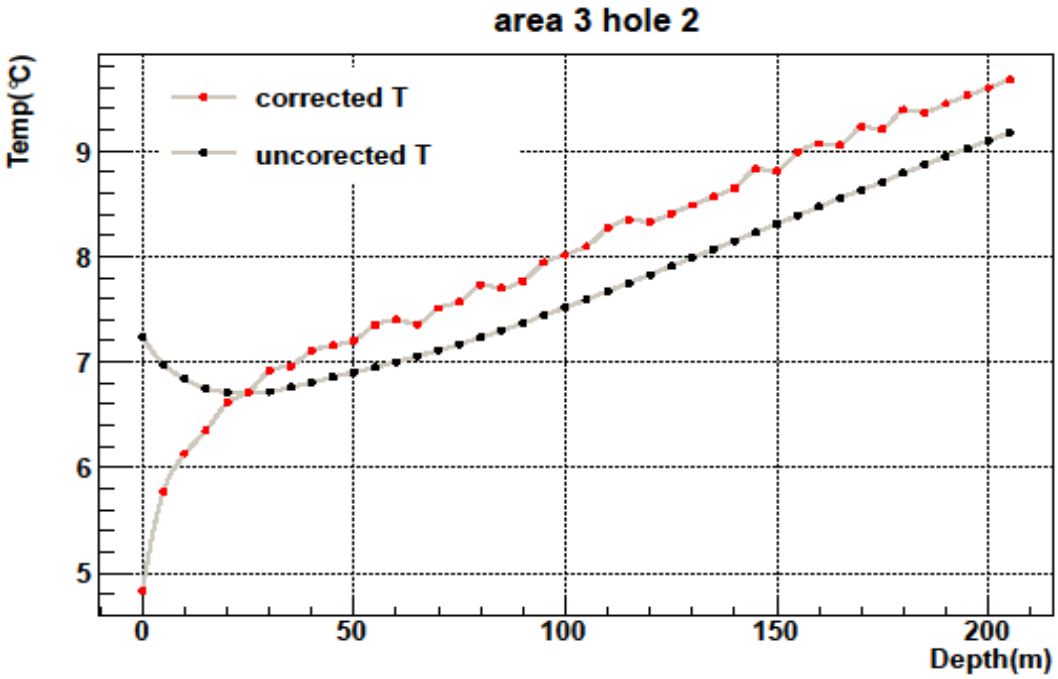

Figure 5.14: The distribution of the measured and corrected temperature data for area3 hole 2, results show variation in some a few points below the surface.

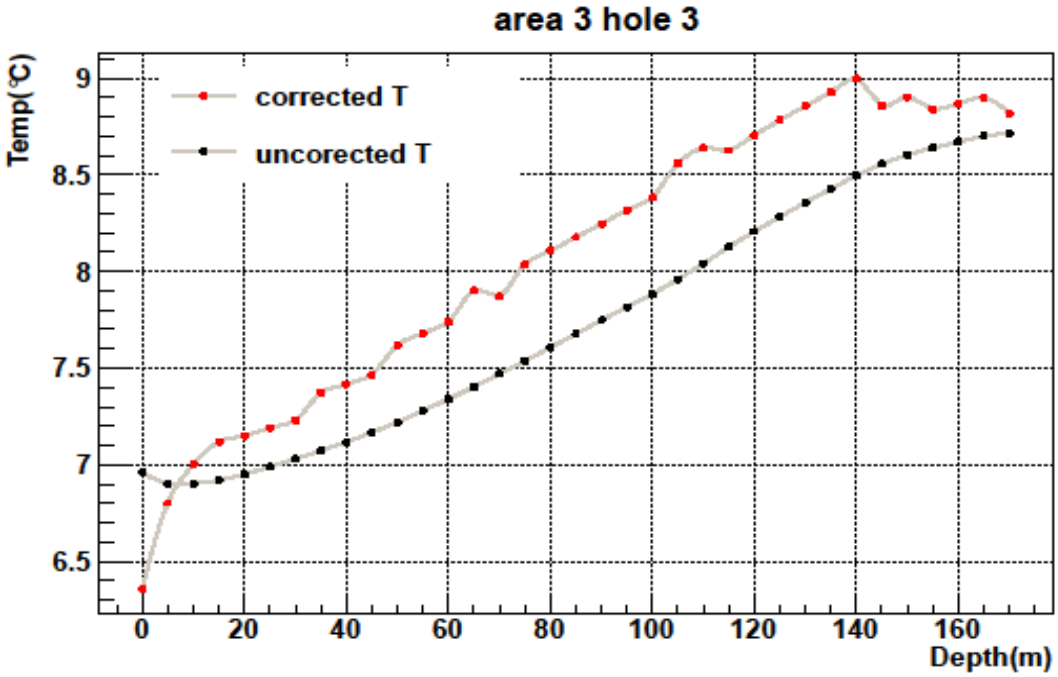

Figure 5.15: The distribution of measured and corrected data for area 3 hole3. Results show no significant variation between the two measurements.

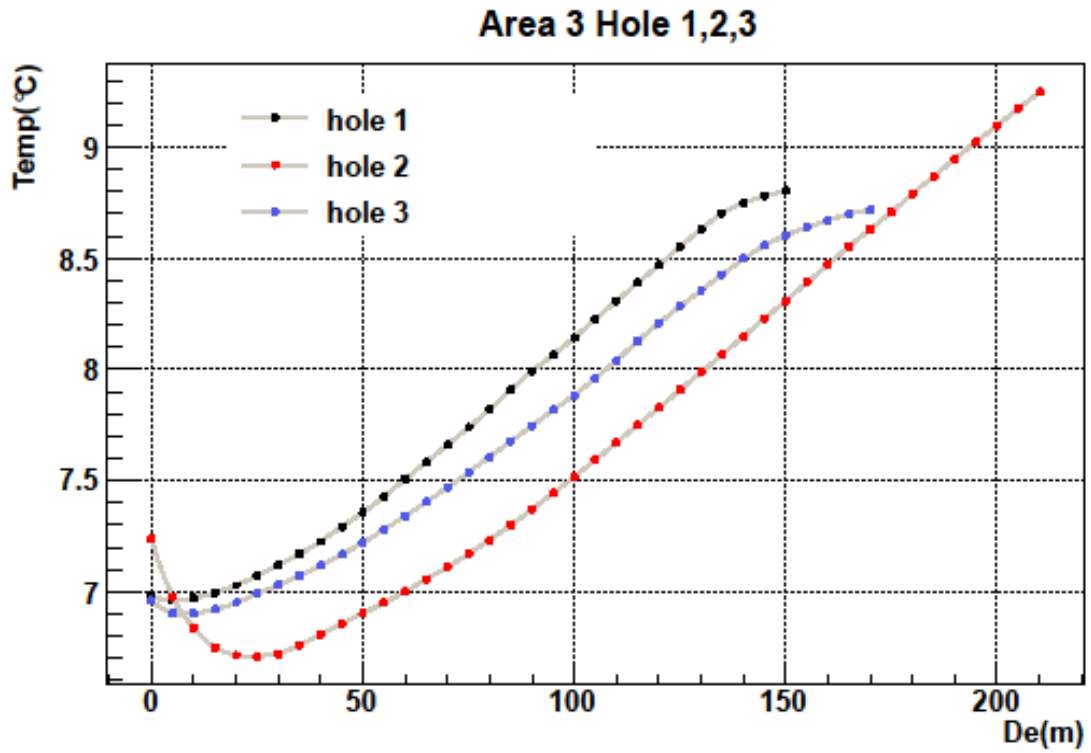

Figure 5.16: The distribution of the measured temperature data of all boreholes in area 2 in one plot.

6. Part two- Field Works

6.1 Measurement of radon concentration in the boreholes

6.1.1 Overview

The activity for radon was measured from boreholes filled with ground water. The aim of the work was to measure the radon concentration with gamma spectroscopy. The rn-222 activity concentration in borehole water was determined using charcoal boxes and a canary meter (see appendix b). After each sample collection, the charcoal was heated for two hours at 150 c degree in order to de-absorb any background radiation that can affect the results before being used for a new measurement. Variations in short-term measurements were noticed in all boreholes. The field measurements for seven boreholes were done in autumn, which is very rainy in this region, while five boreholes were measured in spring months. It is likely that taking measurements after rainfall directly might affect the expected results, as the change of water level affected the value of rn-222 activity. However, the occurrence and distribution of radon in ground water depends mostly on the source of radon emanation that may be a result of natural processes. The amount of radon is principally controlled by its production from its immediate parent isotope, radium-226.

As a principle, most rocks contain small amounts of U and Th and their progeny. From U decay series, a part of Rn-222 is known to recoil out (emanate) of the solids and enters the adjoining pores. The pores are in the top of soil or completely below the water table, which is filled with ground water. The process for radon movement from one place in the soil to another, known as diffusion, and is always operative.

Variation of radon concentration has many influencing parameters, such as soil moisture condition, atmospheric temperature, wind speed and atmospheric pressure. These parameters have been reported in previous studies to be important factors affecting its concentration in the soil. A relation between air temperature and radon emanation has been indicated, moreover, in underground environments Rn-222 concentration is often characterized by large temporal atmospheric pressure variation.

Other research done in Bergen measured different radon activity, outside atmospheric temperature, and underground tunnel. They suggested that this correlation is used by temperature difference between tunnels and outside atmospheric air temperature.

In the present work, the variability of radon activity is noted in different boreholes, and different type of rocks. The previous study recorded low radon activity, however the present research result in Ostrøy showed higher levels.

6.2 Experimental set-up:

The tools for measurement used in this detector were a borehole, coal box, canary meter (digital radon monitor) (see appendix c) [39] and lab equipment like a sodium scintillation detector (NaI) (see section 6.3).

At the physics department, they have instituted a lab to study our samples. Special boxes were designed (figure 6.1) for the sampling procedure. As the figure shows these boxes were structured in a way that we put the lower orifice on the outlet of the borehole to accumulate the radon gas. To avoid the leaking of the gas out of the boxes the upper orifice must carefully seal. The experimental set-up was left for three days and it is because the half-life for radon gas is around 3.8 days. As shown in figure 6.1. *This process was repeated for the other boreholes, but only one of them was equipped with the digital radon monitor in addition to the coal canister box.*

Figure 6.1 Coal box inside a closed box on the top of borehole in order to absorb radon gas in area3.

6.3 Gamma ray spectrometry

Gamma-ray spectroscopy is the science of quantification of radionuclides by analysis of the gamma-ray energy spectrum produced in a gamma ray source, which has an energy level equal to the energy difference ΔE between two nuclear energy levels. Almost all radioactive nuclei emit γ –rays with one or many certain type's energy. Uranium, thorium and potassium decay series have radioisotopes producing gamma rays of sufficient energy and intensity for gamma- ray spectrometry measurements. The common method to

measure the abundance of these radioisotopes such as radon is by looking at gamma-ray spectrometer readings (beards more and cull, 2001) [24]. In order to determine the source of the radiation we need to measure the energies of these gamma-ray photons (see spectrum from Osterøy boreholes). [We should also remember most of gamma rays are higher in energy than X-ray and therefore they can cause a large energy release]. In this thesis, we analyse the gamma-ray spectrum from the coal boxes by using sodium Iodide scintillation detector.

6.4 Gamma-ray detection.

The coal boxes are analysed by a sodium iodide (NaI) scintillation detector coupled to a photo multiplier (PMT) for measuring the intensity of γ-ray. Data acquisitions are controlled through a PC.
The PMT coupled to the NaI detector converts the scintillation light to an amplified electrical signal. When **γ**-rays enter the NaI crystal, they interact primarily with the bound K or L electrons from the iodine atoms in the crystals. The most important interaction mechanism is the photoelectric effect. Gamma rays interact in the crystal, where they can transfer energy to an electron either by elastic scattering or by photo absorption, which will transmit the original **γ** energy to the electron. This causes ionization and electronic and thermal excitation in the crystal when radiation is absorbed. X-ray peaks can be produced by photons that hit the lead shield and some of these x-rays will interact with sodium detector and produce a peak at 74.96 keV, which was visible in the entire spectra that we analysed from the charcoal boxes.

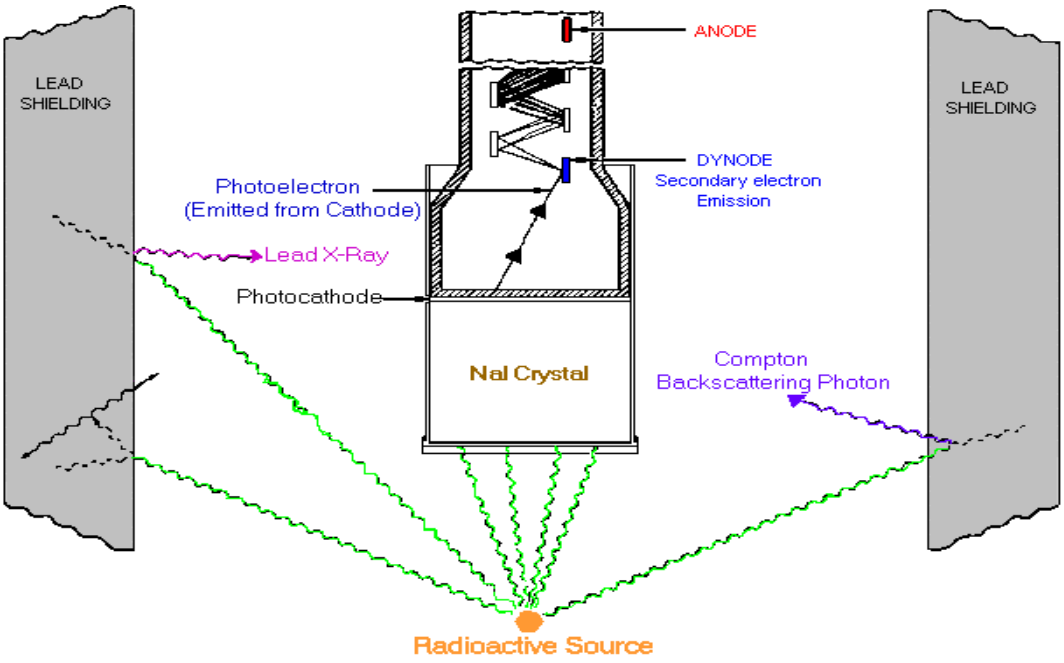

Figure 6.2 Detection gamma rays from radioactive isotopes by NaI scintillation detector as the interactions happens [40].

6.2 Energy calibration of the detector

Energy scale should be calibrated in order to convert detector signal into energy.

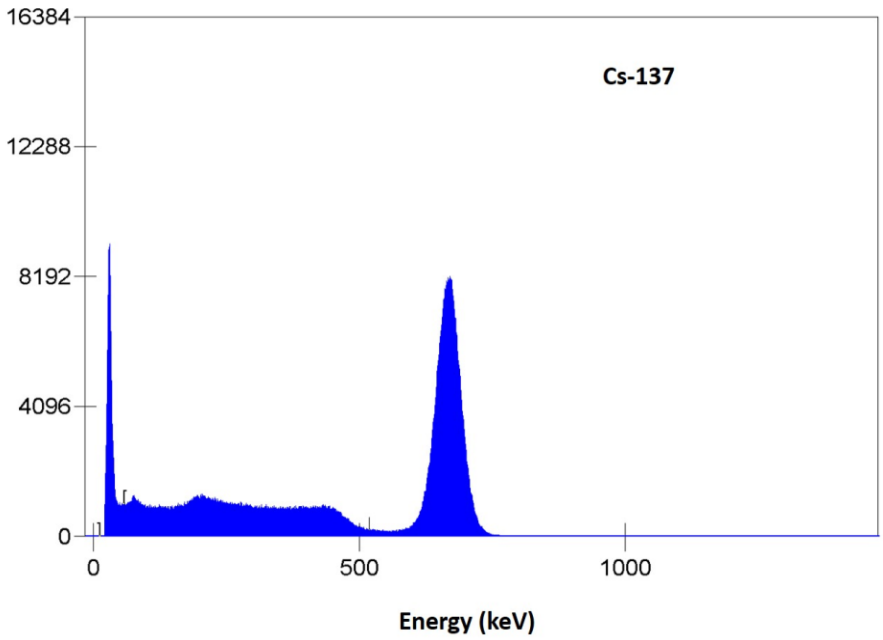

Figure 6.3 Gamma spectrum of Cs- 137 with a single γ energy peak.

For energy calibration, several known sources are used to determine the relationship between the channel number and the energy of the detected emission. The aim for the calibration is to detect the energy from unknown sources, because the channel scale can be converted to an energy scale.

Spectrums should acquire until a well-defined peak can be observed. Since energy of Cs-137 is known we need to record the channel number of the photo peak position by using peak analysis from the software (including uncertainty). The same settings are used for the other isotopes, which are replaced on the detector. We then measure the channel numbers of the centroids of the photo peak and compare against the known photo peak energies for each source.

The data extracted can make a linear plot of the energy of the photo peak against the channel number of the centroid of the photo peak, fitting a straight line to determine the relation between energy and channel.

Using obtained data from the calibration, the graph 6.4 and table 6.1 can be used to identify the unknown radioactive sources.

Table 6.1: Calibration measurement data from several radioactive sources.

Decay	Measured channel	Expected peaks[keV]	Extracted peaks [keV]
Ra226->Ra222	140	187	185,45
Po218->Pb214	181	242	244,70
Po218->Pb215	215	295	293,83
Po218->Pb216	256	353	353,07
Pb214->Bi214	433	609	608,84
Na 22	366	511	512,02
Cs 137	469	661	660,86

Since the expected energy known, we can plot the energy for all the isotopes with channel number in a linear range fitted with linear function.

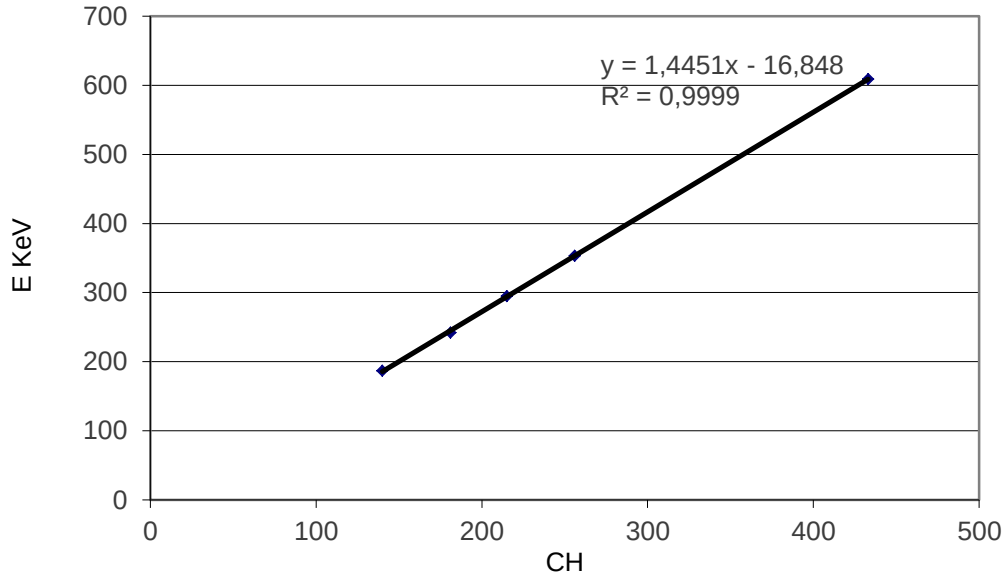

Figure 6.4: The energy calibration of NaI detector (linear function) using known sources of gamma-rays emitters.

$Y(x) = ax + b$ **(6.1)**

$= 1.44x - 16.848$ (from the calibration slope)

$E = -b\ kev + a \frac{kev}{cH} \times CH$ **(6.2)**

6.7 Calibration of radon measurement

For determining the conversion constant "K" (see Eq. 6.3). We rely on the readings of the canary. The canary, the charcoal boxes and a Ra-226 source were enclosed in a sealed box for three days. By using a radon monitor, we calculated the average value for R over three days. The energy calibration is the same for Ra-226. The value for K we have determined can be used as a calibration constant for other samples. We then found the contribution to the spectrum coming from radon by finding the number of counts in the area around the photo peak. We must write down the energy interval and the number of counts in the interval N_{ref}^{box} for the coal box. We repeated the same procedure for all other boxes (4 of them).

There is some radioactivity present everywhere (background radiation), therefore the spectrum should be analyzed when no source is present.

Background radiation must be subtracted from actual measurements N_{ref}^{bac} to be used in further calculation.

Substituting these values in the equation (6.1) yields a value for K. Subsequently we used the K value to find the value of R from Eq. (1) for each measurement.

To calculate the radon concentration, R, we use

$$R = K\frac{N_{ref}C_1}{C_2} \qquad \textbf{(6.3)}$$

Where

K calibration constant

N_{ref} Sums the number of counts in the two intervals.

C_1 and C_2 are correction factors

$$N_{ref} = N_{ref}^{box} - N_{ref}^{bac} \qquad \textbf{(6.4)}$$

$$C_1 = e^{\lambda t} \qquad \textbf{(6.5)}$$

$$C_2 = 1 - e^{-0.01133t} \qquad \textbf{(6.6)}$$

t_1 Is time in unit of hours.

The half-life for radon Rn-222 is 91.68 hours, therefore

$$\lambda = \frac{ln2}{91.68} \qquad \textbf{(6.7)}$$

To compute the uncertainty in R we use formula 6.8

$$\sigma_R = \mathrm{R}\frac{\sqrt{N^{box}-N^{bac}}}{N_{Ref}} \qquad \textbf{(6.8)}$$

In table 6.2 show the calibration constant which obtained by calibrating radon. Radon concentration R was about 218Bq/m^3, the calibration was done in November

Table 6.2: Calibration at the laboratory to determine radon concentration by the canary meter.

	N_{ref}^{BOX}	N_{ref}^{bac}	N_{ref}	*C1*	*C2*	*K*	*Uncertainty*
BOX1	23727	11744	11983	1	0,5577	0,01014	1.58×10^{-14}
BOX2	26619		14875	1	0,5577	0,00817	1.05×10^{-14}
BOX3	26899		15155	1	0,5577	0,00802	1.03×10^{-14}
BOX5	24967		13223	1	0,5577	0,00919	1.33×10^{-14}

6.8 Results

The experimental results for Radon concentration underground from boreholes, which obtained was hole dependent. What we realized is that the radon concentration is higher in inner layers of the Earth than its upper layers that are close to surface. It is because of some geographical and geological factors that influence the experiment's results. Two methods were used in the field measurement to compare and match the readings and results. Identical results were observed in some holes and not in others.

At area 1 radon concentration was low (see table6.3) and its amount was varying significantly in moving from one hole (sample) to another even though the distance between the holes was only a few meters. The results indicate that the radon is unstable and varying from one place to another. Areas 1, 2, 3 and 4 were very different geographically. The difference in depth of boreholes, hole diameter, water level, rock type, and atmospheric temperature all together effect the radon activity measurement.

At area 1 radon activity was low, area 2 radon activity was quite high (see table 6.4). At area 3 it was very low (see table 6.5) and at area 4 even though depths of the borehole was 500m but we still measured very low radon activity.

Results are shown in a list of tables, which describe the amount of radon activity that was measured by using the coal boxes and canary meter for three days. Also a series of figures are showing the gamma energy spectrum.

Table 6.3: Radon concentration measurement at Haukeland. R by canary meter was about 139 Bq/m^3

	K	C1	C2	N_{ref}^{BOX}	N_{ref}^{bac}	N_{ref}	R from callboxes	Uncertainty
Box 1	0.010145	1.0229	0,5425	14485	11896	2589	49.528	3.10
Box 2	0.008173	1.0152	0,5527	12321		425	6.38	2.33
Box 3	0.008022	1	0,5527	13937		2861	41.525	2.33
Box 5	0,00919	1.0152	0,5577	16884		4988	83.479	2.83

Table 6.4: Radon concentration measurement in Osterøy. R by canary meter about 465 Bq/m^3

	K	C1	C2	N_{ref}^{BOX}	N_{ref}^{bac}	N_{ref}	R(coal box)	Uncertainty
BOX1	0.010145	1.0229	0,55265	39804	10039	29765	558.958	4.19
BOX2	0.008173	1.0229	0.55769	141863		131824	1974.206	5.83
BOX3	0.008022	1.0152	0.55769	194751		184712	2697.296	6.60

Table 6.5: Radon concentration measurement in Åsane. R by canary meter about 15 Bq/m^3

	K	C1	C2	N_{ref}^{BOX}	N_{ref}^{bac}	N_{ref}	R (coal box)	Uncertainty
Box1	0.0101	1.0173	0.5475	11615	11643	-28	-0.527	5.02
Box2	0.0081	1.0151	0.5475	11869		226	3.42	5.03
Box3	0.0080	1.0151	0.5526	11840		179	2.90	5.03
Box5	0.0091	1.0151	0.5526	1177		135	2.27	5.03

Table 6.6. Radon concentration measurement at Fyllingsdalen. R was about 31 Bq/m^3

	K	C1	C2	N_{ref}^{BOX}	N_{ref}^{bac}	N_{ref}	R	Uncertainty
Box1	0.0101	1.098	0.5526	12677	11391	1286	23.84	5.04
Box2	0.0081	1.0152	0.5526	12532		1141	17.13	5.04

6.9 Gamma –ray spectra from all boreholes

Gamma – ray spectroscopy used for identifying samples of unknown composition. When energy scale are calibrate. From charcoal box analysis as shown in figure ….for area 2 we measured the extracted peaks for gamma energy, which can identify radon meaning from the boreholes. Results shown in table 6.9.

Table 6.9: Calibration results for area-2 boreholes

peak number	Measured channel	Extracted peaks [keV]
1	122	161,00
2	176	240,00
3	215	297,00
4	255	355,00
5	428	608,00

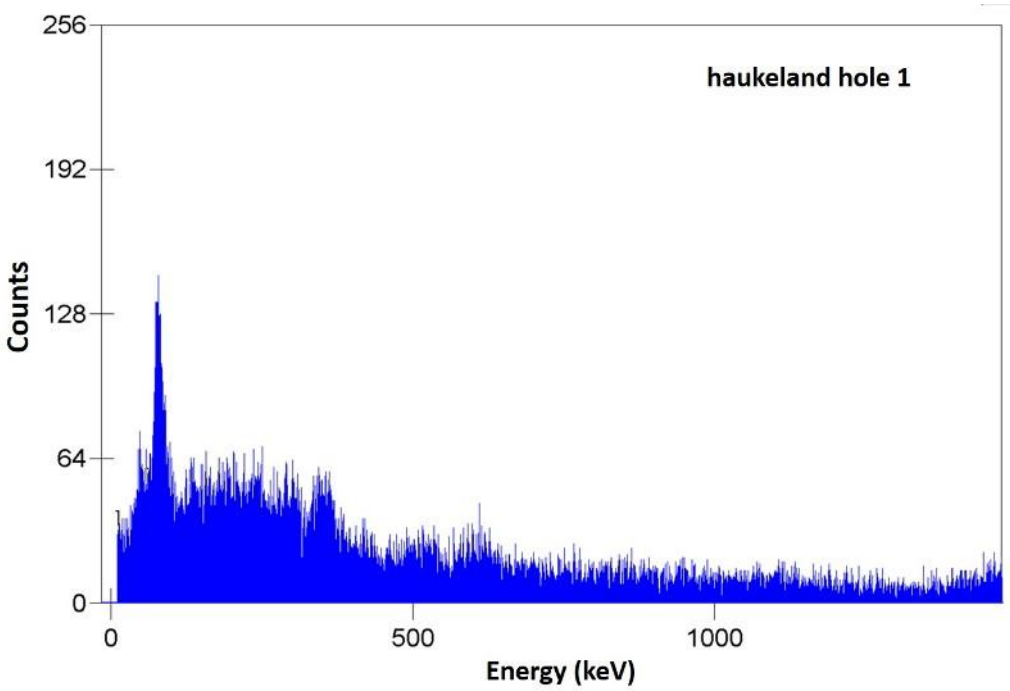

Figure 6.5: area1 hole1, ***Peaks are barely visible, indicating some, but low levels of radon emitting.***

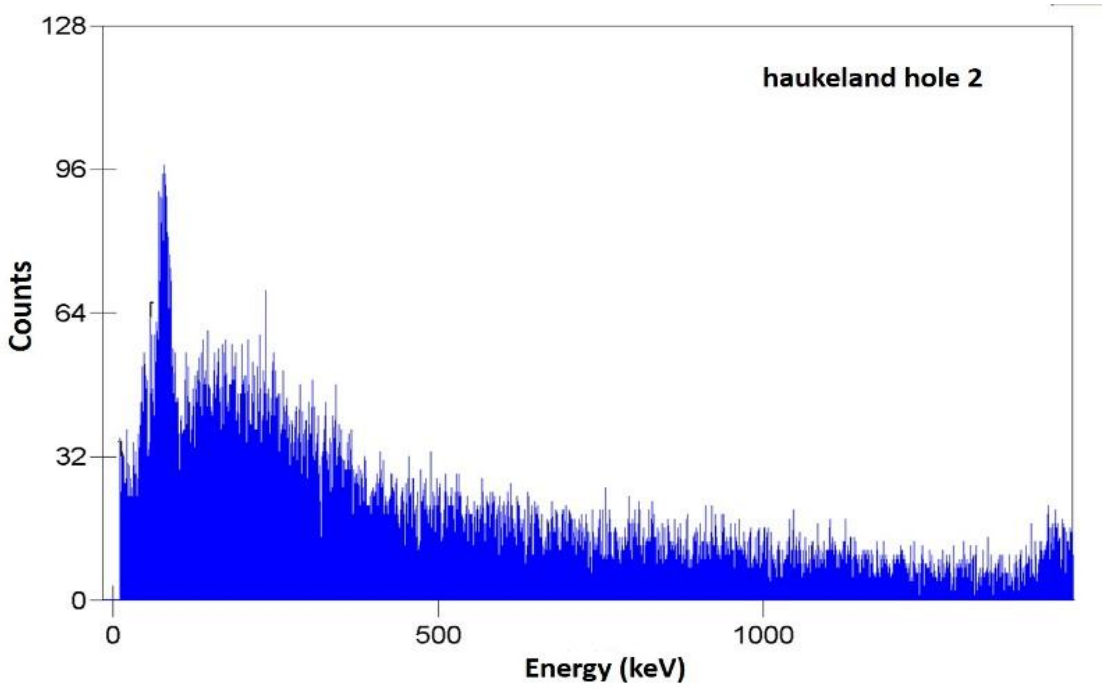

Figure 6.6: area2 hole2, ***Peaks cannot be seen, indicating very low levels of radon.***

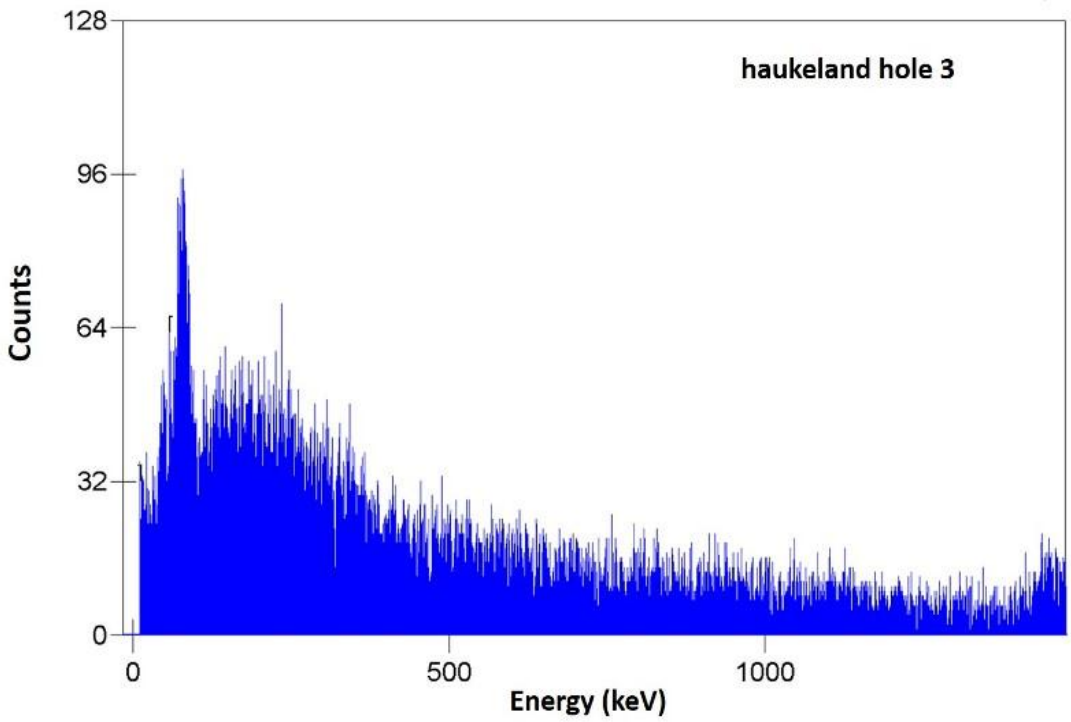

Figure 6.7: area2 hole3, ***Peaks cannot be seen, indicating very low levels of radon.***

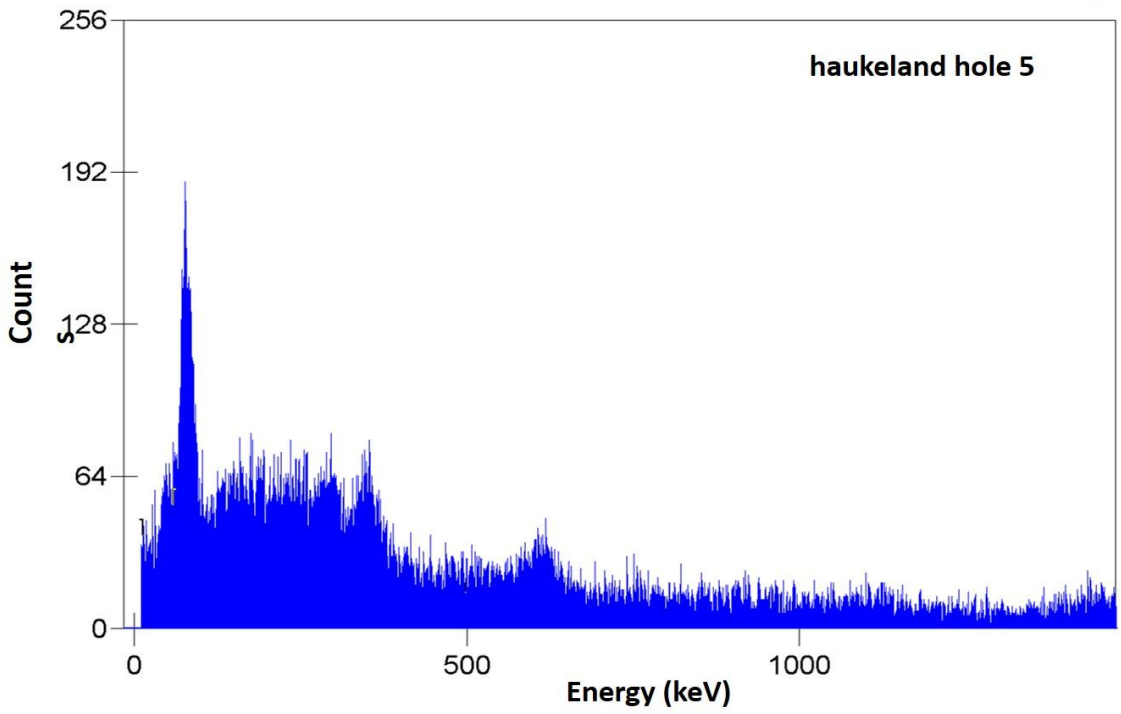

Figure 6.8:area1hole5, ***it is possible to see peaks due to some presence of radon.***

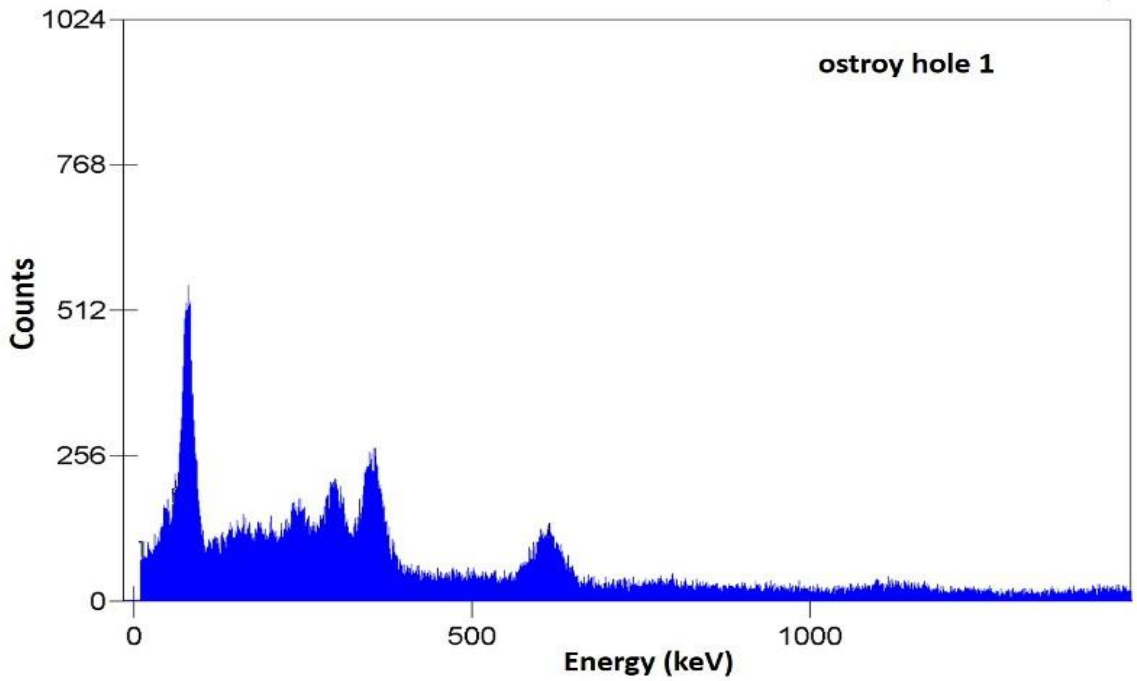

Figure 6.9: area2 hole1, *there are very clear peaks, indicating high level of radon emanation*

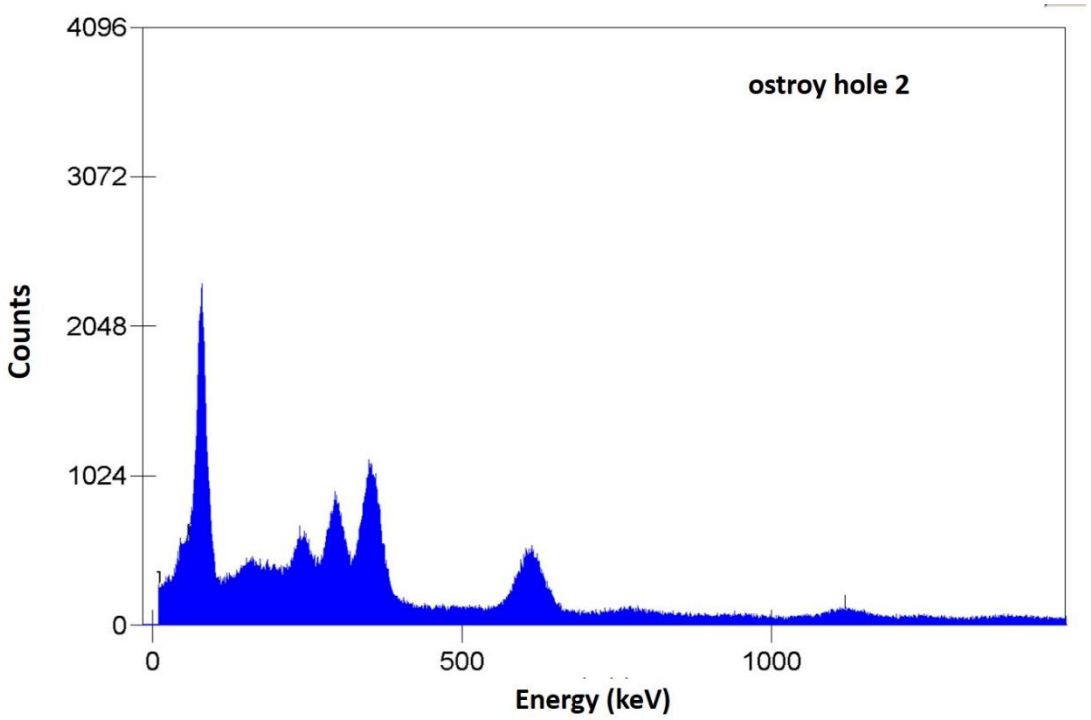

Figure 6.10: ara2 hole2, *very clear peaks, a lot of radon is present.*

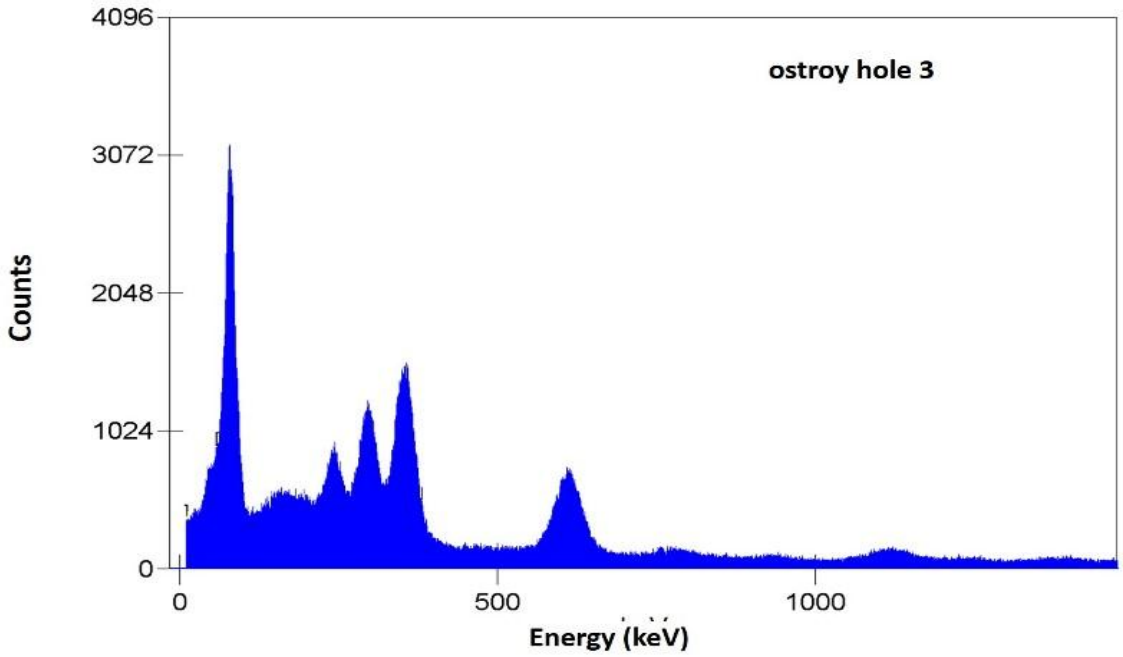

Figure 6.11:area2hole3, *there are very clear peaks. This indicates high level of radon emanation.*

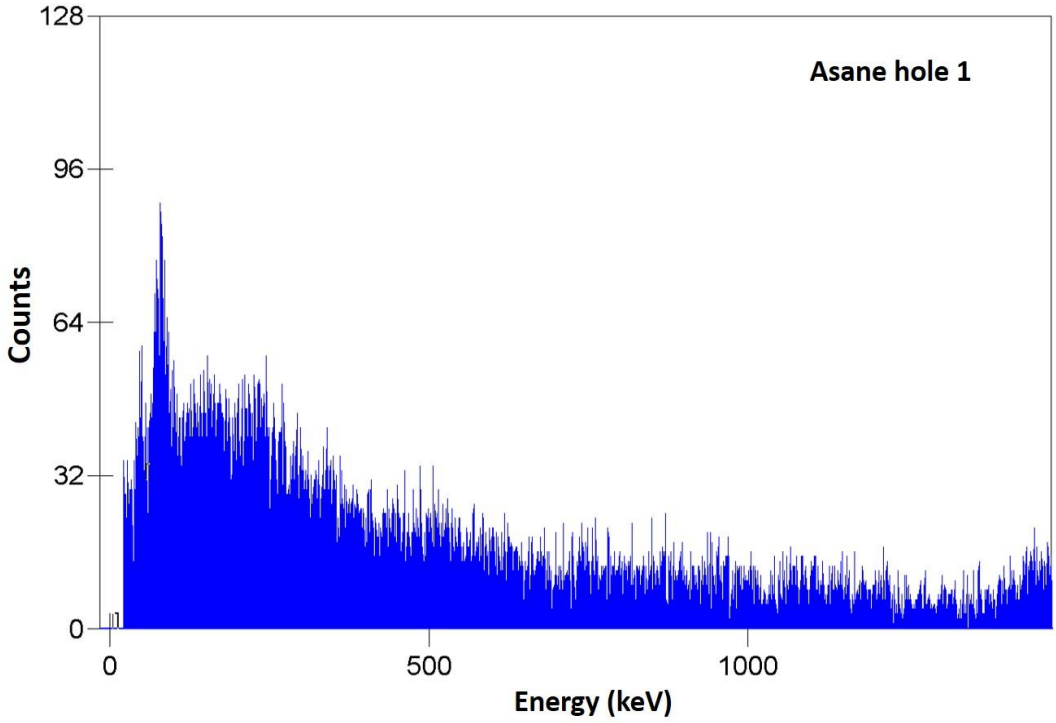

Figure 6.12: area3hole1, ***No peaks to be seen.***

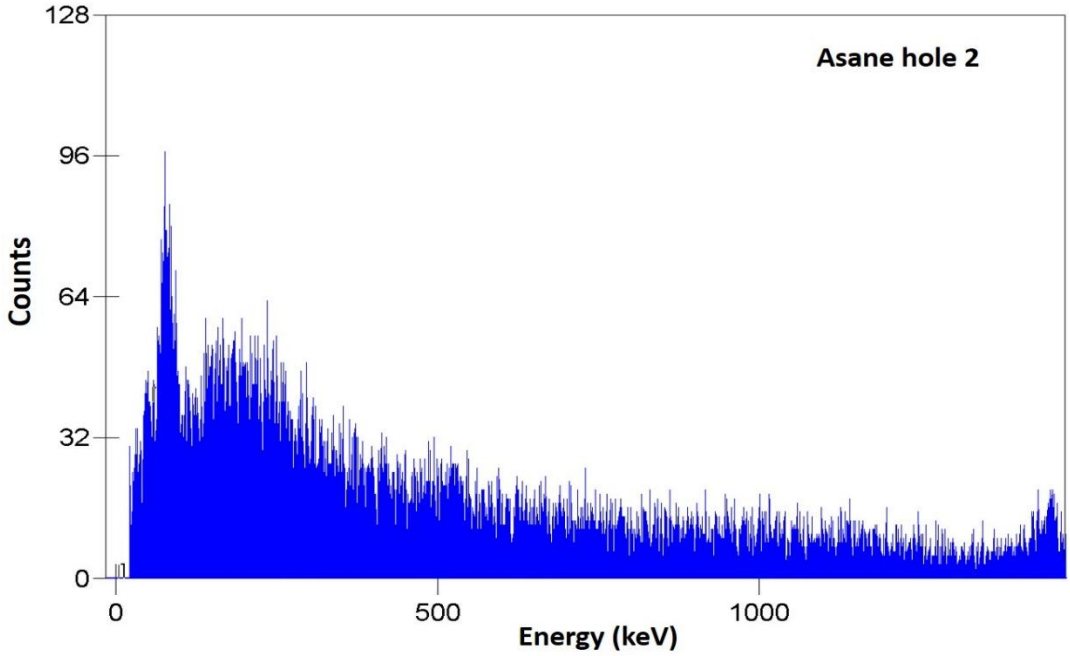

Figure 6.13: *area3 hole2, No peaks can be seen.*

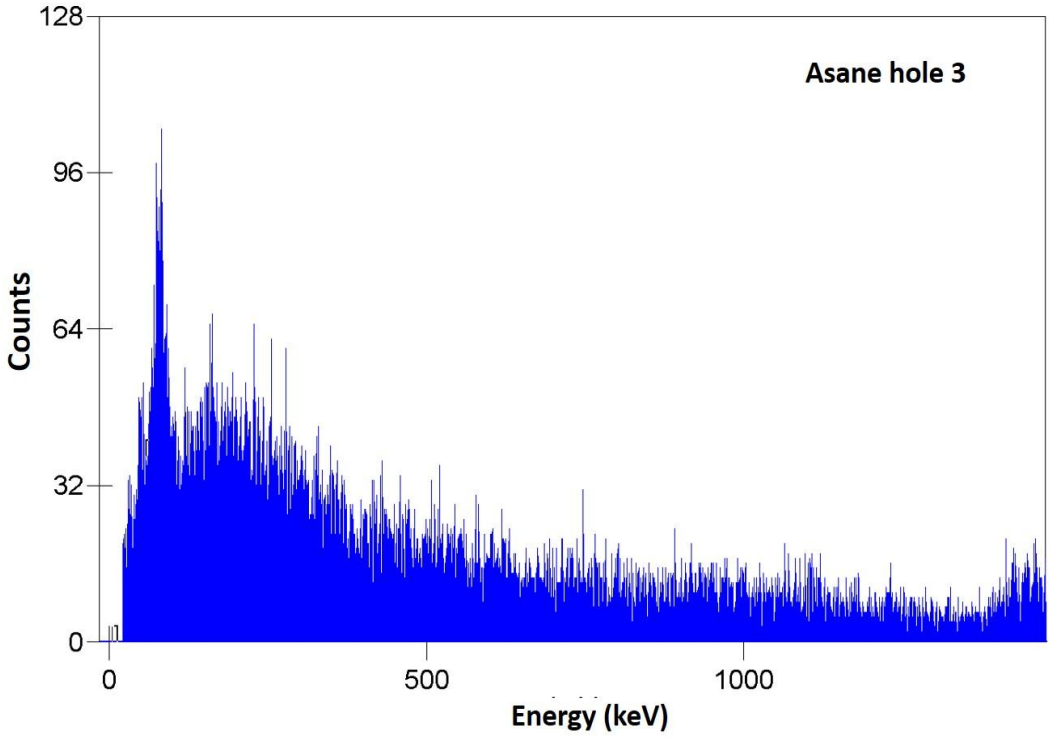

Figure 6.14:area3 hole3, no peaks can be seen.

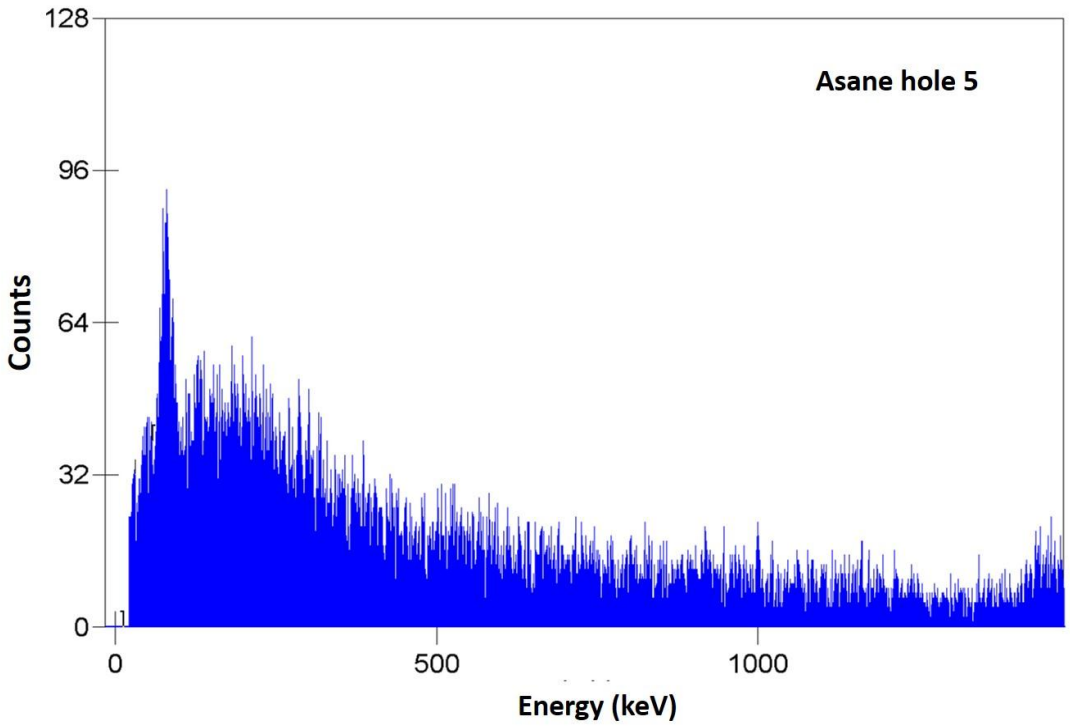

Figure 6.15: area3 hole5, ***No peaks can be seen.***

.

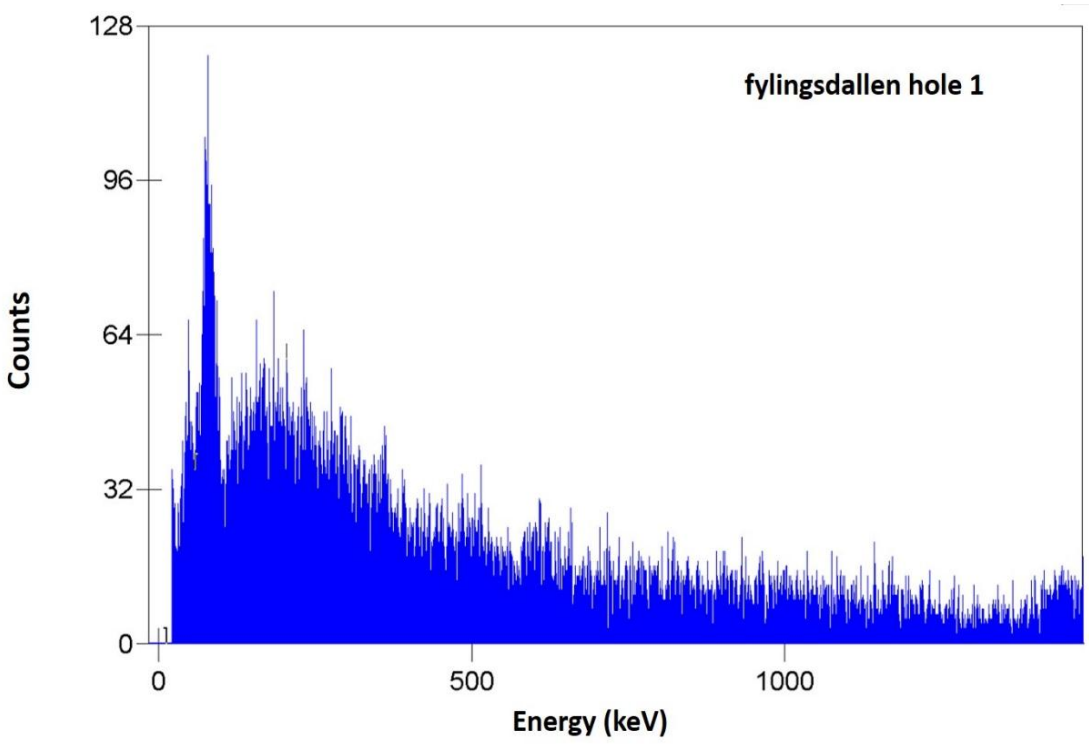

Figure 6.16: area4 hole1, ***No peaks can be seen.***

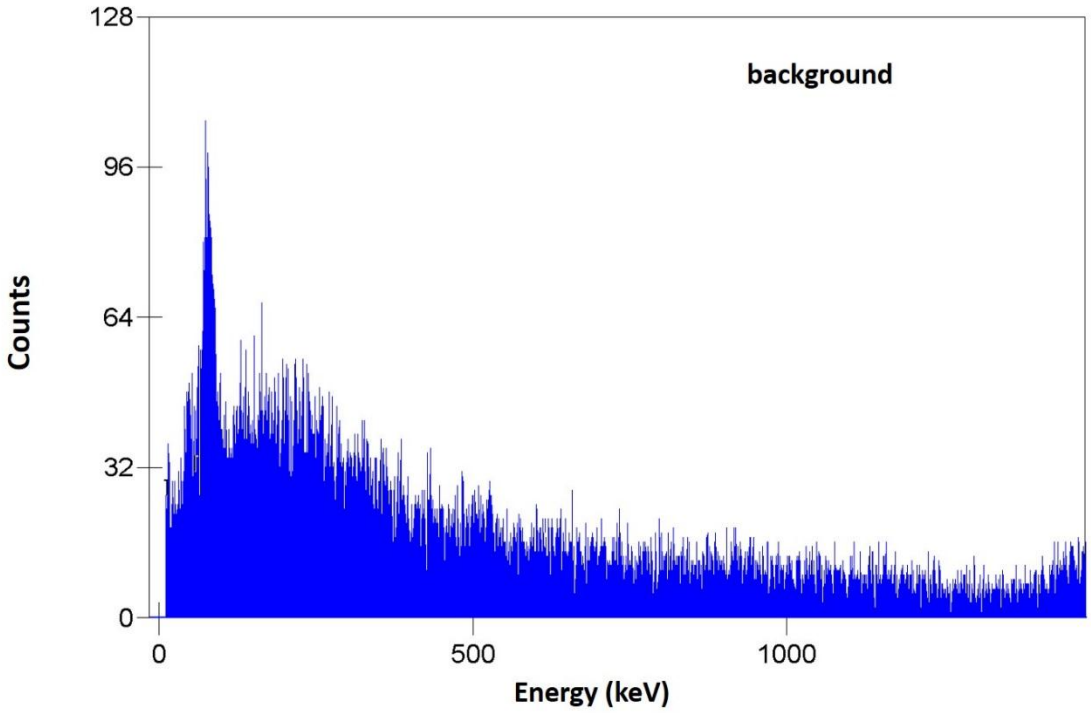

Figure 6.17: Background radiation when no sources are present.

6.10 The relation between radon concentration and temperature gradient.

The results briefly discussed and plotted for a series of radon activity and temperature profiles in boreholes. In this section need to find the correlation between those two measurements. In table 6.7 and 6.8, show no relation between the two-field measurements at 150 m depth, The T remained nearly constant while R measurements showed extreme variation.

Table 6.7: The relation between temperature and radon measurements in area 1, 2, and 3, at average depth 150m.

		$T_{av}\,C^{\circ}$	R(coal box)	R canary
area 1	hole 1	9,90	49,528	
	hole2	9,77	6,380	
	hole 3	9,86	41,525	139
area 2	hole 1	9,08	558,958	
	hole 2	8,96	1974,206	465
	hole 3	8,98	2697,296	
area 3	hole 1	8.80	-0,527	
	hole 2	8.30	3.42	
	hole 3	8.60	2.90	15

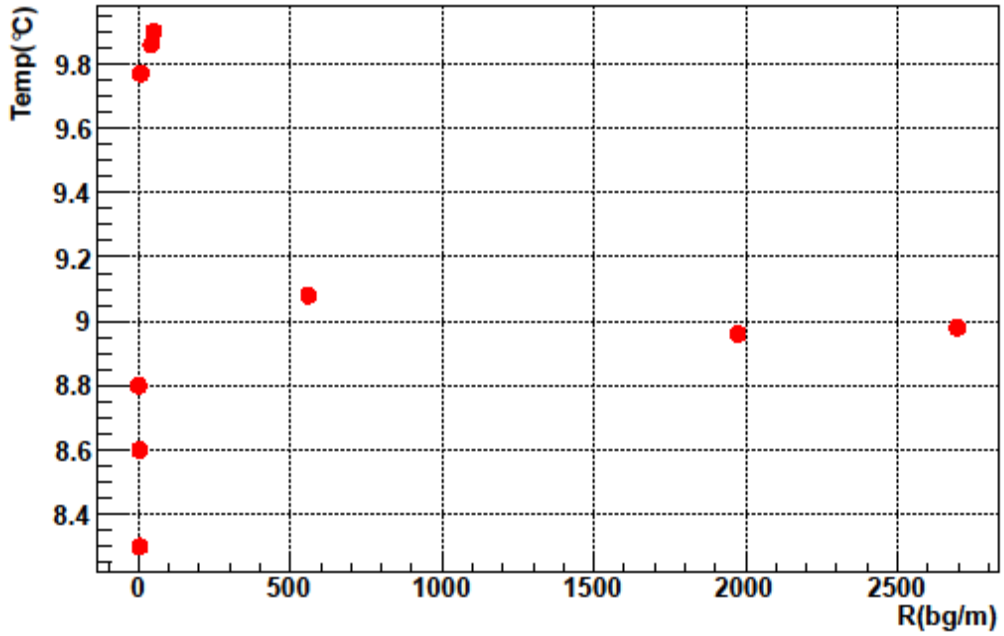

Figure 6.18: The distribution of the measured values of R and T at 150 m depth for area 1, 2, and 3.

Table 6.8: The relation between ΔT/ΔX and R in area1, 2, and 3.

		ΔT/ΔX	R (coalbox)	R (canary)
Area1	hole 1	0,01621	49	139
	hole 2	0,0166	6	
	hole 3	0,01558	41	
Area2	hole 1	0,01395	558	465
	hole 2	0,01474	1974	
	hole 3	0,01266	2697	
Area3	hole 1	0,0134	-0,52	15
	hole 2	0,01585	3	
	hole 3	0,01395	2	

Taking the average radon concentration for each area that measured by using the coal box, with average temperature at 150 m and average thermal gradient with uncertainty on mean. To find any relation between the two measurement.

According to the results in table6.8, no correlation between thermal gradient and radon concentration are observed.

Figure 6.8: the correlation between thermal gradient and radon concentration with the uncertainty.

	R coal box	Tav at 150 m	ΔT/ΔX
Area1	32±11	9,84±0,03	0,0163±0,0003
Area2	1743±544	9,01±0,03	0,0140±0,0005
Area3	1,7±1,2	8,57±0,13	0,0143±0,008

7.Conclusions and discussions

The conclusions are based upon the background information, fieldwork, and results presented in this thesis:

1. Heat generated from decay of naturally radioactive elements, i.e. thorium, uranium and potassium, have a strong influence on heat flow and thermal behavior in the Earth's crust because the presence of these elements varies significantly between different rock types.
2. Radon emanation from the soil varies with soil type and with surface uranium content. All radon isotopes are radioactive and constitute a health hazard.
3. For temperature measurements we have simultaneously performed vertical thermal profiles in the boreholes and estimated thermal gradients.
4. In order to be stable, the thermal gradient must have a constant heat source and available heat sink, in the present research thermal gradient was assumed stable in such areas for all the boreholes.
5. We have corrected the temperature profiles. This has clearly introduced an additional uncertainty. However, this correction is necessary for an unbiased estimate of the temperature at each depth.
6. There is no major variation in temperature gradient underground, it is relatively stable throughout the year.
7. For radon concentration measurements the calibration is done using the canary meter.
8. It is known that the sensitivity of the charcoal boxes change when reused. We have therefore chosen to assign one "K" for each box.
9. We have performed measurements of radon emanating from thermal boreholes in four different locations in the Bergen area.
10. By sealing the holes and measuring radon concentrations as accumulated over three days, we have been able to identify large variations of the amounts of radon emitted in the different locations.
11. Meteorological conditions such as wind, temperature and humidity will affect the results, and we can tentatively assign an overall uncertainty of 30% due to these factors.
12. It has not been possible to identify any correlations between borehole temperatures or thermal gradients and the amount of radon found in the boreholes.

Recommendations to improve similar future research:

- It is necessary to know about the height of water level in borehole before starting to evaluate radon concentration because lower or higher percentage of water in the borehole affected the proportion of radon concentration.

- Measurement of radon concentration in different seasons, specify and extend the duration of the measurement to get the best results.

- Choose different depths in a certain area to compare the results obtained.

- Measurement of short radon activity in water and air borehole to find the effect on radon concentration by these two different environments.

- It is better to collect several samples in one area at different times during the year, so the overall conditions may be better understood.

Appendices

Appendix A

Temperature profile in boreholes

Table 7.1 temperature measurement in area1 hole 1

depth	T1	T2	T3	T4	T5	T6	Tav	derivative	correction	corrected T	**Deviation from real T**
0	11,70	11,57	11,46	11,35	11,25	11,15	11,413	-0,011	2,2	9,213	8,413
5	11,06	10,99	10,93	10,88	10,83	10,79	10,913	-0,0054	1,08	9,833	9,033
10	10,73	10,68	10,62	10,57	10,52	10,47	10,598	-0,0052	1,04	9,558	8,758
15	10,43	10,39	10,34	10,28	10,22	10,16	10,303	-0,0054	1,08	9,223	8,423
20	10,09	10,02	9,97	9,91	9,86	9,82	9,945	-0,0054	1,08	8,865	8,065
25	9,77	9,73	9,68	9,65	9,61	9,58	9,670	-0,0038	0,76	8,910	8,110
30	9,54	9,52	9,49	9,46	9,44	9,42	9,478	-0,0024	0,48	8,998	8,198
35	9,39	9,37	9,35	9,33	9,32	9,3	9,343	-0,0018	0,36	8,983	8,183
40	9,28	9,27	9,25	9,24	9,23	9,22	9,248	-0,0012	0,24	9,008	8,208
45	9,20	9,19	9,18	9,18	9,17	9,16	9,180	-0,0008	0,16	9,020	8,220
50	9,15	9,14	9,13	9,13	9,12	9,12	9,132	-0,0006	0,12	9,012	8,212
55	9,11	9,11	9,10	9,10	9,09	9,09	9,100	-0,0004	0,08	9,020	8,220
60	9,09	9,09	9,08	9,08	9,08	9,08	9,083	-0,0002	0,04	9,043	8,243
65	9,08	9,08	9,08	9,08	9,08	9,08	9,080	0	0	9,080	8,280
70	9,08	9,08	9,08	9,08	9,08	9,08	9,080	0	0	9,080	8,280
75	9,09	9,09	9,09	9,09	9,10	9,10	9,093	0,0002	-0,04	9,133	8,333
80	9,10	9,11	9,11	9,11	9,12	9,12	9,112	0,0004	-0,08	9,192	8,392
85	9,13	9,13	9,13	9,14	9,14	9,15	9,137	0,0004	-0,08	9,217	8,417
90	9,15	9,16	9,16	9,17	9,18	9,18	9,167	0,0006	-0,12	9,287	8,487
95	9,18	9,19	9,20	9,20	9,21	9,21	9,198	0,0006	-0,12	9,318	8,518
100	9,22	9,22	9,23	9,24	9,25	9,25	9,235	0,0006	-0,12	9,355	8,555
105	9,26	9,27	9,27	9,28	9,29	9,3	9,278	0,0008	-0,16	9,438	8,638
110	9,31	9,32	9,33	9,34	9,35	9,36	9,335	0,001	-0,2	9,535	8,735
115	9,37	9,39	9,40	9,41	9,43	9,44	9,407	0,0014	-0,28	9,687	8,887
120	9,45	9,47	9,48	9,49	9,50	9,51	9,483	0,0012	-0,24	9,723	8,923
125	9,52	9,53	9,54	9,56	9,57	9,58	9,550	0,0012	-0,24	9,790	8,990
130	9,59	9,60	9,61	9,63	9,63	9,65	9,618	0,0012	-0,24	9,858	9,058
135	9,66	9,67	9,68	9,69	9,71	9,72	9,688	0,0012	-0,24	9,928	9,128
140	9,73	9,74	9,76	9,77	9,78	9,79	9,762	0,0012	-0,24	10,002	9,202
145	9,80	9,82	9,83	9,84	9,85	9,86	9,833	0,0012	-0,24	10,073	9,273
150	9,87	9,88	9,89	9,91	9,92	9,93	9,900	0,0012	-0,24	10,140	9,340
155	9,94	9,95	9,96	9,98	9,98	10,00	9,968	0,0012	-0,24	10,208	9,408
160	10,01	10,02	10,03	10,04	10,05	10,07	10,037	0,0012	-0,24	10,277	9,477
165	10,08	10,09	10,10	10,12	10,13	10,14	10,110	0,0012	-0,24	10,350	9,550
170	10,16	10,17	10,18	10,19	10,21	10,22	10,188	0,0012	-0,24	10,428	9,628
175	10,24	10,25	10,27	10,28	10,30	10,31	10,275	0,0014	-0,28	10,555	9,755
180	10,33	10,35	10,36	10,38	10,39	10,41	10,370	0,0016	-0,32	10,690	9,890
185	10,42	10,44	10,45	10,47	10,48	10,49	10,458	0,0014	-0,28	10,738	9,938
190	10,51	10,52	10,53	10,55	10,56	10,57	10,540	0,0012	-0,24	10,780	9,980
195	10,59	10,60	10,62	10,63	10,64	10,66	10,623	0,0014	-0,28	10,903	10,103
200	10,67	10,68	10,70	10,71	10,72	10,74	10,703	0,0014	-0,28	10,983	10,183

205	10,75	10,77	10,78	10,79	10,81	10,82	10,787	0,0014	-0,28	11,067	10,267
210	10,83	10,85	10,86	10,88	10,89	10,90	10,868	0,0014	-0,28	11,148	10,348
215	10,92	10,94	10,95	10,97	10,98	11,00	10,960	0,0016	-0,32	11,280	10,480
220	11,01	11,03	11,04	11,06	11,07	11,09	11,050	0,0016	-0,32	11,370	10,570
225	11,10	11,12	11,13	11,14	11,16	11,16	11,135	0,0012	-0,24	11,375	10,575
230	11,18	11,19	11,20	11,21	11,22	11,23	11,205	0,001	-0,2	11,405	10,605
235	11,24	11,25	11,25	11,26	11,27	11,27	11,257	0,0006	-0,12	11,377	10,577
240	11,28	11,28	11,29	11,29	11,30	11,30	11,290	0,0004	-0,08	11,370	10,570
245	11,30	11,31	11,31	11,31	11,32	11,32	11,312	0,0004	-0,08	11,392	10,592
250	11,32	11,32	11,33	11,33	11,33	11,33	11,327	0,0002	-0,04	11,367	10,567

Table 7.2 temperature measurement in area1 hole 2

depth	T1	T2	T3	Tav	derivative	correction	corrected T	**Deviation from real T**
0	10,03	9,99	9,94	9,987	-0,0045	0,90000	9,087	8,287
5	9,89	9,85	9,80	9,847	-0,0045	0,90000	8,947	8,147
10	9,76	9,72	9,68	9,720	-0,004	0,80000	8,920	8,120
15	9,65	9,63	9,60	9,627	-0,0025	0,50000	9,127	8,327
20	9,57	9,55	9,52	9,547	-0,0025	0,50000	9,047	8,247
25	9,50	9,48	9,46	9,480	-0,002	0,40000	9,080	8,280
30	9,44	9,43	9,41	9,427	-0,0015	0,30000	9,127	8,327
35	9,39	9,38	9,37	9,380	-0,001	0,20000	9,180	8,380
40	9,35	9,34	9,33	9,340	-0,001	0,20000	9,140	8,340
45	9,32	9,31	9,29	9,307	-0,0015	0,30000	9,007	8,207
50	9,29	9,28	9,27	9,280	-0,001	0,20000	9,080	8,280
55	9,27	9,26	9,25	9,260	-0,001	0,20000	9,060	8,260
60	9,25	9,25	9,24	9,247	-0,0005	0,10000	9,147	8,347
65	9,24	9,24	9,23	9,237	-0,0005	0,10000	9,137	8,337
70	9,23	9,23	9,23	9,230	0	0,00000	9,230	8,430
75	9,23	9,23	9,23	9,230	0	0,00000	9,230	8,430
80	9,24	9,24	9,24	9,240	0	0,00000	9,240	8,440
85	9,25	9,25	9,26	9,253	0,0005	-0,10000	9,353	8,553
90	9,26	9,27	9,27	9,267	0,0005	-0,10000	9,367	8,567
95	9,28	9,28	9,29	9,283	0,0005	-0,10000	9,383	8,583
100	9,30	9,31	9,32	9,310	0,001	-0,20000	9,510	8,710
105	9,32	9,33	9,34	9,330	0,001	-0,20000	9,530	8,730
110	9,35	9,37	9,38	9,367	0,0015	-0,30000	9,667	8,867
115	9,39	9,40	9,42	9,403	0,0015	-0,30000	9,703	8,903
120	9,43	9,44	9,45	9,440	0,001	-0,20000	9,640	8,840
125	9,47	9,49	9,50	9,487	0,0015	-0,30000	9,787	8,987
130	9,52	9,54	9,55	9,537	0,0015	-0,30000	9,837	9,037
135	9,57	9,59	9,61	9,590	0,002	-0,40000	9,990	9,190
140	9,63	9,65	9,67	9,650	0,002	-0,40000	10,050	9,250
145	9,69	9,71	9,74	9,713	0,0025	-0,50000	10,213	9,413
150	9,75	9,78	9,80	9,777	0,0025	-0,50000	10,277	9,477
155	9,82	9,84	9,86	9,840	0,002	-0,40000	10,240	9,440
160	9,89	9,91	9,93	9,910	0,002	-0,40000	10,310	9,510
165	9,95	9,98	10,00	9,977	0,0025	-0,50000	10,477	9,677
170	10,03	10,05	10,08	10,053	0,0025	-0,50000	10,553	9,753
175	10,10	10,12	10,15	10,123	0,0025	-0,50000	10,623	9,823

180	10,17	10,20	10,23	10,200	0,003	-0,60000	10,800	10,000
185	10,25	10,28	10,31	10,280	0,003	-0,60000	10,880	10,080
190	10,34	10,36	10,39	10,363	0,0025	-0,50000	10,863	10,063
195	10,42	10,45	10,48	10,450	0,003	-0,60000	11,050	10,250
200	10,51	10,54	10,57	10,540	0,003	-0,60000	11,140	10,340
205	10,60	10,63	10,66	10,630	0,003	-0,60000	11,230	10,430
210	10,68	10,71	10,74	10,710	0,003	-0,60000	11,310	10,510
215	10,77	10,80	10,82	10,797	0,0025	-0,50000	11,297	10,497
220	10,85	10,88	10,90	10,877	0,0025	-0,50000	11,377	10,577
225	10,93	10,95	10,98	10,953	0,0025	-0,50000	11,453	10,653
230	11,00	11,02	11,05	11,023	0,0025	-0,50000	11,523	10,723
235	11,07	11,09	11,10	11,087	0,0015	-0,30000	11,387	10,587
240	11,12	11,13	11,14	11,130	0,001	-0,20000	11,330	10,530
245	11,15	11,16	11,16	11,157	0,0005	-0,10000	11,257	10,457
250	11,16	11,16	11,15	11,157	-0,0005	0,10000	11,057	10,257

Table 7.3 temperature measurement in area1 hole 3

depth	T1	T2	T3	Tav	derivative	correction	corrected T	**Deviation from real T**
0	12,45	12,31	12,17	12,310	-0,014	2,8	9,510	8,710
5	12,05	11,92	11,80	11,923	-0,0125	2,5	9,423	8,623
10	11,68	11,57	11,47	11,573	-0,0105	2,1	9,473	8,673
15	11,36	11,26	11,17	11,263	-0,0095	1,9	9,363	8,563
20	11,08	10,99	10,91	10,993	-0,0085	1,7	9,293	8,493
25	10,83	10,75	10,67	10,750	-0,008	1,6	9,150	8,350
30	10,60	10,53	10,47	10,533	-0,0065	1,3	9,233	8,433
35	10,41	10,35	10,29	10,350	-0,006	1,2	9,150	8,350
40	10,24	10,19	10,14	10,190	-0,005	1	9,190	8,390
45	10,09	10,05	10,00	10,047	-0,0045	0,9	9,147	8,347
50	9,96	9,92	9,89	9,923	-0,0035	0,7	9,223	8,423
55	9,86	9,82	9,80	9,827	-0,003	0,6	9,227	8,427
60	9,77	9,74	9,71	9,740	-0,003	0,6	9,140	8,340
65	9,69	9,67	9,65	9,670	-0,002	0,4	9,270	8,470
70	9,63	9,62	9,60	9,617	-0,0015	0,3	9,317	8,517
75	9,59	9,57	9,56	9,573	-0,0015	0,3	9,273	8,473
80	9,55	9,54	9,54	9,543	-0,0005	0,1	9,443	8,643
85	9,53	9,52	9,52	9,523	-0,0005	0,1	9,423	8,623
90	9,52	9,51	9,51	9,513	-0,0005	0,1	9,413	8,613
95	9,51	9,51	9,51	9,510	0	0	9,510	8,710
100	9,51	9,52	9,52	9,517	0,0005	-0,1	9,617	8,817
105	9,52	9,52	9,53	9,523	0,0005	-0,1	9,623	8,823
110	9,54	9,54	9,55	9,543	0,0005	-0,1	9,643	8,843
115	9,56	9,57	9,57	9,567	0,0005	-0,1	9,667	8,867
120	9,58	9,60	9,60	9,593	0,001	-0,2	9,793	8,993
125	9,62	9,63	9,64	9,630	0,001	-0,2	9,830	9,030
130	9,65	9,66	9,68	9,663	0,0015	-0,3	9,963	9,163
135	9,69	9,70	9,72	9,703	0,0015	-0,3	10,003	9,203
140	9,74	9,75	9,77	9,753	0,0015	-0,3	10,053	9,253
145	9,79	9,80	9,82	9,803	0,0015	-0,3	10,103	9,303

150	9,84	9,86	9,88	9,860	0,002	-0,4	10,260	9,460
155	9,90	9,92	9,94	9,920	0,002	-0,4	10,320	9,520
160	9,96	9,98	10,01	9,983	0,0025	-0,5	10,483	9,683
165	10,03	10,05	10,08	10,053	0,0025	-0,5	10,553	9,753
170	10,10	10,12	10,15	10,123	0,0025	-0,5	10,623	9,823
175	10,17	10,19	10,22	10,193	0,0025	-0,5	10,693	9,893
180	10,23	10,25	10,27	10,250	0,002	-0,4	10,650	9,850
185	10,30	10,31	10,34	10,317	0,002	-0,4	10,717	9,917
190	10,36	10,38	10,41	10,383	0,0025	-0,5	10,883	10,083
195	10,43	10,45	10,48	10,453	0,0025	-0,5	10,953	10,153
200	10,50	10,53	10,55	10,527	0,0025	-0,5	11,027	10,227
205	10,58	10,60	10,63	10,603	0,0025	-0,5	11,103	10,303
210	10,66	10,68	10,71	10,683	0,0025	-0,5	11,183	10,383
215	10,73	10,76	10,79	10,760	0,003	-0,6	11,360	10,560
220	10,81	10,84	10,87	10,840	0,003	-0,6	11,440	10,640
225	10,89	10,92	10,95	10,920	0,003	-0,6	11,520	10,720
230	10,97	10,99	11,02	10,993	0,0025	-0,5	11,493	10,693
235	11,04	11,06	11,08	11,060	0,002	-0,4	11,460	10,660
240	11,10	11,11	11,13	11,113	0,0015	-0,3	11,413	10,613
245	11,14	11,16	11,16	11,153	0,001	-0,2	11,353	10,553
250	11,17	11,17	11,17	11,170	0	0	11,170	10,370

Table 7.4 temperature measurement in area2 hole1

depth	t1	t2	t3	t4	t5	t6	av	deritive	corection	corected T	deviation
0	6,42	6,30	6,16	6,05	5,96	5,91	6,133	-0,0102	2,04	4,093	3,293
5	5,87	5,84	5,83	5,82	5,83	5,83	5,837	-0,0008	0,16	5,677	4,877
10	5,84	5,84	5,85	5,88	5,94	6,02	5,895	0,0036	-0,72	6,615	5,815
15	6,11	6,19	6,27	6,23	6,43	6,51	6,290	0,008	-1,6	7,890	7,090
20	6,58	6,64	6,7	6,76	6,82	6,87	6,728	0,0058	-1,16	7,888	7,088
25	6,92	6,97	7,02	7,06	7,09	7,13	7,032	0,0042	-0,84	7,872	7,072
30	7,17	7,2	7,23	7,26	7,28	7,31	7,242	0,0028	-0,56	7,802	7,002
35	7,33	7,36	7,38	7,4	7,42	7,44	7,388	0,0022	-0,44	7,828	7,028
40	7,46	7,47	7,49	7,51	7,52	7,54	7,498	0,0016	-0,32	7,818	7,018
45	7,55	7,57	7,58	7,59	7,61	7,62	7,587	0,0014	-0,28	7,867	7,067
50	7,64	7,65	7,67	7,68	7,69	7,71	7,673	0,0014	-0,28	7,953	7,153
55	7,72	7,73	7,74	7,76	7,77	7,78	7,750	0,0012	-0,24	7,990	7,190
60	7,79	7,81	7,82	7,83	7,84	7,86	7,825	0,0014	-0,28	8,105	7,305
65	7,78	7,89	7,90	7,91	7,93	7,94	7,892	0,0032	-0,64	8,532	7,732
70	7,96	7,97	7,99	8,00	8,02	8,03	7,995	0,0014	-0,28	8,275	7,475
75	8,04	8,05	8,06	8,07	8,08	8,09	8,065	0,001	-0,2	8,265	7,465
80	8,10	8,11	8,12	8,13	8,14	8,15	8,125	0,001	-0,2	8,325	7,525
85	8,17	8,18	8,18	8,20	8,21	8,22	8,193	0,001	-0,2	8,393	7,593
90	8,23	8,24	8,25	8,26	8,27	8,28	8,255	0,001	-0,2	8,455	7,655
95	8,29	8,30	8,31	8,32	8,33	8,34	8,315	0,001	-0,2	8,515	7,715
100	8,35	8,37	8,38	8,39	8,40	8,41	8,383	0,0012	-0,24	8,623	7,823
105	8,42	8,43	8,44	8,46	8,47	8,48	8,450	0,0012	-0,24	8,690	7,890
110	8,48	8,50	8,51	8,52	8,53	8,55	8,515	0,0014	-0,28	8,795	7,995
115	8,56	8,56	8,58	8,59	8,60	8,61	8,583	0,001	-0,2	8,783	7,983

120	8,62	8,63	8,64	8,66	8,67	8,68	8,650	0,0012	-0,24	8,890	8,090
125	8,69	8,70	8,72	8,72	8,73	8,75	8,718	0,0012	-0,24	8,958	8,158
130	8,76	8,77	8,78	8,79	8,80	8,82	8,787	0,0012	-0,24	9,027	8,227
135	8,83	8,84	8,85	8,87	8,88	8,89	8,860	0,0012	-0,24	9,100	8,300
140	8,90	8,92	8,93	8,94	8,95	8,97	8,935	0,0014	-0,28	9,215	8,415
145	8,98	8,99	9,00	9,01	9,03	9,04	9,008	0,0012	-0,24	9,248	8,448
150	9,05	9,06	9,08	9,09	9,10	9,11	9,082	0,0012	-0,24	9,322	8,522
155	9,13	9,14	9,15	9,16	9,17	9,18	9,155	0,001	-0,2	9,355	8,555
160	9,18	9,19	9,20	9,20	9,21	9,23	9,202	0,001	-0,2	9,402	8,602
165	9,24	9,26	9,27	9,29	9,31	9,33	9,283	0,0018	-0,36	9,643	8,843
170	9,34	9,36	9,38	9,40	9,42	9,43	9,388	0,0018	-0,36	9,748	8,948
175	9,45	9,46	9,48	9,49	9,50	9,52	9,483	0,0014	-0,28	9,763	8,963
180	9,53	9,54	9,55	9,56	9,57	9,57	9,553	0,0008	-0,16	9,713	8,913

Table 7.5 temperature measurement in area2 hole2

depth	t1	t2	t3	tav	deritive	corection	corected T	deviation
0	8,30	8,27	8,24	8,270	-0,003	0,6	7,670	6,870
5	8,21	8,18	8,15	8,180	-0,003	0,6	7,580	6,780
10	8,12	8,10	8,08	8,100	-0,002	0,4	7,700	6,900
15	8,06	8,04	8,03	8,043	-0,0015	0,3	7,743	6,943
20	8,01	8,00	7,99	8,000	-0,001	0,2	7,800	7,000
25	7,99	7,98	7,98	7,983	-0,0005	0,1	7,883	7,083
30	7,97	7,97	7,97	7,970	0	0	7,970	7,170
35	7,98	7,98	7,99	7,983	0,0005	-0,1	8,083	7,283
40	7,99	8,00	8,01	8,000	0,001	-0,2	8,200	7,400
45	8,01	8,02	8,04	8,023	0,0015	-0,3	8,323	7,523
50	8,05	8,06	8,08	8,063	0,0015	-0,3	8,363	7,563
55	8,09	8,10	8,12	8,103	0,0015	-0,3	8,403	7,603
60	8,13	8,15	8,17	8,150	0,002	-0,4	8,550	7,750
65	8,18	8,20	8,22	8,200	0,002	-0,4	8,600	7,800
70	8,23	8,25	8,27	8,250	0,002	-0,4	8,650	7,850
75	8,28	8,30	8,32	8,300	0,002	-0,4	8,700	7,900
80	8,34	8,35	8,37	8,353	0,0015	-0,3	8,653	7,853
85	8,39	8,41	8,43	8,410	0,002	-0,4	8,810	8,010
90	8,44	8,46	8,48	8,460	0,002	-0,4	8,860	8,060
95	8,49	8,51	8,53	8,510	0,002	-0,4	8,910	8,110
100	8,55	8,56	8,58	8,563	0,0015	-0,3	8,863	8,063
105	8,60	8,61	8,63	8,613	0,0015	-0,3	8,913	8,113
110	8,64	8,66	8,68	8,660	0,002	-0,4	9,060	8,260
115	8,69	8,71	8,72	8,707	0,0015	-0,3	9,007	8,207
120	8,73	8,75	8,76	8,747	0,0015	-0,3	9,047	8,247
125	8,78	8,79	8,80	8,790	0,001	-0,2	8,990	8,190
130	8,81	8,83	8,84	8,827	0,0015	-0,3	9,127	8,327
135	8,85	8,86	8,87	8,860	0,001	-0,2	9,060	8,260
140	8,87	8,89	8,90	8,887	0,0015	-0,3	9,187	8,387
145	8,91	8,92	8,94	8,923	0,0015	-0,3	9,223	8,423
150	8,95	8,96	8,98	8,963	0,0015	-0,3	9,263	8,463
155	8,99	9,00	9,02	9,003	0,0015	-0,3	9,303	8,503
160	9,03	9,04	9,06	9,043	0,0015	-0,3	9,343	8,543
165	9,08	9,11	9,15	9,113	0,0035	-0,7	9,813	9,013
170	9,18	9,22	9,25	9,217	0,0035	-0,7	9,917	9,117

175	9,28	9,31	9,33	9,307	0,0025	-0,5	9,807	9,007
180	9,35	9,37	9,39	9,370	0,002	-0,4	9,770	8,970

Table 7.6 temperature measurement in area2 hole3

depth	t1	t2	t3	av	deritive	corection	corected T	deviation
o	8,42	8,44	8,44	8,433	0,001	-0,2	8,633	7,833
5	8,43	8,42	8,40	8,417	-0,0015	0,3	8,117	7,317
10	8,37	8,31	8,24	8,307	-0,0065	1,3	7,007	6,207
15	8,18	8,12	8,07	8,123	-0,0055	1,1	7,023	6,223
20	8,03	7,99	7,96	7,993	-0,0035	0,7	7,293	6,493
25	7,93	7,91	7,90	7,913	-0,0015	0,3	7,613	6,813
30	7,88	7,87	7,86	7,870	-0,001	0,2	7,670	6,870
35	7,85	7,84	7,84	7,843	-0,0005	0,1	7,743	6,943
40	7,84	7,84	7,84	7,840	0	0	7,840	7,040
45	7,84	7,84	7,85	7,843	0,0005	-0,1	7,943	7,143
50	7,85	7,86	7,87	7,860	0,001	-0,2	8,060	7,260
55	7,87	7,89	7,90	7,887	0,0015	-0,3	8,187	7,387
60	7,92	7,94	7,96	7,940	0,002	-0,4	8,340	7,540
65	7,98	8,00	8,02	8,000	0,002	-0,4	8,400	7,600
70	8,04	8,06	8,08	8,060	0,002	-0,4	8,460	7,660
75	8,10	8,12	8,14	8,120	0,002	-0,4	8,520	7,720
80	8,16	8,18	8,21	8,183	0,0025	-0,5	8,683	7,883
85	8,23	8,25	8,27	8,250	0,002	-0,4	8,650	7,850
90	8,29	8,31	8,33	8,310	0,002	-0,4	8,710	7,910
95	8,36	8,38	8,40	8,380	0,002	-0,4	8,780	7,980
100	8,42	8,45	8,47	8,447	0,0025	-0,5	8,947	8,147
105	8,49	8,51	8,53	8,510	0,002	-0,4	8,910	8,110
110	8,55	8,56	8,59	8,567	0,002	-0,4	8,967	8,167
115	8,60	8,62	8,64	8,620	0,002	-0,4	9,020	8,220
120	8,66	8,68	8,70	8,680	0,002	-0,4	9,080	8,280
125	8,72	8,74	8,76	8,740	0,002	-0,4	9,140	8,340
130	8,78	8,8	8,81	8,797	0,0015	-0,3	9,097	8,297
135	8,83	8,85	8,87	8,850	0,002	-0,4	9,250	8,450
140	8,88	8,90	8,92	8,900	0,002	-0,4	9,300	8,500
145	8,93	8,95	8,96	8,947	0,0015	-0,3	9,247	8,447
150	8,97	8,98	9,00	8,983	0,0015	-0,3	9,283	8,483
155	9,02	9,04	9,06	9,040	0,002	-0,4	9,440	8,640
160	9,08	9,10	9,12	9,100	0,002	-0,4	9,500	8,700
165	9,14	9,16	9,18	9,160	0,002	-0,4	9,560	8,760
170	9,20	9,22	9,24	9,220	0,002	-0,4	9,620	8,820
175	9,26	9,28	9,30	9,280	0,002	-0,4	9,680	8,880
180	9,32	9,34	9,36	9,340	0,002	-0,4	9,740	8,940

Table 7.7 temperature measurement in area3 hole1

depth	t1	t2	t3	t4	t5	t6	tav	deritive	correction	corrected T	deviation
0	7,00	6,99	6,98	6,97	6,97	6,97	6,98	-0,001	0,12	6,860	6,060
5	6,96	6,96	6,96	6,96	6,96	6,96	6,96	0,000	0	6,960	6,160
10	6,96	6,97	6,97	6,97	6,98	6,98	6,972	0,000	-0,08	7,052	6,252
15	6,98	6,99	6,99	7,00	7,00	7,01	6,995	0,001	-0,12	7,115	6,315
20	7,01	7,02	7,03	7,03	7,04	7,04	7,028	0,001	-0,12	7,148	6,348
25	7,05	7,06	7,07	7,08	7,08	7,09	7,072	0,001	-0,16	7,232	6,432
30	7,10	7,11	7,12	7,12	7,13	7,14	7,120	0,001	-0,16	7,280	6,480
35	7,15	7,16	7,17	7,17	7,18	7,19	7,170	0,001	-0,16	7,330	6,530
40	7,20	7,21	7,22	7,23	7,24	7,25	7,225	0,001	-0,2	7,425	6,625
45	7,26	7,28	7,29	7,30	7,31	7,32	7,293	0,001	-0,24	7,533	6,733
50	7,33	7,34	7,35	7,36	7,37	7,38	7,355	0,001	-0,2	7,555	6,755
55	7,39	7,41	7,42	7,43	7,45	7,46	7,427	0,001	-0,28	7,707	6,907
60	7,47	7,49	7,50	7,51	7,53	7,54	7,507	0,001	-0,28	7,787	6,987
65	7,55	7,56	7,58	7,59	7,60	7,62	7,583	0,001	-0,28	7,863	7,063
70	7,63	7,64	7,65	7,67	7,68	7,69	7,660	0,001	-0,24	7,900	7,100
75	7,71	7,72	7,73	7,74	7,76	7,77	7,738	0,001	-0,24	7,978	7,178
80	7,78	7,80	7,81	7,83	7,84	7,86	7,820	0,002	-0,32	8,140	7,340
85	7,87	7,89	7,90	7,92	7,93	7,94	7,908	0,001	-0,28	8,188	7,388
90	7,96	7,97	7,99	8,00	8,01	8,03	7,993	0,001	-0,28	8,273	7,473
95	8,04	8,05	8,06	8,07	8,08	8,09	8,065	0,001	-0,2	8,265	7,465
100	8,11	8,12	8,13	8,15	8,16	8,18	8,142	0,001	-0,28	8,422	7,622
105	8,19	8,20	8,22	8,23	8,25	8,26	8,225	0,001	-0,28	8,505	7,705
110	8,27	8,29	8,30	8,32	8,33	8,34	8,308	0,001	-0,28	8,588	7,788
115	8,36	8,37	8,38	8,40	8,41	8,42	8,390	0,001	-0,24	8,630	7,830
120	8,44	8,45	8,46	8,47	8,49	8,50	8,468	0,001	-0,24	8,708	7,908
125	8,52	8,53	8,55	8,56	8,57	8,58	8,552	0,001	-0,24	8,792	7,992
130	8,60	8,61	8,63	8,64	8,65	8,66	8,632	0,001	-0,24	8,872	8,072
135	8,68	8,69	8,70	8,71	8,72	8,72	8,703	0,001	-0,16	8,863	8,063
140	8,73	8,74	8,75	8,75	8,76	8,76	8,748	0,001	-0,12	8,868	8,068
145	8,77	8,77	8,78	8,78	8,79	8,79	8,780	0,000	-0,08	8,860	8,060
150	8,79	8,80	8,80	8,81	8,81	8,81	8,803	0,000	-0,08	8,883	8,083

Table 7.8 temperature measurement in area3 hole2

depth	t1	t2	t3	tav	deritive	corection	corrected T	deviation
0	7,36	7,23	7,12	7,237	-0,012	2,4	4,837	4,037
5	7,04	6,97	6,92	6,977	-0,006	1,2	5,777	4,977
10	6,87	6,84	6,8	6,837	-0,004	0,7	6,137	5,337
15	6,77	6,75	6,73	6,750	-0,002	0,4	6,350	5,550
20	6,72	6,71	6,71	6,713	0,000	0,1	6,613	5,813
25	6,71	6,71	6,71	6,710	0,000	0	6,710	5,910
30	6,71	6,72	6,73	6,720	0,001	-0,2	6,920	6,120
35	6,75	6,76	6,77	6,760	0,001	-0,2	6,960	6,160
40	6,79	6,81	6,82	6,807	0,002	-0,3	7,107	6,307
45	6,84	6,86	6,87	6,857	0,002	-0,3	7,157	6,357
50	6,89	6,90	6,92	6,903	0,002	-0,3	7,203	6,403
55	6,93	6,95	6,97	6,950	0,002	-0,4	7,350	6,550
60	6,98	7,00	7,02	7,000	0,002	-0,4	7,400	6,600
65	7,04	7,06	7,07	7,057	0,002	-0,3	7,357	6,557

70	7,09	7,11	7,13	7,110	0,002	-0,4	7,510	6,710
75	7,15	7,17	7,19	7,170	0,002	-0,4	7,570	6,770
80	7,21	7,23	7,26	7,233	0,002	-0,5	7,733	6,933
85	7,28	7,30	7,32	7,300	0,002	-0,4	7,700	6,900
90	7,35	7,37	7,39	7,370	0,002	-0,4	7,770	6,970
95	7,42	7,44	7,47	7,443	0,002	-0,5	7,943	7,143
100	7,49	7,52	7,54	7,517	0,002	-0,5	8,017	7,217
105	7,57	7,59	7,62	7,593	0,002	-0,5	8,093	7,293
110	7,64	7,67	7,7	7,670	0,003	-0,6	8,270	7,470
115	7,72	7,75	7,78	7,750	0,003	-0,6	8,350	7,550
120	7,80	7,83	7,85	7,827	0,002	-0,5	8,327	7,527
125	7,88	7,91	7,93	7,907	0,002	-0,5	8,407	7,607
130	7,96	7,99	8,01	7,987	0,002	-0,5	8,487	7,687
135	8,04	8,07	8,09	8,067	0,003	-0,5	8,567	7,767
140	8,12	8,15	8,17	8,147	0,003	-0,5	8,647	7,847
145	8,20	8,23	8,26	8,230	0,003	-0,6	8,830	8,030
150	8,28	8,31	8,33	8,307	0,003	-0,5	8,807	8,007
155	8,36	8,39	8,42	8,390	0,003	-0,6	8,990	8,190
160	8,44	8,47	8,5	8,470	0,003	-0,6	9,070	8,270
165	8,53	8,55	8,58	8,553	0,003	-0,5	9,053	8,253
170	8,60	8,63	8,66	8,630	0,003	-0,6	9,230	8,430
175	8,68	8,71	8,73	8,707	0,003	-0,5	9,207	8,407
180	8,76	8,79	8,82	8,790	0,003	-0,6	9,390	8,590
185	8,84	8,87	8,89	8,867	0,003	-0,5	9,367	8,567
190	8,92	8,95	8,97	8,947	0,003	-0,5	9,447	8,647
195	9,00	9,02	9,05	9,023	0,003	-0,5	9,523	8,723
200	9,07	9,10	9,12	9,097	0,002	-0,5	9,597	8,797
205	9,15	9,17	9,2	9,173	0,002	-0,5	9,673	8,873
210	9,22	9,25	9,27	9,247	0,002	-0,5	9,747	8,947

Table 7.9 temperature measurement in area3 hole3

depth	t1	t2	t3	tav	deritive	corection	corrected T	deviation
0	6,99	6,96	6,93	6,96	-0,003	0,6	6,360	5,560
5	6,91	6,90	6,90	6,903	-0,0005	0,1	6,803	6,003
10	6,90	6,90	6,91	6,903	0,0005	-0,1	7,003	6,203
15	6,91	6,92	6,93	6,92	0,001	-0,2	7,120	6,320
20	6,94	6,95	6,96	6,95	0,001	-0,2	7,150	6,350
25	6,98	6,99	7,00	6,99	0,001	-0,2	7,190	6,390
30	7,02	7,03	7,04	7,03	0,001	-0,2	7,230	6,430
35	7,06	7,07	7,09	7,073	0,0015	-0,3	7,373	6,573
40	7,10	7,12	7,13	7,117	0,0015	-0,3	7,417	6,617
45	7,15	7,17	7,18	7,167	0,0015	-0,3	7,467	6,667
50	7,20	7,22	7,24	7,220	0,002	-0,4	7,620	6,820
55	7,26	7,28	7,30	7,280	0,002	-0,4	7,680	6,880
60	7,32	7,34	7,36	7,340	0,002	-0,4	7,740	6,940
65	7,38	7,40	7,43	7,403	0,0025	-0,5	7,903	7,103
70	7,45	7,47	7,49	7,470	0,002	-0,4	7,870	7,070
75	7,51	7,54	7,56	7,537	0,0025	-0,5	8,037	7,237
80	7,58	7,61	7,63	7,607	0,0025	-0,5	8,107	7,307
85	7,65	7,68	7,70	7,677	0,0025	-0,5	8,177	7,377

90	7,72	7,75	7,77	7,747	0,0025	-0,5	8,247	7,447
95	7,79	7,82	7,84	7,817	0,0025	-0,5	8,317	7,517
100	7,86	7,88	7,91	7,883	0,0025	-0,5	8,383	7,583
105	7,93	7,96	7,99	7,960	0,003	-0,6	8,560	7,760
110	8,01	8,04	8,07	8,040	0,003	-0,6	8,640	7,840
115	8,10	8,13	8,15	8,127	0,0025	-0,5	8,627	7,827
120	8,18	8,21	8,23	8,207	0,0025	-0,5	8,707	7,907
125	8,26	8,28	8,31	8,283	0,0025	-0,5	8,783	7,983
130	8,33	8,36	8,38	8,357	0,0025	-0,5	8,857	8,057
135	8,40	8,43	8,45	8,427	0,0025	-0,5	8,927	8,127
140	8,47	8,50	8,52	8,497	0,0025	-0,5	8,997	8,197
145	8,54	8,56	8,57	8,557	0,0015	-0,3	8,857	8,057
150	8,59	8,60	8,62	8,603	0,0015	-0,3	8,903	8,103
155	8,63	8,64	8,65	8,640	0,001	-0,2	8,840	8,040
160	8,66	8,67	8,68	8,670	0,001	-0,2	8,870	8,070
165	8,69	8,70	8,71	8,700	0,001	-0,2	8,900	8,100
170	8,71	8,72	8,72	8,717	0,0005	-0,1	8,817	8,017

Appendix B

Logger calibration profile

T sec	Temperaturs
0	21,19
10	20,06
20	18,93
30	17,83
40	16,8
50	15,83
60	14,94
70	14,13
80	13,38
90	12,67
100	12,02
110	11,39
120	10,81
130	10,25
140	9,72
150	9,23
160	8,76
170	8,33
180	7,92
190	7,54
200	7,17
210	6,83
220	6,5
230	6,19
240	5,91
250	5,64
260	5,38
270	5,14
280	4,9

290	4,67
300	4,45
310	4,24
320	4,04
330	3,86
340	3,69
350	3,53
360	3,38
370	3,24
380	3,1
390	2,97
400	2,83
410	2,72
420	2,61
430	2,51
440	2,42
450	2,34
460	2,26
470	2,18
480	2,1
490	2,03
500	1,96
510	1,89
520	1,83

Appendix C

1. Temperature logger (Vemco) field reader

The vemco field reader, enables user to offload data in the field from the new minilog-11 Temperature data logger and all existing vemco minilog data loggers and copy later to the computer.

It is Bluetooth wireless technology enables high speed data uploads to pc, and reader operating temperature range of -10 c to 40 c, and it's water resistant.

2. Canary digital radon monitor

The canary digital radon monitor provides with continuous radon measurements. Can reads short and long term average measurements of radon concentration can be used in homes, workplaces, and public buildings.

References

1. IPCC. Summary for Policymakers. In: IPCC Special Report on Renewable Energy Sources and Climate Change Mitigation. Abu Dhabi, United Arab Emirates2011.
2. European Parliament C. Promotion of the use of energy from renewable sources. 2010 [cited 2013 April 4]; Available from: europa.eu/legislation-summaries/energy/renewable-energy/en0009_en.htm.
3. Holter Ø, Ingebretsen F, Parr H. Fysikk og energiressurser: Universitetsforlaget; 1998.
4. Sørensen B. Renewable energy: Its physics, engineering, environmental impacts, economics and planning. Second ed. DK: Roskilde University; 2000.
5. Pollack HN, Chapman DS. On the regional variation of heat flow, geotherms, and lithospheric thickness. Tectonophysics. 1977;38(3–4):279-96.
6. Bank D. An introduction to thermogyology ground source heating and cooling. Second ed: John Wiley & Sons; 2012.
7. Boyd TL. The Oregon Institute of Technology geothermal heating system-then and now. Geo-Heat Center Quarterly Bulletin. 1999;20(1):10-3.
8. Tester J, Drake E, Driscoll M, Golay M, Peters W. Sustainable energy: Choosing among options: The MIT press; 2005.
9. Metz B. Climate Change 2007-Mitigation of Climate Change: Working Group III Contribution to the Fourth Assessment Report of the IPCC: Cambridge University Press; 2007.
10. Lund JW. Direct utilization of geothermal energy. Energies. 2010;3(8):1443-71.
11. NGU. Groundwater. NGU; 2008 [cited 2013 May 20]; Available from: http://www.ngu.no/en-gb/hm/Resources/Groundwater/.
12. Gehlin S. Thermal response test: method development and evaluation. 2002.
13. Mogensen P. Fluid to duct wall heat transfer in duct system heat storages. Document-Swedish Council for Building Research. 1983(16):652-7.
14. Austin Iii WA. Development of an in situ system for measuring ground thermal properties: Oklahoma State University; 1998.
15. Signorelli S, Bassetti S, Pahud D, Kohl T. Numerical evaluation of thermal response tests. Geothermics. 2007;36(2):141-66.
16. GECCO. Thermal Response Test Report: Geothermal Borehole. Northwich2012 Nov 16. Report No.: CO474-12.

17. Jessop AM. Thermal geophysics: Elsevier Amsterdam; 1990.

18. Allen P, Allen J. Basin analysis, principles and applications. Second ed: Blackwell Publishing; 2005.

19. Turcotte DL, Schubert G. Geodynamics: Cambridge University Press; 2002.

20. Lederer CM, Shirley VS, Browne E, Shihab-Eldin AA. Table of isotopes: Wiley New York; 1978.

21. ENC. Radioactive Decay. Energy without Carbon; 2011-2013 [cited 2013 June 24]; Available from: http://www.energy-without-carbon.org/RadioactiveDecay.

22. Serway RA, Jewett Jr JW. Physics for Scientists and Engineers with Modern Physics, Volume 2. 2008.

23. Thorsteinsen T. Strålingsfysikk-FYS233. [Kompendium]. In press 1995.

24. Beardsmore GR, Cull JJP. Crustal heat flow: a guide to measurement and modelling: Cambridge University Press; 2001.

25. Ievy J. Radon: Understanding the element of periodic table2009.

26. EPA. EPA Assessment of Risks from Radon in Homes. Washington, DC: United States Enviromental Protection Agency2003.

27. Roper WL. Toxicological Profile for Radon. Agency for Toxic Substances and Disease Registry, US Public Health Service in collaboration with the US Environmental Protection Agency. 1990.

28. Harley J. Nobel gases1975.

29. Zdrojewicz Z, Strzelczyk J. Radon treatment controversy. Dose-Response. 2006;4(2):106-18.

30. No ISS. 115, International Basic Safety Standards for Protection against Ionizing Radiation and for the Safety of Radiation Sources. International Atomic Energy Agency, Vienna. 1996.

31. AEA. Radiation Protection against Radon in Workplaces other than Mines. Vienna2003 Contract No.33.

32. Løvø G. Kart viser radioaktivitet på vestlandet. NGU; 2011; Available from: http://www.ngu.no/en-gb/Aktuelt/2011/Kart-viser-radioaktivitet-pa-Vestlandet/.

33. NRPA. Government launched the national radon strategy, Norwegian Radiation protection Authority. 2009

34. U.S. Geological Survey, Mineral Commodity Summaries. 2004; Available from: http://minerals.usgs.gov/minerals/pubs/commodity/thorium/thormcs04.pdf.

35. Map available from: *http://www.hordaland.no/Hordaland-fylkeskommune/Regional-utvikling/Kart-og- statistikk /Kart/).*

36. Fossen, H. & Dunlap, W.J. 2006: Age constraints on the late Caledonian deformation in the Major Bergen Arc, SW Norway. Norwegian Journal of Geology 86, 59-70.

37. *VEMCO Company, http://vemco.com/ field –reader*

38. A. Erdal: Notes for course PHYS114, experimental physics.

39. WWW. Canary.no/no/radon

40. The University of Sheffield Department of Physics and Astronomy, Gamma-ray spectroscopy using a Sodium Iodide Scintillation Detector